Università degli studi di Napoli "Federico II"

Dottorato di Ricerca in Scienze Chimiche

XX *ciclo*

Integrated Computational Approach to Modelling Physico-Chemical Processes of Biological and Technological Relevance

Michele Pavone

TUTORE	COORDINATORE
Prof. Vincenzo Barone	Prof. Aldo Vitagliano

Novembre 2007

Table of Contents

Introduction

Modern research in chemical sciences tries to discover new molecules and materials, to understand their properties, and to design new systems with tailored functions. Such an aim has been stimulating the set-up and tuning of extremely sensitive spectroscopic techniques that are able to investigate the deep and subtle features of the matter. However, an experimental apparatus records the overall response of the matter to an external perturbation: in many cases, the collected data could be only indirectly related to the microscopic structure and dynamics of the system. Thus, the theoretical description at the atomistic level of the undergoing physico-chemical processes provides the framework for an unbiased interpretation of experimental data and could also suggest new experimental directions.[1] Indeed, in recent years, the margin of interaction between computational chemistry and most branches of experimental chemistry has increased at a fast pace. The characterization of new systems relies more and more on molecular modelling techniques, e. g., for the evaluation of structural, energetic, electronic and dynamical features. In particular, the use of reliable quantum mechanical (QM) methods[2] to obtain accurate estimates for several spectroscopic parameters has given rise to many successful, synergic interactions between experimentalists and theoretically oriented chemists. As a matter of fact, even within reliable and well tested spectroscopic characterization protocols, computational approaches can play an important role.[3] Thus, for example, the choice among alternative structural hypotheses can be often guided by the agreement between measured and computed spectroscopic parameters. Moreover, instances where the computed parameters have disproven a seemingly reliable assignment are not unusual, and it is quite conceivable that this kind of validation may become routine in a short time, at least in those fields of molecular spectroscopy where complications due to flexibility and chemical heterogeneity of the investigated system are not overwhelming.

From another perspective, the theoretical modelling of physico-chemical processes for molecular systems is usually feasible, but rarely trivial. In particular, when dealing with the response of the matter to external electromagnetic fields or with the breaking and forming of chemical bonds, the successful application of computational approaches in molecular spectroscopy, chemical reactivity, and design of new materials, relies on the

accurate description of the QM behaviour of interacting electrons and nuclei. On the other hand, the size of the systems imposes obvious limitations on the theory levels that can be employed. Despite the terrific development of electronic structure methods and the availability of high performance computing facilities, state-of-the-art first-principle approaches provide molecular parameters that could be directly related to experimental observables just in the cases of medium-to-large systems (up to few hundreds of atoms). The introduction of effective methods rooted in the Density Functional Theory (DFT)[4] has certainly been instrumental in widening the range of applications, from calculations of spectroscopic parameters to molecular dynamics (MD) simulations.[5] Needless to say, experimental efforts are mostly devoted to complex chemical systems in condensed phases: from biological macromolecules in the living cell to reactions of heterogeneous catalysts, the number of interacting atoms and molecules exceeds by far the aforementioned limits of first-principle methods. Therefore, the development and validation of effective computational approaches represent the main focus of active research in the field of theoretical chemistry. Many physico-chemical processes are "local": the reactions at the active site of enzymes, the adsorption of molecules on the surface of heterogeneous catalysts, and the chemical shift in nuclear magnetic resonance molecular parameters are only some examples of a large class of processes where the phenomena under investigation take place in a well defined region of space and occur in a rather fast time. Under such circumstances, the theoretical description could effectively exploit a scaling of space and time by using an integrated hierarchy of theory levels,[6] each of which addresses a specific space and time framework. Thus, in favourable cases, the system under investigation could be divided into concentric layers, the focus being the portion of space where the atoms or molecules undergoing the physico-chemical process are located. This represents the "core" region of the system and needs a proper description by means of QM techniques. However, the QM region is not treated as an isolated system, but it "feels" the chemical surroundings thanks to the formulation of an effective Hamiltonian that includes perturbative potentials accounting for the effects of the embedding regions of space. Thus, each of the subsequent layers, and, consequently, its effect on the QM region, could be described at a different level of theory, the best compromise being reached by the use of methods with decreasing accuracy and increasing efficiency when going outward from the focus of the process.

This thesis reports the results on the development and validation of a computational scheme that integrates this kind of multi-scale approach with the description of short-time dynamics for complex molecular systems. Notwithstanding the general applicability of the proposed scheme, we tuned our approach toward the reliable prediction of spectroscopic parameters, as discussed below: spectroscopy, indeed, represents a common ground for the experimental investigations in both Life and Material Sciences.

The issue of structural flexibility, which has been already hinted at, may well represent the main bottleneck in the formulation of a general computational protocol: in favourable cases, grid searches and relaxed potential energy scans can be used; but when the complexity of the problem increases, the involved computational effort rules out these simple approaches, and other conformational search techniques must be brought into play. Of course, for these screening phases one wants to employ lower levels of theory than for the more demanding computation of spectroscopic parameters: in particular, exploration of the potential energy surface would be made much easier by the use of reliable force fields based on molecular mechanics (MM).[7] Unfortunately, in some cases these are still not available: the development of a tailored force-field is a possibility, albeit probably not the most attractive one from the viewpoint of a non-specialist. Conceptually, solvent effects can also be related to structural flexibility: in both cases the central issue is the difficulty of sampling a proper phase space adequately. Concerning solvation effects, approaches in which the solvent degrees of freedom are accounted for in an average way, e.g., in terms of a reaction field, have proven particularly effective. The polarizable continuum model (PCM)[8-10] probably represents the best known example. The model consists of embedding the solute molecule within a cavity made by the envelope of atom-centred spheres whose radii have been parameterized for reproducing experimental solvation free energies; inside the cavity, the relative dielectric constant has the same value as in a vacuum ($\varepsilon = 1$), and it steeply goes to the solvent bulk value outside (e.g., $\varepsilon = 78.4$ for water). The presence of the solute perturbs the polarisable medium, which undergoes new equilibration acting back onto the solute molecular parameters by means of an effective reaction field. Such phenomenon is described by the PCM in terms of a pattern of effective charges on the cavity surface. The simple introduction of the PCM often provides substantial

improvements in energies, geometries and spectroscopic parameters computed for molecular systems in a variety of solvent media. However, the PCM may also display limitations in some cases, e. g., when highly specific interactions, like hydrogen bonds, come into play.[11] Cluster approaches can provide a straightforward route to describe localised phenomena, including the spectroscopic transitions of molecules; once again, the PCM can be brought into play to account for the "bulk" solvent, and thus to reduce the number of solvent molecules to be described explicitly.[12] In other words, such a discrete-continuum scheme takes into account both the quantum mechanical nature of specific solute-solvent interaction, i.e. hydrogen bonds, and the classical Coulomb long-range effects tuned by the dielectric properties of the solution. The resulting cluster-PCM description represents a very versatile tool that can be adapted to different structural and spectroscopic situations; of course, which and how many solvent molecules need to be explicitly described is a question that has to be defined case by case. Moreover, a single structure of the solute-solvent cluster or supra-molecular frame could not be representative of a very flexible situation.[13] This means that the structures of the solute and its closest solvent molecules must be statistically averaged among all the energetically accessible configurations. Thus, the cluster-PCM approach is also attractive for the computation of averaging effects brought about by dynamics. Physically, when a spectroscopic transition is fast with respect to the time scale of a dynamic phenomenon, the measured energetic parameters of the transition reflect the contribution of different populated configurations. From a computational viewpoint (and assuming ergodicity holds), if a representative MD simulation has been generated, the statistical distribution of the parameter values in the system can be reproduced by extracting from the trajectory a sufficient number of uncorrelated frames, and repeating a cluster-PCM calculation on each of them. Thus, averaging the computed values provides an estimate of the observable measured spectroscopically. As far as the nature of the simulation is involved, classical MD presents many advantages connected to the cheapness of the MM approach, but the difficulties with respect to the availability of reliable force fields represent a concrete limitation. As alternative, classical simulations employing energies and gradients computed by QM methods, i.e., Born-Oppenheimer dynamics and, especially, extended-Langrangian approaches based on the Car-Parrinello scheme,[14] are starting to provide dynamical trajectories which are long

enough to allow for reasonable averaging of spectroscopic parameters. In this connection, it is worth noting that the quality of the potential-energy landscape underlying Car-Parrinello simulations, which at present rely on conventional density functional models, may well turn out to be insufficient for a direct use in the computation of structurally sensitive parameters. As a matter of fact, there are still situations where application of currently available density functionals fails to capture the correct physics: dispersion or van der Waals interactions represent probably the most well-known DFT failure.[15] Local and semi-local exchange-correlation functionals fail to correctly describe these subtle non-local and non-classical electronic interactions across regions of very sparse electron densities.[16] Expensive post-Hartree-Fock methods,[17] especially coupled clusters (CC) approaches, offer, to-date, the most reliable and comprehensive representation of dispersion forces. However, while CC results for simple molecular systems are very accurate, these methods are so computer-time consuming that both the dimension of the system and the region of the investigated electronic potential energy surface are severely limited. But, beyond the accurate reproduction of experimental energies and static structures, a simple concept must be pointed out: weak interactions do correspond to large-amplitude motions. Therefore, the accurate description of a weakly bound molecular complex should include a proper investigation of its dynamical behavior, either in a time-independent (harmonic and anharmonic force fields) or a time-dependent (MD) approach. Thus, there is the need of reliable and cheap first-principle methods, for computing analytical gradients (MD simulations/geometry optimizations) and Hessians (harmonic and anharmonic frequencies): in both cases, the chance of extensively exploring the phase space of weakly bound molecular complexes could be only effectively pursued within the framework of density functional theory. Indeed, the consistent inclusion of dispersion in density-functional models is an active field of research and several routes are being explored. In our opinion, the most effective scheme to describe van der Waals interactions without losing computational effectiveness has been achieved, to-date, by consistently adding to the density-functional a semi-empirical dispersion term (DFT-D),[18] in the form of a long-range attractive pair-potential (proportional to R^{-6}) multiplied by a dumping function that shuts it off at short range. Thus the present thesis also reports the implementation of the DFT-D energy, analytical gradients and Hessians.

As pilot application, we discuss the minimum-energy structures, vibrational frequencies and *ab initio* molecular dynamics of a prototypical van der Waals complex, the benzene dimer.

In summary, this thesis reports the development and validation of an integrated computational tool, rooted in density functional theory, polarizable continuum model, and classical/Car-Parrinello molecular dynamics, which has been purposely tuned to study physico-chemical processes occurring in complex chemical systems. The reported results and future further developments toward the integration of effective theoretical models within a single and easy-to-use computer program may represent an important contribution toward filling the gap between *in vitro* and *in silico* chemistry.

General background

As briefly outlined in the introduction, experimental investigations have already been, and could further benefit by the use of reliable and accurate computational protocols to predict spectroscopic observables. The standard route to this aim has become the computation of molecular parameters for isolated systems at their minimum-energy structure: in other terms, it means to compute the spectroscopic parameters of rigid molecules in the gas phase. Of course, such a picture is well far from the experimental collection of data, which in many cases occurs at finite temperatures, and in condensed phases. Therefore, the last generations of theoretical methods try to include all the effects that modulate the spectroscopic parameters in the calculation. However, there are no general and accepted methodologies to account for the effects of structural fluctuations and chemical surroundings. On these grounds, we developed an integrated computational procedure, as described below, and applied it for the prediction of optical and magnetic parameters, as discussed in the next chapters.

The issue of molecular vibrations is directly addressed by Infrared and Raman spectroscopic techniques, but they could also have a direct or indirect effect on other spectroscopic properties.[19] In the case of electronic transitions, the vibrations are responsible for the fine structure of ultraviolet-visible adsorption and fluorescence emission spectra; as a matter of fact, the *Franck-Condon* selection rules depend on the nuclear wave-functions of the ground and the excited electronic states (direct effect).[20-22] In the case of magnetic resonance spectroscopies, which involve much lower energies than those of vibrational transitions, the temperature has the effect of averaging out the magnetic parameters over the structural fluctuations of the molecules (indirect effect).[6] In the framework of the Born-Oppenheimer (BO) approximation,[23] after obtaining a reliable description of the electronic potential-energy surface (PES), the most accurate theoretical description of molecular vibrations is achieved within the vibrational Hamiltonian formalism.[19] Within the harmonic approximation, the calculation of normal mode frequencies is made affordable by the available analytical second derivatives of the quantum chemical method used for solving the electronic Schrödinger equation.[24] The introduction of density functional theory has been instrumental also in this context in order to get correlation-consistent description of the

PES, and its analytical Hessian, for molecular systems larger than those feasible by post-HF methods. On these grounds, semi-rigid molecules are well described in terms of the harmonic scheme, but a second-order perturbative inclusion of principal anharmonicities provides much improved results at a reasonable cost.[25, 26] Both these approaches ensure the maximum possible accuracy since they account for the QM nature of nuclear motions. Therefore, the expected values of the observables (e.g., the hyperfine coupling constant) are obtained by averaging the different molecular parameters with respect to the normal modes.[11] At this level, the vibrationally averaged value of a property P at 0 K is given by:

$$\langle P \rangle_0 = P_{eq} + 0.25 \sum_k \left(P''_{kk} - \sum_l P'_l F_{kll} / \omega_k \omega_l \right) / \omega_k$$

Where where P_k' and P_{kk}'' are first and second derivatives of the property with respect to normal modes, ω_k, ω_l are normal mode frequencies and F_{kll} are third energy derivatives with respect to normal modes. The harmonic approximation is recovered neglecting the term involving first derivatives of the property. Despite the excellent results for medium-sized molecules in the gas phase, these so-called "Hessian-based" methods become computationally prohibitive for large systems and could not be exploited for describing large-amplitude motions like, e.g., those of fluxional molecules.[27] Complementary to the former stationary-state approach, an alternative route could be achieved by a dynamic picture of the system, i.e., by the sampling of nuclear motions in the classical phase space via molecular dynamics techniques. MD simulations are based on following the classical trajectory of the nuclei by solving the Newton's equation of motion on the force-field corresponding to the electronic PES.[28] Normal mode frequencies and Infrared spectra can be computed, in this case, following the standard statistical mechanics formalism, via the Fourier transform analysis of the time correlation functions of atomic velocities and dipole moment, respectively.[29] Besides, magnetic parameters can be averaged on a time-based criterion by extracting a consistent set of configurations from the trajectories, and averaging the parameter values computed on each of them.[30] Within this context, it is worth noting the importance of the quality of the force field governing the nuclear dynamics.[13] The most accurate result is achieved by using the forces on the PES self-consistently computed at

each step along the trajectories. This scheme is usually referred as BOMD; however, a typical trajectory has 50-to-100 thousands of time steps, and the corresponding computational burden would be unaffordable. Alternatively, Car and Parrinello in a seminal paper[14] proposed an effective scheme for performing classical MD on forces computed from first principles, within the framework of DFT. The Car-Parrinello (CP) method approximates the BOMD through the classical dynamical evolution of both the electronic and nuclear variables generated by the Lagrangian:

$$L_{CP} = \mu \sum_i \int \left|\dot{\psi}_i(\mathbf{r})\right|^2 d\mathbf{r} + \frac{1}{2}\sum_I M_I \dot{\mathbf{R}}_I^2 - E_{KS}\left[\{\psi_i\}, \mathbf{R}_I\right] + \sum_{i,j}\left(\int \psi_i^*(\mathbf{r})\psi_j(\mathbf{r})\, d\mathbf{r} - \delta_{ij}\right)$$

where ψ_i are the electronic molecular orbitals (regarded as classical fields), M_I are the ionic masses, E_{KS} is the Kohn-Sham density functional, μ is a mass-like parameter with dimensions of an energy times a squared time, and the last term ensures the ortho-normality of the wave functions (this constraint does not perform any work on the system and no dissipation occurs due to its presence). Extensive reviews of the CPMD equations can be easily found in recent literature: it has been well demonstrated that the CP scheme properly approximates the molecular dynamics along the true BO surface at an affordable computational cost.[31, 32] However, the inaccuracy due to the use of approximated density functionals still affects the CPMD dynamics. The original CP method implements a plane-wave expansion of the electronic wave function; in this way the ortho-normality of the wave function is always achieved, but only local density functional models could be used, since the direct calculation of non-local HF exchange is too expensive.[33] Recently, the CP method has been extended to DFT-based MD simulations with localized basis sets: the Atom-centered Density Matrix Perturbation (ADMP)[34] scheme allows the use of Gaussian-type orbitals to expand the electronic degrees of freedom, thus also allowing the use of more reliable hybrid HF-DFT density functional.[5] Notwithstanding the many successful applications of these density functionals,[35] as for example in hydrogen-bonded systems, there are situations where all the available density functionals fail to capture the correct physics: the description of van der Waals forces is one of the most known cases.[15] Within this context, in this thesis we propose the use of a semi-empirical corrected density functional that accounts for dispersion (DFT-D).[18] As described in the first chapter, we validated our approach

on the prototypical case of the benzene dimer. While the dispersion interaction is completely neglected by commonly employed density functional, the DFT-D scheme provides molecular structures and binding energies in close agreement with the most refined post-HF methods. Besides, the implementation of DFT-D within the ADMP scheme allowed us to get not only a quantitative agreement with micro-wave experiments, but also to highlight the importance of accounting dynamical effects in all the cases ruled by non-covalent forces, since weak interactions usually correspond to large amplitude motions.

The second issue in the prediction of accurate spectroscopic properties is related to the effect of the chemical surroundings. In this thesis we address the case of isotropic solutions, so the environmental effects are essentially due to the solvent. From a general perspective, it is possible to identify two ways by which the surrounding medium affects the molecular properties of the solute: it induces structural modifications (indirect effect), and, for a given molecular structure, it modifies the electron density distribution (direct effect). Since both optical and magnetic spectroscopic parameters depend explicitly on the accurate description of the electron spin density, a full QM model of the molecule itself (the solute) and of its interaction with the solvent is mandatory. The QM calculation of the solute plus a very large number of solvent molecules via a brute-force approach is unbearable; thus, one should rely on implicit solvation schemes. An extensive review of all continuum-based method of implicit solvation can be found in recent literature.[8, 9, 36] Briefly, the most general approach to the problem of solvent effects is traditionally based on a system-bath decomposition. The solvation process can then be dissected into the creation of a cavity for the solute (spending energy E_{cav}), and the successive switching-on of dispersion-repulsion (with energy $E_{dis\text{-}rep}$) and electrostatic (with energy E_{el}) interactions with surrounding solvent molecules. The polarisable continuum model (PCM) provides a unified and well-sound framework for the evaluation of all these contributions, in both isotropic and anisotropic solutions. Within this model, the solute molecule is embedded in a cavity formed by the envelope of spheres centred on the solute atoms. The procedures to assign the atomic radii and to form the cavity have been described in detail together with effective classical approaches for evaluating E_{cav} and $E_{dis\text{-}rep}$.[8, 9, 37] The solvent is polarized by the presence of the solute molecule and undergoes a new equilibration, giving rise to a

reaction field that acts back onto the solute molecule. The cavity surface is finely subdivided into small tiles (*tesserae*), and the solvent reaction field determining the electrostatic contribution (E_{el}) is described in terms of a pattern of apparent point charges appearing in *tesserae* and self-consistently adjusted with the solute electron density. Within the framework of effective Hamiltonian schemes, it is possible to write the solute molecular Hamiltonian as perturbed by a reaction field operator:

$$\hat{H} = \hat{H}^0 + \hat{V}_{RF}$$
$$\hat{V}_{RF} = \frac{1}{2}\int_{surface} \phi(\mathbf{r}')\, D(\mathbf{r}', \mathbf{r})\phi(\mathbf{r})\, d\mathbf{r}' d\mathbf{r}$$

where H^0 is the Hamiltonian of the isolated molecule, ϕ(r) is the electrostatic potential on the cavity surface, and D(r′,r) is a function depending on cavity geometry and solvent dielectric constant. Solvation charges (q) depend, in turn, on the electrostatic potential (V) on *tesserae* through a geometrical matrix Q (q = QV), related to the position and size of the surface *tesserae*, so that the free energy in solution G can be written:

$$G = E[\rho] + V_{NN} + \frac{1}{2}\mathbf{V}^{\dagger}\mathbf{Q}\mathbf{V}$$

here $E[\rho]$ is the free-solute energy, but with the electron density (ρ) polarized by the solvent, and V_{NN} is the repulsion between solute nuclei. The core of the model is then the definition of the Q matrix, which in the most recent formulations of PCM depends only on the electrostatic potentials, takes into the proper account the part of the solute electron density outside the molecular cavity, and allows the treatment of conventional, isotropic solutions, and anisotropic media like liquid crystals. Starting from these definitions, very effective linear-scaling algorithms[38] have been implemented for cavity construction and evaluation of energy and of its first and second derivatives with respect to geometric, electric and magnetic parameters, thus allowing for the inclusion of PCM contributions in the calculation of optical and magnetic spectroscopic parameters.[12, 39-41] Moreover, the PCM could easily be extended to situations where a simple continuum model is not sufficiently accurate due to the presence of specific solute-solvent interactions (e.g., hydrogen bonds). Under these circumstances, the PCM could be integrated by including some solvent molecules into the QM region together with the solute. Such a discrete-continuum scheme is very effective, since it takes into

the proper account the short-range solvent effects (at the QM level) and the classical Coulomb effects from the bulk of the solvent. Unfortunately, how many solvent molecules and which solute-solvent configurations should be taken into account have to be determined case-by-case. To this aim, here, we propose an effective scheme that integrates the afore-mentioned CPMD and discrete-continuum approaches in order to compute reliable EPR observables of nitroxide spin-probes in aqueous and in methanolic solutions, as discussed in the second chapter. Our approach consists of (i) performing a first-principle MD simulation of the solute-solvent system, (ii) extracting a consistent set of snapshots (i.e., configurations) along the trajectory, (iii) analyzing the dynamical features of the solute-solvent specific interactions, and (iv) carrying out on each configuration the calculation of spectroscopic parameters within the discrete-continuum scheme, by selecting the number of explicit solvent molecules on the basis of the former analysis. Beyond the importance of properly accounting specific and bulk solvent effects, the case of nitroxide free radicals represents an enlightening example of how crucial is the description of the dynamical features of the H-bond networks in order to achieve a quantitative agreement with available experimental EPR data: we found a variable number of solvent molecules H-bonded to the NO moiety,[42] depending on the flexibility of the nitroxide molecule and on the solvent nature (e.g., water vs. methanol). Furthermore, as first step of the proposed approach, it would be preferable to perform a classical MD simulation by exploiting "cheap" molecular mechanics force-fields, in order to achieve a better statistical sampling of the solute-solvent phase space than in the case of CPMD.[7] However, the available parameterizations of empirical force fields are not always suited to describe the molecular structures at the level of accuracy that is mandatory for the *a posteriori* calculation of spectroscopic properties.[13, 43] Therefore, in the third chapter, we propose a protocol to obtain the intra- and inter-molecular force-field of the acetone-water system on the basis of high level QM calculation and CPMD simulations, thus tuning the empirical parameters on both static and dynamical properties. The acetone-water system represents the simplest prototypical system for the carbonyl-group water interactions, for which experimental spectroscopic data are available. Moreover, we exploit a new developed mean field (MF) method to perform MD simulation of liquid solutions with non-periodic boundary conditions. Briefly, the MF is a continuum model suited for simulation of solute-solvent systems: the solute

molecule (in this case the acetone) is placed at the center of a spherical cavity embedded in a dielectric continuum and solvated with a large number (thousands) of explicit solvent molecules within the cavity. In a recent work,[44] it was shown that the MF model is very effective in reproducing the structural and thermodynamic properties of bulk water as well as aqueous solutions of simple solutes, as compared to conventional simulations using periodic boundary conditions. In this context, the use of the MF model is very well-suited, because it elegantly allows retention of the same explicit molecular system, as obtained from the simulated trajectory, in the QM calculations of spectroscopic properties: for each snapshot extracted along the trajectory, the whole molecular system is considered, which also includes the dielectric continuum for consistency. Only few solvent molecules along with the solute need to be treated at the QM level for obtaining accurate spectroscopic parameters, whereas the remaining molecules are included as point charges in what can be more properly named a QM/MM/MF calculation. Remarkably, the QM/MM/MF approach has also been recently used for effective MD simulations of liquids and solutions,[45, 46] by allowing the use of localized basis sets instead of plane waves. In the case of acetone in aqueous solution, our results on the electronic n-π^* transition energy, and on ^{13}C and ^{17}O magnetic shielding tensors are in quantitative agreement with experiments, thus providing a further validation of our integrated computational approach.

Chapter 1

Ab initio molecular dynamics of the benzene dimer

Abstract: this chapter addresses a case where currently available density-functionals fail: the accurate theoretical prediction of structure, energetics and molecular dynamics of weakly bound molecular complexes. The case of benzene dimer, which represents the prototypical system of aromatic π-π interactions, has been exploited in order to validate a semi-empirical correction to DFT for taking into account the Dispersion interaction (DFT-D). Thanks to our implementation of DFT-D for energies, analytical gradients, and Hessians, the potential energy surface of the benzene dimer has been explored by means of a complete set of first-principle methods. Therefore, it has been possible to dissect the impact of non-bonding interactions on structures, binding energies and zero-point energy contributions as well as on first-principle molecular dynamics trajectories, thus unraveling the dynamic features of the benzene-benzene interaction.

Introduction

Despite being usually identified as weak forces, non-covalent interactions of the aromatic π-π type play a relevant role in many physico-chemical processes like, e. g., folding of bio-molecules, supra-molecular assembly, and molecular recognition.[47-49] The systems undergoing these processes have a complex macro-molecular nature; therefore computational techniques, able to describe all their subtle features, could represent an invaluable complement to experimental investigations.

Density Functional Theory has become the method of choice for first-principle modelling of complex molecular systems,[4, 5] thanks to its accuracy and computational feasibility. However, there are still situations where currently available functionals fail to capture the correct physics; dispersion or van der Waals (vdW) interactions are probably among the most well known DFT failures. As a matter of fact, local (LDA) and semi-local (GGA) exchange-correlation (xc) functionals fail to correctly describe these subtle non-local and non-classical electronic interactions across regions of very sparse electron densities.[15] Expensive post-HF methods (especially coupled clusters (CC) approaches)[17] offer, to-date, the most reliable and comprehensive representation of dispersion forces. However, while CC results for simple molecular systems are very accurate, these methods are such computer-time consuming that both the dimensions of the systems and the regions of the investigated electronic potential energy surface (PES) are severely limited, also because converged computations require huge basis sets.[50] But beyond the accurate reproduction of experimental energies and rigid structures, in the present chapter we ought to point out a simple concept: weak interactions do correspond to large-amplitude motions. Therefore, the accurate description of a weakly bound molecular complex should include a proper investigation of its dynamical behaviour, either in a time-independent (harmonic and anharmonic force fields) or a time-dependent (molecular dynamics, MD) approach. Thus, there is the need of reliable and cheap first-principle methods, for computing analytical gradients (geometry optimizations and MD simulations) and Hessians (harmonic and anharmonic frequencies): in both cases, the chance of extensively exploring the PES of weakly bound molecular complexes could be only effectively pursued within the framework of DFT. Indeed, the consistent inclusion of dispersion in density-functional models is an

active field of current research: several routes are being explored ranging from electron-density based approximations,[51, 52] to symmetry-adapted perturbation theory,[53] solution of the adiabatic connection formula for the long-range part of the interaction energy,[16] use of effective core potentials including a dispersion term,[54] *ad hoc* reparametrization of semi-local GGA functionals.[55] However, in our opinion, the most effective scheme to describe vdW interactions without losing computational effectiveness has been achieved by consistently adding to the density-functional a semi-empirical dispersion term (DFT-D), in the form of a long-range attractive pair-potential (proportional to R^{-6}) multiplied by a dumping function that shuts it off at short range.[56-59]. Thus, in the present chapter, we report the implementation of DFT-D energy, analytical gradients and Hessians, exploiting the parameterization recently proposed by Grimme, [18] for computing the minimum-energy structures, vibrational frequencies and *ab initio* molecular dynamics of a prototypical vdW complex, the benzene dimer.[60]

The three most investigated structures of the benzene dimer are the T-shaped (B2T), the parallel (B2P) and the parallel displaced (B2D) configurations, as depicted below.

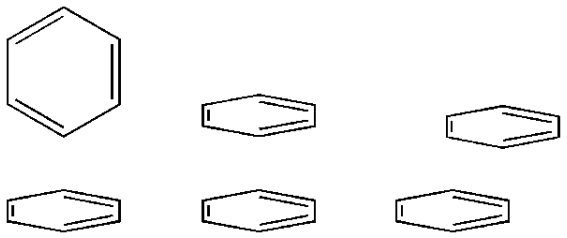

B2T (C_{2v}) ***B2P (D_{6h})*** ***B2D (C_{2h})***

From experimental investigations, the T-shaped structure seems to be the most stable, the parallel-displaced has also been observed in some experiments; nevertheless, in molecular crystals, T-shaped structures have been observed much less frequently than the parallel-displaced ones.[60-62] Therefore, a great theoretical effort has been devoted to explore the differences between these two conformers of the benzene dimer.[50, 60, 63-65] Dispersion is certainly the most relevant contribution for the benzene-benzene PES; electrostatic interactions (quadrupole-quadrupole) play an important role too, especially for the T-shaped conformer. At any rate, the computed binding energies for the different structures and their relative ordering are remarkably sensitive to the level of correlation

treatment and/or basis set. CC based benchmarking calculations[65] predict nearly isoenergetic B2T and B2D structures, whose binding energy (~2.6 kcal/mol) is very close to the best experimental estimate (2.4 ±0.4 kcal/mol).[62] The most recent results[50] favour the T-shaped structure with respect to its B2D counterpart by just 0.02 kcal/mol, whereas the B2P structure is significantly less stable (by about 1 kcal/mol). Several DFT-based results for the benzene dimer are also available,[66-68] involving different correction schemes (semi-empirical or not) to the basic density functional, and mostly confirming the reference CC results. However, once again it must be noted that both post-HF and DFT-based investigations have been restricted to the characterization of stationary points, neglecting wider sampling of the PES. A viable solution to this problem is offered by first-principle molecular dynamics [14, 34] enforcing the DFT-D model. In the present study we will exploit, in particular, the Atom-centred Density Matrix Propagation (ADMP) method[34] for *ab initio* molecular dynamics (MD) simulations of the T-shaped benzene dimer. The ADMP approach is an extended-Lagrangian MD scheme, similar to the Car-Parrinello method, but employing localized basis functions (GTO) in place of plane waves (PW), and propagating the electronic density matrix together with nuclear coordinates. While the ADMP is well suited for exploiting hybrid HF-DFT functionals, the finite size of localized basis sets leads to the well known basis-set superposition error (BSSE).[69] Since there are no practical on-the-fly methods to correct the BSSE, when running ADMP simulations, the size consistency of the chosen basis-set must be well proven: here, we also present, as side result, a brand new GTO triple-ζ basis set, optimized for DFT-based calculations, ensuring in the case of the benzene dimer a very small BSSE, at a reasonable computational cost.

Methods and computational details

In the DFT-D scheme, the total dispersion energy is computed as a sum of all possible pair-wise atomic contributions and then added to the usual DFT energy:

$$E_{DFT-D} = E_{DFT} - s_6 \sum_{i=1}^{N_{at}-1} \sum_{j=i+1}^{N_{at}} \frac{C_6^{ij}}{R_{ij}^6} f_{damp}\left(R_{ij}\right) \quad (1).$$

The interatomic attractive potential of the C_6R^{-6} form is damped by the following function:

$$f_{damp}\left(R_{ij}\right) = 1 / \left(1 + e^{-d\left(\frac{R_{ij}}{R_{vdW}} - 1\right)} \right) \quad (2).$$

The s_6 and d constants are scaling parameters, optimized with respect of the density-functional form and the dumping function, respectively. R_{vdW} is the sum of the atomic vdW radii, and the C_6^{ij} coefficients are given by the geometric mean of atomic values ($C_6^{ij} = \sqrt{C_6^i C_6^j}$). Each of the C_6 atomic coefficients is proportional to the ionization potential and atomic polarizability; they have been obtained, as well as vdW radii, on the basis of first-principle calculations, as recently proposed by Grimme.[18] The contributions of the dispersion term to the DFT energy, gradient and Hessian have been implemented in a local version of the Gaussian suite of programs for quantum chemistry.[70] We compared the well known B3LYP hybrid functional [71] with its dispersion-corrected counterpart (B3LYP-D).

The augmented triple-ζ correlation-consistent basis set of the Dunning series (Aug-cc-pVTZ)[72] has been used as reference for tuning our brand new triple-ζ basis set optimized for Khon-Sham DFT calculations (N07T).[73] Single-point energy calculations were carried out on the benzene monomer and B2T, B2D, B2P dimer structures, optimized at the CCSD(T) level of theory;[64] then the basis-set superposition error (BSSE) has been evaluated via the counterpoise method.[69] Once proven the effectiveness of the proposed basis set, full geometry optimizations were carried out at the B3LYP-D/N07T level of theory. The nature of the stationary points we found has been investigated by means of harmonic frequency calculations.

At the same level of theory, we carried out ADMP simulations of the T-shaped benzene dimer, and of the benzene monomer for comparison. The simulations were performed within the micro-canonical ensemble (NVE), for a total simulation time of 4.0 ps. The Verlet algorithm[74] for the integration of the equations of motions and a time step of 0.20 fs were used, while the Cholesky decomposition[34] was chosen to obtain the unitary transformation of the density matrix into an ortho-normal basis set. The fictitious mass parameter of the electron was set to 0.50 atomic units. The stability of the simulations was monitored by checking the idempotency of the density matrix (within a 10^{-12} threshold) and the so-called adiabaticity index (within a 10^{-4} threshold).[34]

Results and discussion

Table I compares the results regarding the benzene molecular structure, harmonic frequencies, the relative IR intensity and average polarizability, as obtained by the B3LYP density-functional with the N07T basis set and the well converged Aug-cc-pVTZ set of the Dunning' series. In all the cases, the N07T basis set provides quantitative agreement with the Aug-cc-pVTZ, and the results are always close to the available experimental data.[75, 76] Table II lists the BSSE computed with the two different basis-sets on the standard set of reference structures[64] of the benzene dimer isomers; the BSSE values are always very close, despite the much reduced number of basis functions of N07T w.r.t. Aug-cc-pVTZ (396 vs. 828).

Table II compares also the interaction energies [$E(benzene)_2 - 2E(benzene)$] obtained with the B3LYP and the dispersion corrected B3LYP-D functionals: as expected, B3LYP does not provide favourable binding energies, whereas the B3LYP-D scheme succeeds in predicting the existence of bound molecular complexes. The computed binding energies are comparable to those obtained at the CCSD(T) complete basis level of theory, that are around 2.6-2.7 kcal/mol in the B2T and B2D cases[50] and 1.7 in the B2P one. The slight underestimation of the interaction energy for the B2P structure is consistent with other results obtained by related DFT-D models,[18] and does not undermine the remarkable improvement over pure DFT when enforcing the proposed

semi-empirical correction scheme. Such an improvement has been highlighted by performing rigid-scan calculations relative to the benzene-benzene intermolecular distances, as depicted by Figure 1: it is apparent that the B3LYP density functional does not predict any energy minimum at finite distances between the benzene molecules, while B3LYP-D provides the expected positions of minima.

Table I. *Molecular properties of the benzene monomer (point group D_{6h}) computed at the B3LYP level of theory: distances in Å, computed harmonic frequencies in cm^{-1} and IR intensities in Km/mol, polarizability in atomic units and quadrupole moments in Debye·Å*

Geometry	**N07T**	**Aug-cc-pVTZ**	
C – C	1.39	1.39	
C – H	1.08	1.08	
Quadrupole	**N07T**	**Aug-cc-pVTZ**	**Exp[a]**
Q_{xx}	2.6	2.5	2.8
Q_{yy}	2.6	2.5	2.8
Q_{zz}	-5.1	-5.0	-5.6
	N07T		**Aug-cc-pVTZ**	
	Freq.	**IR int.**	**Freq.**	**IR int.**
out-of-plane bnd (A_{2u})	685	117.0	693	110.1
in-plane bnd (E_{1u})	1060	5.7	1060	5.1
in-plane bnd (E_{1u})	1517	7.1	1516	6.3
CH str (E_{1u})	3183	32.8	3182	34.5
Polarizability	**N07T**	**Aug-cc-pVTZ**	**Exp[b]**	
$1/3(2P_{aa} + P_{cc})$	68.0	69.3	68.7	

(a) Ref. [75]; (b) Ref. [76]

Table II. *Interaction energies (kcal/mol) relative to the B2T, B2P and B2D configurations, inter parenthesis the BSSE*

B3LYP	**B2P**	**B2D**	**B2T**
Aug-cc-pVTZ	2.42 (0.14)	2.12 (0.17)	0.46 (0.16)
N07T	2.41 (0.19)	2.17 (0.19)	0.46 (0.17)
B3LYP-D	**B2P**	**B2D**	**B2T**
Aug-cc-pVTZ	-1.21	-2.33	-2.91
N07T	-1.22	-2.28	-2.91

(a) 828 basis functions; (b) 396 basis functions

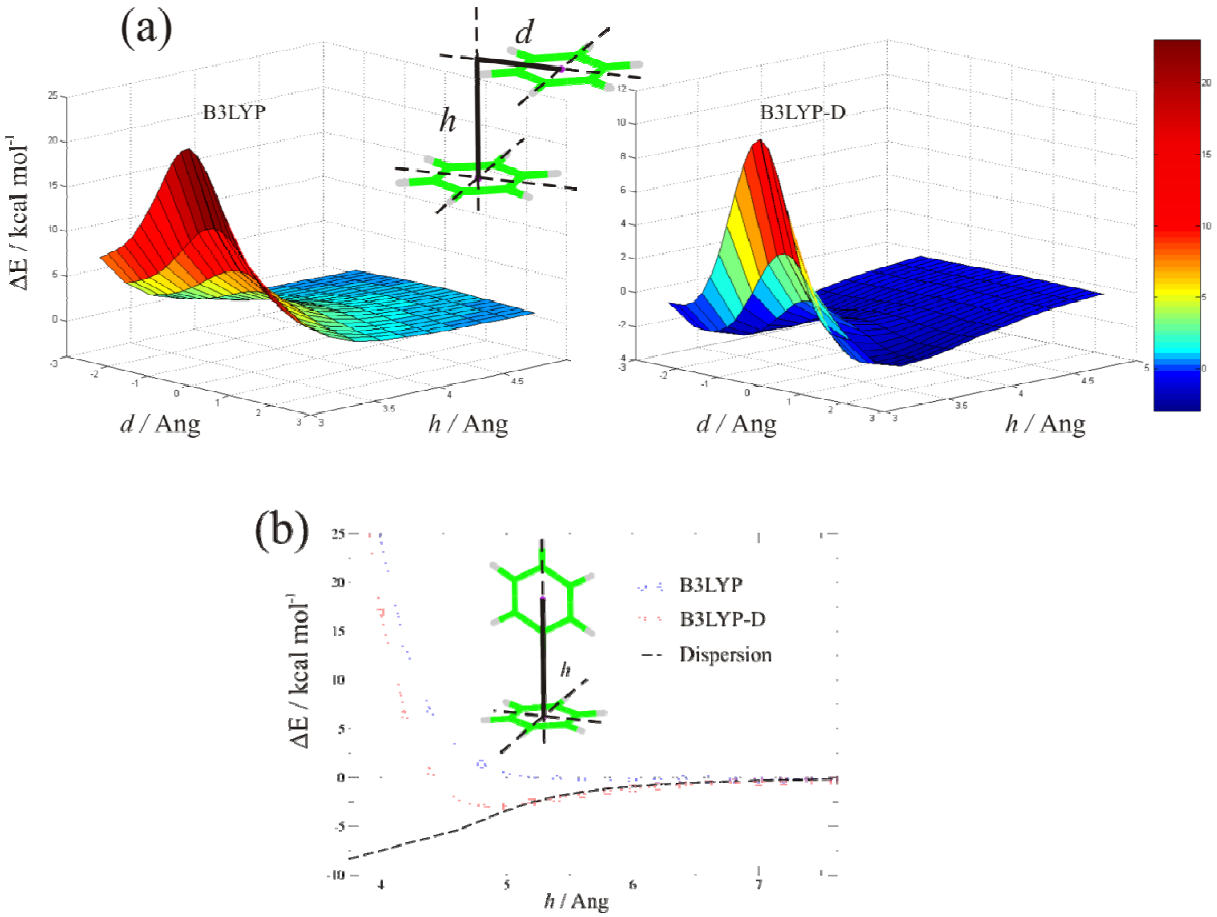

Figure 1. Potential *Energy Surface scan of the benzene dimer: (a) parallel and (b) T-shaped isomers*

Table III. *Calculated and experimental frequencies (cm^{-1}) of the benzene monomer*

	B3LYP/N07T		**B3LYP-D/N07T**		**Experiment**[a]
	Harmonic	**Anharmonic**	**Harmonic**	**Anharmonic**	
ν_{13} (B_{1u})	3158	3002	3153	2994	3015[b]
ν_{20} (E_{1u})	3183	3030	3176	3021	3047.9
ν_{7} (E_{2g})	3168	3039	3161	3030	3056.7[b]
ν_{2} (A_{1g})	3193	3049	3185	3040	3073.9[b]

(a) Ref. [77]; (a) Not IR active;

The implementation of analytic gradients and Hessian of the B3LYP-D model allowed us to perform geometry-optimization and harmonic-frequency calculations of the benzene monomer and dimer; estimation of the anharmonic contribution to normal mode frequencies has been also performed for the semirigid monomer by a second-order perturbative approach[25] providing results in quantitative agreement with experiments,[77] as listed by Table III. However, perturbative anharmonic computations are not appropriate for the large amplitude intermolecular motions of the dimer. Four stationary points out of the aforementioned B2T, B2D and B2P isomers have been found; all the structures and relative labelling are reported by Figure 2. Table IV lists the optimised geometrical parameters for each structure: in all the cases, the intra-molecular parameters of the benzene molecules are not appreciably affected by the formation of the dimer.

Table IV. *Structural parameters of the benzene dimer isomers optimized at the B3LYP-D/N07T level of theory: distances in Å, angles in degrees*

	TSP	**MD1**	**MD2**	
C – C	1.39	1.39	1.39	
C – H	1.08	1.08	1.08	
h [a]	3.88	3.43	3.42	
d [a]	0.00	1.77	1.79	
	TST1	**TST2**	**MT1**	**MT2**
C – C	1.39	1.39	1.39	1.39
C – H	1.08	1.08	1.08	1.08
h [b]	4.85	4.85	4.79	4.79
α [b]	90.0	90.0	67.4	67.9

(a) see Figure 1; (b) see Figure 3

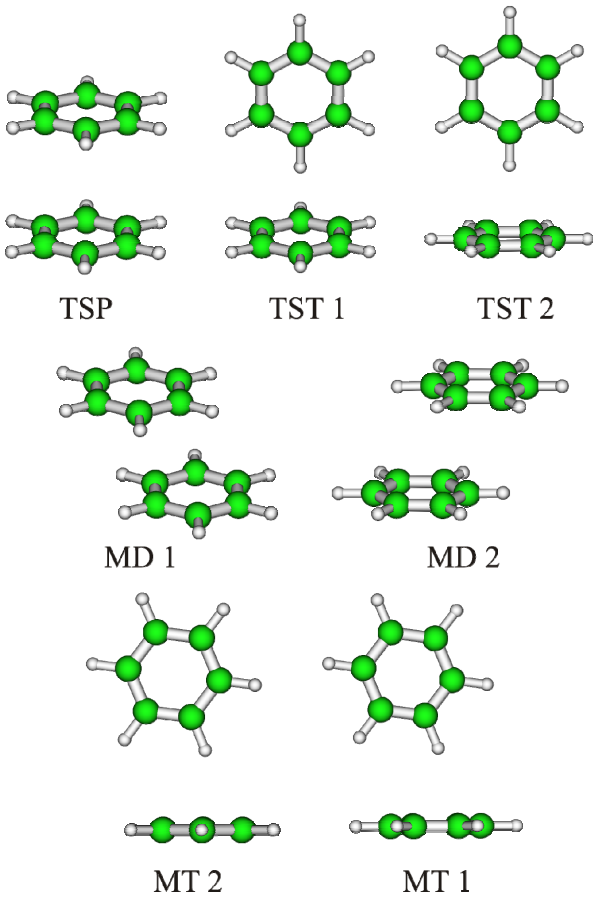

Figure 2. *Structures and labeling of the benzene dimer isomers*

The sandwich parallel configuration TSP is a second order saddle point: the imaginary frequencies correspond to the normal modes going toward the two parallel displaced minima MD1 and MD2, where the displacement vector is orthogonal to a C – C bond or parallel to a C – H bond, respectively. The MD1 and MD2 inter-plane distances (*h*) are shorter (~0.45 Å) than in the transition state, the displacement vector (*d*) of MD2 is slightly longer (~0.02 Å) than in the MD1 case. The obtained data of the TSP and MD1 isomers, usually referred as the B2P and B2D structures, are in reasonable agreement with post-HF accurate results: *h* values are 3.9 and 3.6 Å in the B2P and B2D cases, respectively, and the *d* value (for the B2D/MD1 case) is 1.6 Å.[65] Concerning the T-shaped configurations, we found two first-order saddle points TST1 and TST2, both with C_{2v} point group symmetry, where the molecular plane of the vertical benzene is orthogonal to the C – C bond of the molecule in the horizontal plane (TST1) or parallel to the C – H bond (TST2), thus implying a rotation of 30° of the vertical benzene along the C_2 axis. The distance between the two centres of mass (*h*) is the same in the TST1 and TST2 cases (4.85 Å), once again we found a fair comparison with the post-HF data (5.0 Å) with a slight overestimation of the attractive interaction. The TST1/2 structures correspond to the two different minima MT1 and MT2, with C_S symmetry, where the vertical molecule rotates in its own plane, forming an angle of ~67° with the plane of the horizontal molecule. The distance between the centres of mass is ~4.8 Å for both the MT1 and MT2, in good agreement with the experimental value of 4.9 (±0.1) Å.[78]

Table V. *Interaction energies (kcal/mol) of the benzene dimers*

	ΔE	**Δ(E+ZPE[a])**	**$\Delta E_{dispersion}$**
TSP	-1.23	-1.14	-3.70
MD1	-2.43	-2.15	-5.36
MD2	-2.45	-2.12	-5.38
TST1	-3.05	-2.49	-4.15
MT1	-3.16	-2.60	-4.54
TST2	-3.06	-2.50	-4.15
MT2	-3.16	-2.60	-4.55

(a) Zero Point Energy correction evaluated at the harmonic level.

Table V lists the formation energies of the different structures characterized for the benzene dimer, including the zero-point energy (ZPE) and decoupling the contribution of the dispersion term. Starting from the parallel structures, and considering the ZPE corrected interaction energies, the MD1 and MD2 present the same binding energy (~2.1 kcal/mol), whereas the energy barrier toward the TSTP transition state is ~ 1.0 kcal/mol. Also in the case of the T-shaped structures, the TST1/2 and MT1/2 couples present an energetic picture that does not change upon rotation of the vertical molecule along the C_2 axis. Indeed, by performing a scan of the PES along such rotation angle we did not find any significant energy barrier. The ZPE-corrected interaction energies at the minima (~ 2.6 kcal/mol) are consistent with the experimental estimation of 2.4 ± 0.4 kcal/mol.[62] The energy barriers for going from the C_S to the C_{2v} structures are very low (0.1 kcal/mol) with respect to the cases of parallel displaced configurations. It is worth noting that the ZPE corrections are not negligible, ranging between ~7% of ΔE in the TSP case, and ~11% for MD1/2 or ~18% for TST1/2 and MT1/2 cases. Eventually, the contribution of dispersion to the interaction energies is determinant in all the cases, thus implying that the bare B3LYP functional does not predict bound complexes, in contrast to the experimental observations.

The ADMP simulation of the benzene dimer dynamics in the NVE micro-canonical ensemble was carried out starting from the TST1 structure, and the average kinetic energy corresponds to a temperature of 65K. The time evolutions of the structural parameters ruled by the dispersion interaction are plotted in Figure 3: the distance between the centres of mass (*h*), the only one directly related to an experimental observable, the angle between the two benzene planes (ϕ) and the inclination angle (α) are all computed along the 4ps trajectory. Among the aforementioned structural parameters, *h* appears to be the most flexible, the corresponding average value, plotted in the dashed line of Figure 3a, converges very rapidly to a value of ~4.9 Å, remarkably close to the experimental data, while several oscillations are observed between the extreme values of 5.3 and 4.5 Å. Such behaviour shows remarkably well how strong the connection between weak interactions and large amplitude motions is.

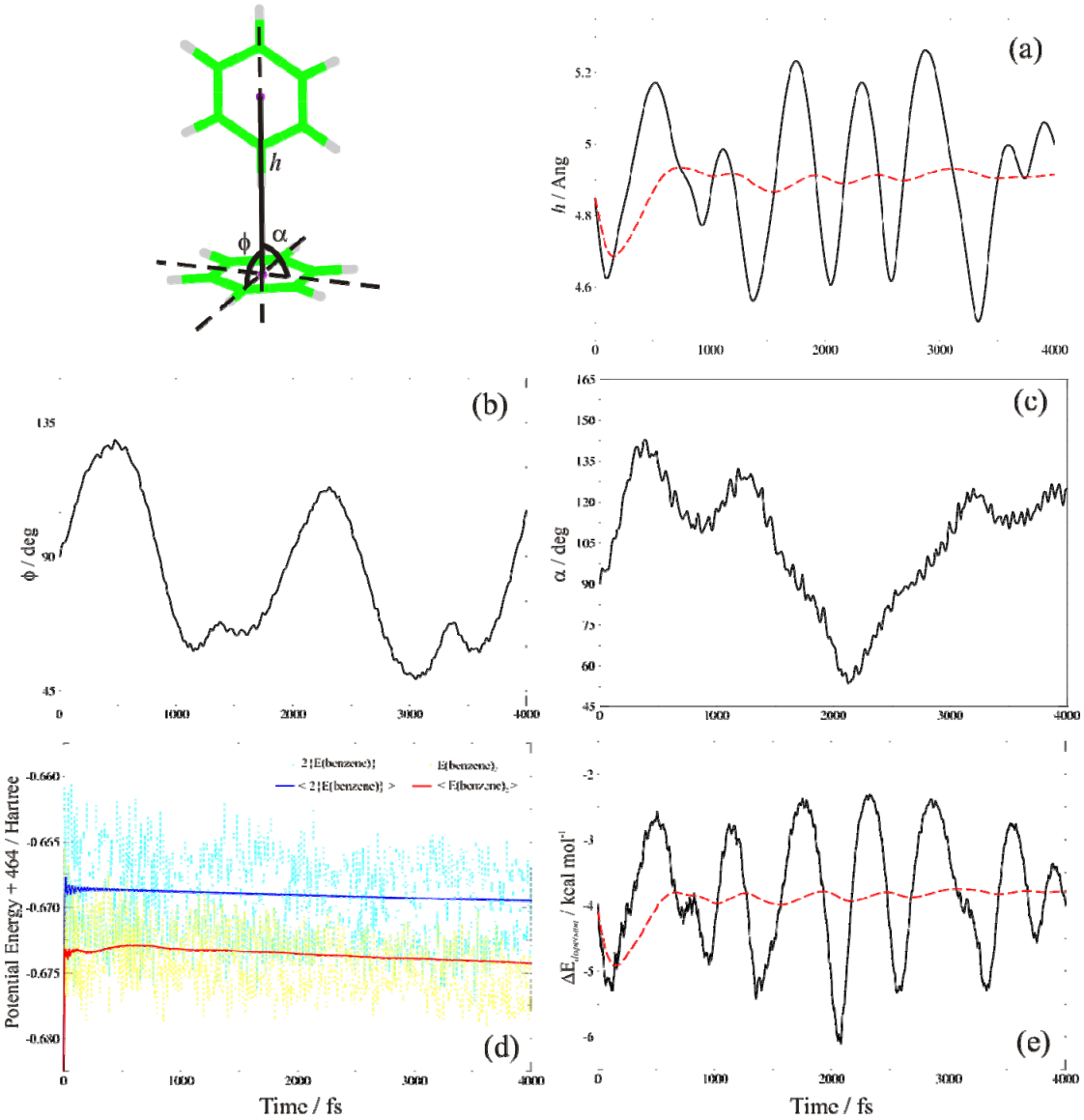

Figure 3. *Structural and energetic analysis from the ADMP trajectories:*
(a) black full line, h value at time t; red dashed line, average of the h values up to time t;
(b) angle ϕ and (c) angle α values along the trajectories;
(d) plot of the potential energy values and their average of the benzene dimer and benzene monomer;
(e) plot of the dispersion interaction between the two benzene molecules along the benzene dimer ADMP simulation, black full line, and corresponding average value at time t, red dashed line.

Regarding the ϕ and α angles, the statistics of the 4 ps trajectory does not allow to dissect average values or general behaviours. Nevertheless, some considerations could be done. The plot of ϕ values demonstrates that the system did never undergo a conversion to the parallel configuration; it rather passed through the orthogonal minimum-energy structure with a slow oscillation, the period being ~2 ps. For what

concerns the α angle, the 90° value corresponds now to the transition-state between the inclined minimum energy isomers; thus the α value oscillated across the minimum energy values (65° ≡ 115°), and in the 4 ps trajectory it went only twice through the transition-state value of 90°. Once again, the reported data highlight the high flexibility of the system. On examination of the average values of the potential energies, depicted by Figure 3d, for both the benzene dimer and monomer dynamics, carried out under the same conditions, we could evaluate an interaction energy of ~ 2.7 kcal/mol, with a standard deviation of 0.8 kcal/mol, which is consistent with the ZPE-corrected and experimental values. Eventually, Figure 3e plots the value of the dispersion interaction between the two benzene molecules along the dimer trajectory: it is apparent that, as expected, the most relevant parameter influencing such a value is the distance between the centres of mass of the benzene molecules.

Conclusions

This chapter reports the main results of a first validation of DFT-D for structural and dynamical characterizations of molecular complexes ruled by dispersion forces. The benzene dimer has been taken as case study since it represents the prototypical system for π-π interactions. Structural and energetic parameters of different minima are in remarkable agreement with sophisticated post-HF results in a fraction of the computer time. First principle molecular dynamics simulations show, however, that static considerations are not sufficient to provide a reliable picture of processes ruled by weak forces due to the presence of large amplitude motions: meaningful comparison with experiment is then possible only upon averaging of physico-chemical properties along dynamical trajectories. The favourable scaling of DFT-D dynamics with the number of active electrons, the concurrent development of effective and reliable localized basis sets, and the implementation of the whole approach in an effective computational tool pave the route toward the investigation of large systems of technological and biological significance.

Chapter 2

Magnetic parameters of nitroxide radicals in aqueous and methanolic solutions

Abstract: this chapter discusses the interplay of different factors in determining the structural and magnetic properties of nitroxide free radicals in aqueous and methanolic solutions. Thanks to their long-lived spin-unpaired electronic ground state and to molecular parameters strongly sensitive to the chemical surroundings, nitroxide radicals have been widely employed as spin labels or spin probes in electron paramagnetic resonance experiments to investigate the local structure and dynamics of complex systems. Our integrated approach provided not only a qualitative understanding of the undergoing physico-chemical processes, but also a remarkable quantitative agreement of computed spectroscopic data with those obtained from experiments. Several interesting aspects are pointed out in order to achieve a correct interpretation of experimental results: (1) the structure of the hydrogen bonding network, related to more or less effective compensation between steric and electrostatic contributions to solute-solvent and solvent-solvent interactions; (2) the sensitiveness of hyperfine and gyromagnetic tensors to different structural parameters, so that accurate equilibrium structures and proper vibrational averaging are mandatory for quantitative results. From a more general point of view, the reliability and advantages of our integrated approach for the study of fast physico-chemical processes of biological and technological interest involving organic free radicals are well evidenced. Connected to this chapter, Appendix A reports the theoretical background for the prediction of electron paramagnetic resonance parameters.

Introduction

Nitroxide free radicals are characterized by a long-lived spin-unpaired electronic ground state[79] and by molecular properties strongly sensitive to the chemical surroundings.[6] Thanks to ongoing developments in electron paramagnetic resonance (EPR) and electron-nuclear double-resonance (ENDOR) spectroscopies, these electronic features have led to widespread application of nitroxide derivatives as spin labels, spin probes, redox probes, and contrast agents. [80-83] More recently, high field EPR has allowed to use nitroxides as probes of local polarity in investigations of micelles and membrane proteins: once again, values of magnetic tensors have been used to infer structural aspects.[84, 85]. EPR and ENDOR are still the most accurate methods to experimentally determine the nuclear hyperfine tensors ($\boldsymbol{A}_X$), which account for the interaction between the unpaired electron and the different nuclei (X), and the gyromagnetic tensor ($\boldsymbol{g}$), which measures the interaction of the external magnetic field with the electron spin. The isotropic parts of $\boldsymbol{A}_X$ (usually referred to as hyperfine coupling constants, a_X) are local parameters that depend on the spin-density on each atom and are mainly affected by the molecular structure; by contrast, the dipolar parts of $\boldsymbol{A}_X$ tensors (hereafter, $\boldsymbol{T}_X$) and, especially, the $\boldsymbol{g}$ tensor are sensitive to the spin density distribution over the whole molecule, and convey significant information about the nature of the molecules interacting with the radical active species. Unfortunately, the interpretation of spectroscopic data may suffer from ambiguities, especially when different kinds of environmental effects operate together to tune the intrinsic values of magnetic tensors. In particular, it has been shown that the nitrogen hyperfine coupling constant (hereafter, a_N) increases and the isotropic g-value (hereafter, g_{iso}) decreases going from low to high polarity environments.[86] The isotropic values are obtained from EPR at room temperature and represent rotational averages of the different tensors. Use of frozen solutions has allowed to resolve anisotropic tensor components showing that the terms most sensitive to the polarity of the local environment and to interactions with surrounding molecules are $\boldsymbol{g}_{xx}$ (directed along the NO bond) and $\boldsymbol{A}_{N,zz}$ (perpendicular to the plane of the R_2NO moiety). Together with bulk effects, specific hydrogen bonding between the nitroxide oxygen and protic solvents leads to remarkable shifts of g_{iso}, a_N, $\boldsymbol{g}_{xx}$, and $\boldsymbol{A}_{N,zz}$ when the radicals are dissolved in aqueous or alcoholic solutions.[87] All the above trends have been rationalized in terms of the selective stabilization by high

dielectric constant solvents of a charge-separated resonance form with the unpaired electron on the nitrogen atom,[6] as depicted below.

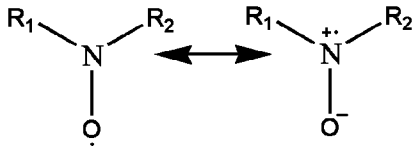

Scheme 1

Nevertheless, within the framework of simple mean field theories, no linear relationship or predictive formula has been found capable of correlating the experimental data in a variety of different solvents.[86] In favourable cases, a satisfactory interpretation of experimental results can be achieved based on refined, yet well established, QM calculations of solvent-nitroxide clusters. However, a deeper analysis calls for an explicit description of the dynamic behaviour in solution.[82, 88] While in aprotic media the dielectric contribution is the feature that mostly affects the molecular properties, additional problems arise for protic solvents: not only the internal dynamics of the nitroxide radical needs to be accounted for, but also the strength and geometrical features of the solute-solvent H-bonding network, as well as their fluctuations, must be described in an effective and balanced fashion, since all these factors significantly impact on the structure and/or on the spectroscopic parameters of the solute. Moreover, conceptual as well as practical difficulties are emphasized when nitroxide radicals are located at the interface between physically or chemically inhomogeneous systems.[89]

The accurate computation of magnetic tensors remains a desirable goal in a much more general sense than for the unusual or problematic situations hinted above. As a matter of fact, the experimental determination of $\boldsymbol{g}$ and $\boldsymbol{A}$ tensor components usually involves fitting of the experimental EPR and/or ENDOR spectra by simulated datasets: an initial guess for all the unique spin Hamiltonian tensor components, as well as for the diffusion tensor, must be provided in order to start the simulation. When the number of magnetic nuclei is large, or when the magnetic tensors differ significantly from the available reference values, it may be difficult to guess the components in advance, and as a result the fitting procedure can well converge to a spurious minimum. Thus, a viable alternative is to resort to computed $\boldsymbol{A}$, $\boldsymbol{g}$ (and possibly diffusion) tensors, averaged over

fast internal and solvent librational motions. In favourable cases, the simulated spectra issuing from the computed parameter values are in quantitative agreement with experiment, without any need for fitting.[90] More generally, some parameters will still need to be optimized by fitting to the experimental dataset, but the starting guesses will be close enough to the optimal values to ensure convergence to the true minimum. Together with slow- and fast-motion limit cases, use of the stochastic Liouville equation approach (SLE) pioneered by Freed and co-workers [91-93] allows to correctly account for the whole range of possible motional regimes. The EPR line shape of a nitroxide radical in dilute solutions is dominated by the rotational averaging of the $\boldsymbol{g}$ and $\boldsymbol{A}_N$ tensors. Moreover, the effects on the line shape due to the anisotropic magnetic couplings of the protons may be important, and they can be clearly detected when the proton hyperfine components are well resolved. Although QM computations provide, of course, the whole set of hyperfine tensors, proton contributions will be not discussed in detail in the following, since they usually show negligible solvent shifts and are not necessarily central to the interpretation of experimental results.

Overall, it seems clear that a synergic use of experimental data and refined theoretical approaches will allow to gain further insights about the tuning of the magnetic parameters by intrinsic, environmental, and dynamic effects. This issue has been recently highlighted by Majda and co-workers,[89] who investigated aqueous vapour/liquid interface exploiting the redox properties of a nitroxide probe and obtained a satisfactory interpretation of experimental results by means of quantum chemical calculations of water-nitroxide interactions. However, the authors pointed out that a deeper analysis would have required reliable theoretical descriptions of the dynamics of nitroxide probe molecules in solution, which were still lacking. Recently nitroxide radicals in aqueous solution have been investigated by classical MD [94] as well as by Monte-Carlo simulations [95], but both studies employed empirical force fields from MM, whose reliability is questionable, especially concerning the angular distribution around the nitroxide moiety.[88] Moreover, the QM methods used for the computation of hyperfine coupling constants and the representations of water molecules directly bound to the nitroxide oxygen only in term of point charges cast further doubts about the reliability of the results. In order to overcome the limitations of available empirical force field parameterizations, we exploited Car-Parrinello (CP)[14] MD simulations of

real-size nitroxide radicals in the gas phase, in aqueous and in methanolic solutions: namely, the di-methyl nitroxide (DMNO), di-*tert*-butyl-nitroxide (DTBN), and 2,2,5,5-tetramethyl-1-pyrrolidinyloxy (PROXYL) radicals have been investigated. Magnetic parameters were computed on frames extracted at regular time intervals from the CPMD trajectories: compared to other *on-the-fly* approaches,[96] the proposed *a posteriori* calculations of spectroscopic properties allow to exploit different electronic structure methods for the molecular dynamic simulations and for the more demanding computation of first- (a_X) and second- order ($\boldsymbol{g}$) molecular parameters.[2] The quite small spin polarization contribution to the isotropic hyperfine couplings of non-hydrogen atoms results from the nearly exact compensation between core and valence contributions. Since the plane-wave implementation of CPMD replaces core electrons by pseudopotentials, computation of this term requires *ad hoc* procedures,[97] whose general validity has not been extensively proven yet. On the other hand, purposely tailored basis sets allow reliable computations when using localized gaussian-type orbitals.[6]

Each frame extracted from the trajectory can be regarded as a static cluster, in which the nitroxide molecule is embedded in a large number of solvent molecules. In order to compute spectroscopic parameters on such clusters, it is quite sensible to adopt a hierarchization of theory levels for the description of the spin probe itself, of the solvent molecules directly involved into hydrogen bonds with the nitroxyl group, and of the further portions of the solvent. As a matter of fact, several different approaches have been proposed to account for the solvent in these situations, a description of solvent molecules in terms of partial atomic charges being one of the most popular.[30, 98, 99] However, the charges adopted come usually from MM parameterizations, and they may vary among different force fields. By considering the simplest realistic model for the family of nitroxide radicals, the DMNO, in aqueous solution we tested the consistency of the proposed discrete-continuum approach (QM/PCM) based on the PCM implicit solvation model,[8, 37] in comparison with full QM calculations as well as to a QM/MM description. Solvent effects on magnetic tensors can indeed be described by means of discrete-continuum calculations, provided that some of the closest solvent molecules are explicitly included in the QM layer: in particular, taking into account at the QM level the two water molecules closest to the nitroxide oxygen is necessary and sufficient to

account for the short-range solvent-solute interactions; the rest of the solution affects the solute by an essentially electrostatic effect, and thus both the PCM and the MM computations, once averaged over the sampled frames, lead to equivalent results. Thus, the choice between PCM and MM approaches is to some extent a matter of taste, and has a marginal influence on the final computed results: for consistency with our previous works, we have then used the PCM to take into account bulk solvent effects. Thus, the proposed CPMD/QM/PCM integrated approach has been validated for predicting the magnetic properties of the DTBN molecule in aqueous solution, which a relevant number of experimental data were available for. Eventually, once validated, the same approach has been exploited to a thorough computational analysis of a five-membered cyclic nitroxide, the PROXYL, in different solutions. The free PROXYL molecule has been widely employed as a spin probe;[100] moreover, covalently attached PROXYL-derived moieties are commonly exploited for the site-specific spin labeling of complex macro-molecules. In view of the computational challenge they represent, and also on account of experimental information that seems to point to a different behavior in the two solvent systems, we focused on the comparison of water and methanol. Interestingly, despite the similarity of the two solvents, remarkably different behaviours also emerged in aqueous and in methanolic solutions.

Methods and computational details

The Car-Parrinello approach was used to generate MD trajectories for the gas-phase, the aqueous and the methanolic solutions. Within the framework of DFT, the CP[14] scheme provides a unified and affordable method for classical MD simulations and first-principle electronic structure calculations. Details about the theory and its implementation in high performance computing facilities are well reviewed in the recent literature. [32] Here, MD simulations were carried out with a parallel version of the official CPMD code.[101] The gradient-corrected density-functional of Perdew, Burke and Ernzerhof (PBE)[102] was adopted, the electronic variables being expanded in a plane-wave basis-set up to a 25 Ry cut-off energy. Core states were projected out by pseudo-potentials built according to Vanderbilt's "ultra-soft" scheme.[103] The time step for integrating the equations of motion was 0.242 fs and fictitious mass parametr was set to 1000 a.u. in both the cases of DMNO and DTBN simulations. A time step of 0.15 fs and a fictitious electronic mass of 700 a.u. have been exploited in the case of PROXYL dynamics for a better accuracy. In all the trajectories, hydrogen atoms were assigned the mass of deuterium. These choices have proved effective for structural investigations within the CP scheme.[104] Periodic boundary conditions were enforced to all the simulations. The initial configuration of DMNO in aqueous solution was obtained by replacing a water molecule by a DMNO molecule from a previously equilibrated liquid water trajectory for a constant volume super-cell including 64 water molecules at a density of 1.00 g/cm^3.[105] The simulation in vacuum was performed starting from the optimised structure of DMNO. Similarly, for DTBN in aqueous solution, the initial configuration was obtained by replacing six water molecules by a DTBN molecule from the same previously equilibrated liquid water trajectory. The gas phase simulation was performed starting from the optimised structure of DTBN. The DTBN and DMNO systems have been equilibrated for 1.5 ps at 300K, applying a Nosé thermostat,[106] which ensures a canonical ensemble (NVT). After equilibration, the systems have been observed for a total time of 4.0 ps for further analysis. In the case of PROXYL, we used a rhombic dodecahedral cell that contained the solute molecule together with 31 waters, or 23 methanol molecules. Trajectories were collected in the NVT ensemble (330 K) for a total time of 11.0 and 17.5 ps for methanol and aqueous solutions, respectively. Starting configurations were extracted from previously

equilibrated classical MD trajectories. For statistical analysis, snapshots were collected at regular time intervals from the last 5 ps (methanol solution) or 7.5 ps (aqueous solution) of the trajectories.

Calculations of minimum-energy structural parameters were carried out by the Gaussian03 package.[70] The nitroxide geometries were fully optimized using the PBE exchange and correlation functional both in its pure semi-local formalism and within the more reliable hybrid Hartree-Fock–DFT scheme, known as PBE0.[35] Moreover, we performed several tests up to convergence of geometrical parameters exploiting both valence-double-ζ and valence-triple-ζ sets, augmented by diffuse and polarization functions, from the Pople[107] and Dunning[108] series. The 6-311++G(3df,2pd) basis set was found to achieve a good convergence while remaining relatively cheap. Employing such basis set together with the PBE0 functional, we calculated the minimum-energy structures of the nitroxide radicals, and their adducts involving a single and a double H-bond with solvent molecules. At the same level of theory we computed, for comparison, the water molecule and its dimer, and the methanol and its dimer as well. All these geometry optimizations were carried out with and without the PCM description of solution bulk. Single-point energy calculations and magnetic properties were also evaluated for comparison to the MD averaged results.

All the calculations of magnetic properties were carried out by the Gaussian03 package too. The details about the theoretical approaches for the calculation of EPR molecular parameters are discussed in the Appendix A. For the calculation of Nitrogen hyperfine coupling constants, we performed DFT computations at the PBE0 level of theory coupled to the purposely tailored EPR-II basis sets.[109] Quadratic Configuration Interaction Single and Double (QCISD) calculations were also performed with the basis set purposely tailored by Chipman for evaluation of EPR parameters.[110] Thus, we combined the DFT description of the nitroxide system with a more accurate and correlation-consistent method for computing the a_N: from the total system a model region is extracted, where the QCISD calculation was carried out and the resulting data were combined as follows:

$$a_N = a_N^{DFT}(\text{total system}) + a_N^{QCISD}(\text{model system}) - a_N^{DFT}(\text{model system})$$

Such an approach has been proven to be particularly efficient. As for hyperfine coupling constants, calculations of *g*-tensor were carried out at the PBE0 level of theory employing the EPR-II basis set; this approach has been proven to be very effective for DFT-based calculations of magnetic properties [41] within the gauge-including atomic orbital scheme (GIAO).[111] Bulk solvent effects have been taken into account by the PCM, using the UAHF parameterization of atomic-group sphere radii.[37] When water molecules are represented by point charges, we have used the vaules adopted be the TIP3P model (-0.834 on oxygen and +0.417 on hydrogen atoms). [112]

Results and discussion

Figure 1 shows the structure and labelling of the investigated nitroxide radicals.

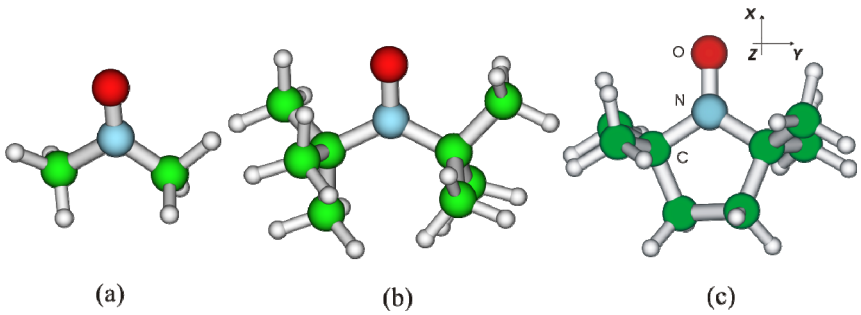

Figure 1. *Nitroxide radicals: (a) DMNO, (b) DTBN and (c) PROXYL plus the reference axes used in the calculation of magnetic tensors*

I. ***DiMethyl-NitrOxide (DMNO)***

Table I lists The average structures of DMNO in the gas phase and in aqueous solution. Solvent effects increase the NO bond length by about 0.02 Å due to a preferential stabilization of the resonance structure involving charge separation. The other geometrical parameters are only negligibly affected by solvent. We carried out an analysis of the hydrogen bonding network of water molecules around DMNO by mean of a standard geometrical definition.[113] A water molecule is considered to be engaged with the nitroxide Oxygen to form an H-bond when these conditions are satisfied:

$$dist(O_{DMNO} - - - O_{WATER}) \leq 3.5\text{Å}$$
$$dist(O_{DMNO} - - - H_{WATER}) \leq 2.6\text{Å}$$
$$angle(O_{DMNO} - - - O_{WATER} - H_{WATER}) \leq 30°$$

Table II lists the average geometrical parameters thus obtained.

Table I. *Average structural parameters from Car-Parrinello Molecular Dynamics. Distances in Å, valence and dihedral angles in degrees. Standard deviations are given in parentheses.*

	Gas phase	**Aqueous solution**
N=O	1.30 (0.03)	1.32 (0.02)
N—C	1.47(0.05)	1.47 (0.04)
C—H	1.11 (0.04)	1.11 (0.03)
C—N=O	118.8 (2.9)	118.4 (4.3)
C—N—C	119.8(3.7)	120.0 (4.9)
N—C—H	109.6 (4.5)	109.1 (5.9)
H—C—H	109.1 (5.1)	109.6 (7.1)
Φ = C—N=O…C	180(17)	180(19)
$< \Phi^2 >^{1/2}$	165.0	163.6

Table II. *H-Bonding average geometrical parameters: distances in Å and angle in degrees.*

Average number of H-bonds	**1.91**
Distance (O … O_{water})	2.87 (0.23)
Distance (O … H_{water})	1.93 (0.24)
Angle (H—O_{water} …O)	17.2

The average (O—O_{water}) and (O—H_{water}) distances are in close agreement with the first peak of the corresponding radial distribution function, reported in Figure 2. The number of H-bonded molecules has an average value of 1.9, so that, as expected, just the two water molecules closest to the nitroxide Oxygen need to be considered in order to have a description of the strong H-bond interaction within a DMNO aqueous solution.

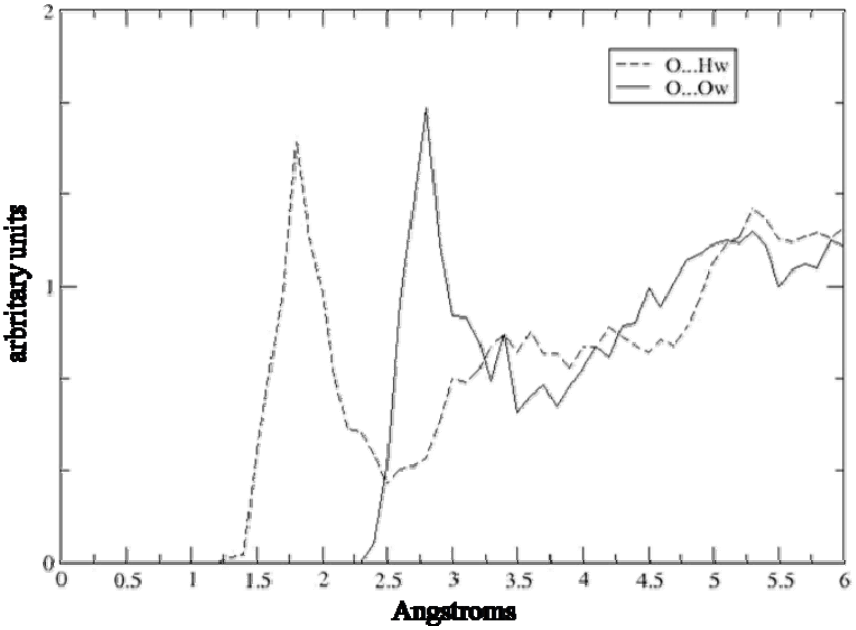

Figure 2. *Radial Distribution Functions for hydrogen (Hw) and oxygen (Ow) atoms of water molecules around the nitroxide oxygen.*

Regarding the hyperfine coupling constants, we have first checked the convergence of nitrogen a_N with the number of frames extracted from the dynamics. As shown in Figure 3(a), the average a_N computed extracting one hundred frames has, with a good approximation, the converged value for both the gas-phase and water-solution simulations.

(a)

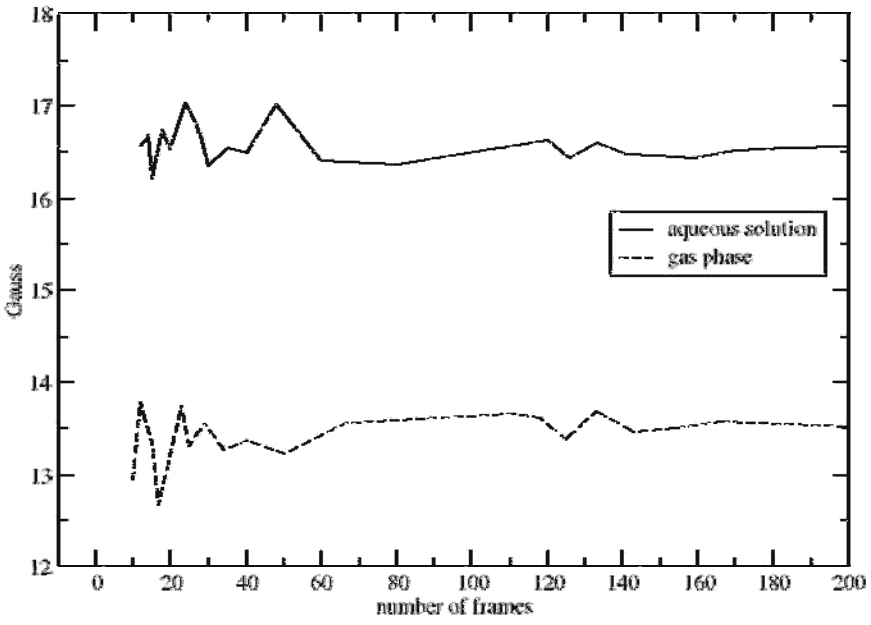

(b)

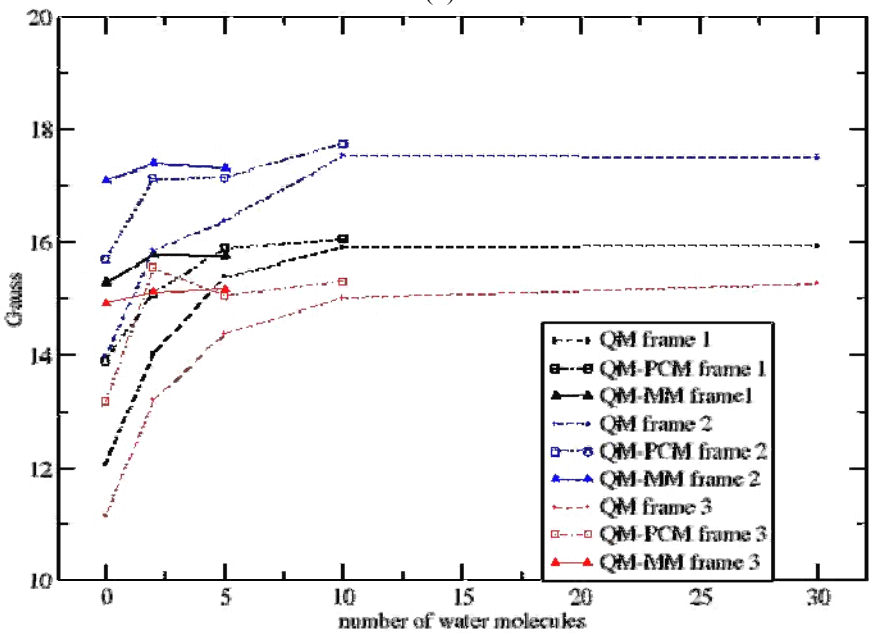

Figure 3. *convergence of the Nitrogen a_N (a) with the number of frames and (b) with the number of explicit water molecules retained in each frame.*

The second step was the definition of the minimum number of explicit water molecules to be included both in the QM/PCM and QM/MM calculations to have values consistent with those computed by full QM computations on clusters formed by DMNO and a large number of water molecules. Figure 3b shows the computed hcc of nitrogen atom computed on 3 different frames extracted from the CP dynamics. It is quite apparent that a cluster with 30 water molecules surrounding DMNO gives a converged value, which is well reproduced by a much smaller cluster including two to five water molecules treated at the QM level and PCM or MM point charges to describe bulk effects. A more complete analysis can be performed in terms of the average value over 100 frames extracted by the dynamics, as reported in Table III. The solvent shift obtained with all the water molecules modelled as point charges is quite larger than that obtained just with the PCM; however the result obtained with 5 explicit water molecules and the PCM is in perfect agreement with those obtained using 2 or 5 QM and 30 MM water molecules. The physical meaning of these results is that the strongest contribution to the solvent shift is due to a pure electrostatic stabilization of the resonance structure with the spin density on the nitrogen atom, but the classical electrostatic effect must be corrected by a full QM treatment of the H-bonded water molecules.

Table III. *Average nitrogen a_N (in Gauss) computed at the PBE0/6-31+G(d) level of theory on frames extracted by the CP simulations. Standard deviations are given in parentheses.*

Gas phase		
a_N	13.3 (2.2)	
Aqueous solution		$\Delta_{solvent}$
NO WATER	13.5 (2.1)	0.2
2 QM	15.3 (2.4)	2.0
2 MM	15.1 (2.3)	1.8
PCM	15.4 (2.2)	2.1
2 QM + PCM	16.7 (2.3)	3.4
5 QM + PCM	16.7 (2.5)	3.4
60 MM	16.5 (2.6)	3.2
2 QM + 58 MM	16.9 (2.6)	3.6
5 QM + 55 MM	16.9 (2.6)	3.6

From another point of view, the relevance of DMNO geometry for obtaining meaningful a_N can be appreciated from Figure 4, which shows the energy and a_N variation as a function of the out of plane displacement of the nitrogen atom (measured by the CNO…C improper dihedral angle).

In this context, it is remarkable that geometry optimisation leads to values of this angle smaller than its dynamical average (152.8 vs.165° at the PBE/6-31+G(d) level in vacuum), which leads, in turn, to an overestimation of average a_N (15.45 vs. 13.3 G). Replacement of the PBE functional by its more reliable hybrid PBE0 counterpart, does not modify this conclusion, but leads to a lower a_N (14.99) due to both an intrinsic difference and to a shorter NO distance. Of course, vibrational averaging by the out of plane nitrogen motion can be taken into account by a proper effective one-dimensional treatment, but, in the present context we prefer to use the average values provided by MD simulations.

Table IV: *Nitrogen hcc computed at the PBE0/6-31+G(d) on DMNO structures optimized at the PBE/6-31+G(d) and PBE0/6-31+G(d) levels of theory.*

	N=O bond (Å)	**C—N=O…C dihedrals (°)**	**a_N (Gauss)**
PBE	1.290	152.77	15.45
PBE0	1.274	153.57	14.99

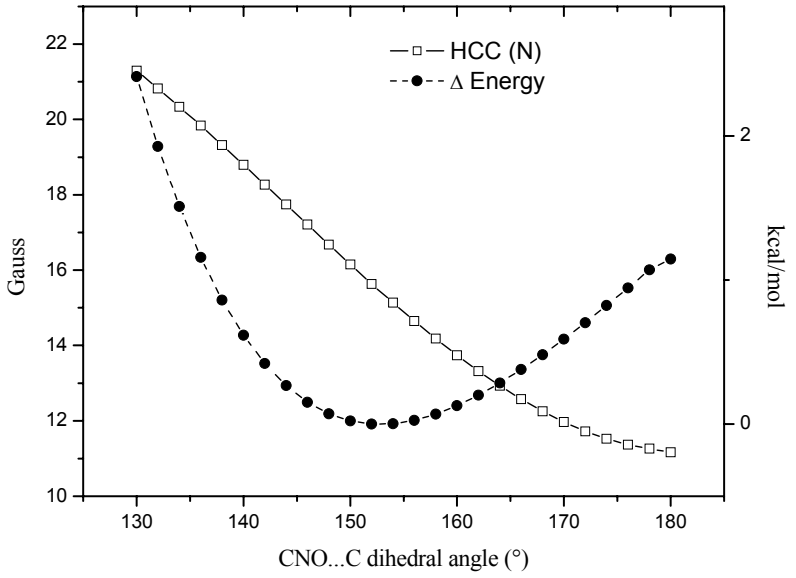

Figure 4*. dependence of the total energy (circles) and nitrogen a_N (diamonds) on the improper dihedral angle CNO…C.*

In particular, it is of interest to compare the results issuing from the present MD simulations in aqueous solution to those obtained from geometry optimisations of suitable clusters. Several previous studies have shown that a clusters formed by the nitroxide radical and two water molecules bound to the oxygen lone pairs provides, when immersed in a dielectric continuum with the dielectric bulk constant of water, remarkably accurate solvent shifts of nitrogen a_N. The results of Table V show that the results delivered by this this model are also in good agreement with MD averages provided that the CNO…C improper dihedral is fixed at its average value (3.4 and 3.2 G from MD and optimisation, respectively at the PBE/6-31+G(d) level). This paves the route for the evaluation of improved absolute values performing single point computations at suitable optimised geometries. For instance the results collected in Table V show that use of PBE0 geometries, whose shorter NO bond distance is in closer

agreement with the available experimental data [6] slightly lowers both the absolute value and the solvent shift of nitrogen a_N. A deeper analysis of this aspect will be discussed dealing with larger nitroxides, DTBN and PROXYL for which experimental data in different solvents are available.

Table V:*Nitrogen a_N computed at the PBE0/6-31+G(d) level on the structures of DMNO-$(H_2O)_2$ cluster optimised at the PBE/6-31+G(d) and PBE0/6-31+G(d) levels of theory including bulk solvent effects by the PCM.*

.	**PBE**	**PBE0**
N=O bond (Å)	1.302	1.281
abs(CNO...C) dihedral angle (°)	158.6	158.7
a_N DMNO (Gauss)	13.9	13.7
a_N DMNO + 2 H_2O QM + PCM (Gauss)	17.1	16.6
a_N DMNO + 2 H_2O MM + PCM (Gauss)	16.7	16.2

II. *Di-Tert-Butyl-Nitroxide (DTBN)*

Structure, labelling and orientation of the DTBN are shown in Figure 1(b). Average geometrical parameters of the DTBN molecule from the Car-Parrinello MD simulations in gas-phase and in aqueous solution are listed in Table VI.

Table VI. *Average geometrical parameters of DTBN from CPMD simulations: bond distances in Å, angles and dihedrals in degrees, standard deviations in parenthesis.*

	Gas phase	**Aqueous solution**
NO	1.30 (0.02)	1.31 (0.02)
NC_α	1.53 (0.04)	1.54 (0.06)
$C_\alpha C_\beta$	1.55 (0.04)	1.55 (0.04)
$C_\alpha NC_\alpha$	128 (3)	127 (4)
ONC_α	114 (4)	115 (4)
abs($C_\alpha NOC_\alpha$)	166 (8)	170 (8)

Only very small variations of the average structure occurred when going from gas-phase to aqueous solution involving essentially lengthening of the NO bond and increasing of the CNOC improper dihedral. A picture of the gas-phase and aqueous-solution DTBN dynamics is provided by the distribution functions along the trajectories of the N–O bond length (Figure 5a) and CNOC improper dihedral (Figure 5b). Concerning the NO bond, both plots present a similar trend, although the peak is sharper in gas-phase than in solution, in close agreement with the above mentioned lengthening of the average value. On the other hand, the distribution of the CNOC improper dihedral angle (related to the out-of-plane motion of the nitroxide backbone) in the gas phase shows two equivalent peaks symmetric with respect to a planar configuration, whereas in aqueous solution there is only one well defined maximum corresponding to a planar arrangement of the CNOC moiety. In agreement with former theoretical predictions about DTBN in the gas phase,[114, 115] the two symmetric maxima of the gas-phase CNOC dihedral distribution are indicative of two equivalent non-planar minima and of a smooth potential energy surface governing the out-of-plane motion of the NO moiety. Therefore, the non negligible probability of finding the DTBN molecule close to a

planar configuration in the gas phase should be taken into account. Such an issue is even more crucial in the case of the aqueous solution dynamics. The water medium enhances the flexibility of the CNOC dihedral angle and the large peak centred at zero degrees is the result of the ease with which the NO moiety undergoes inversion.

(a)

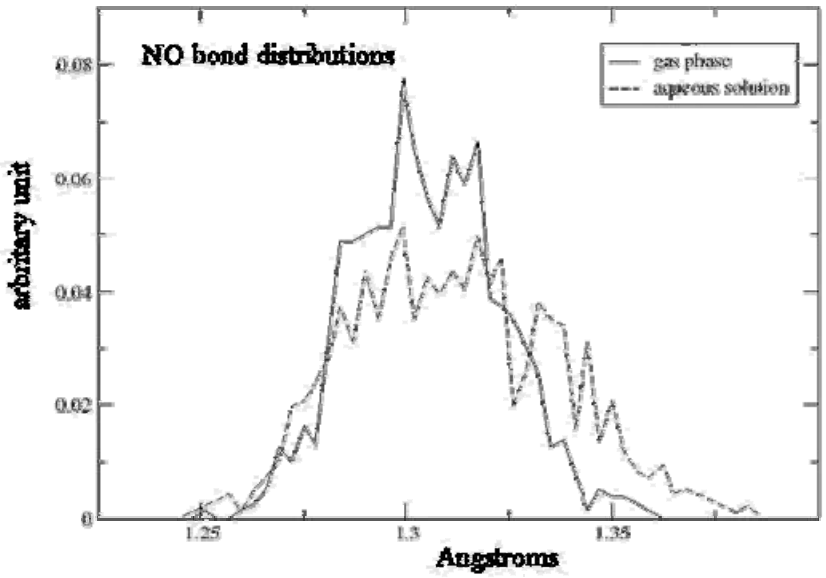

(b)

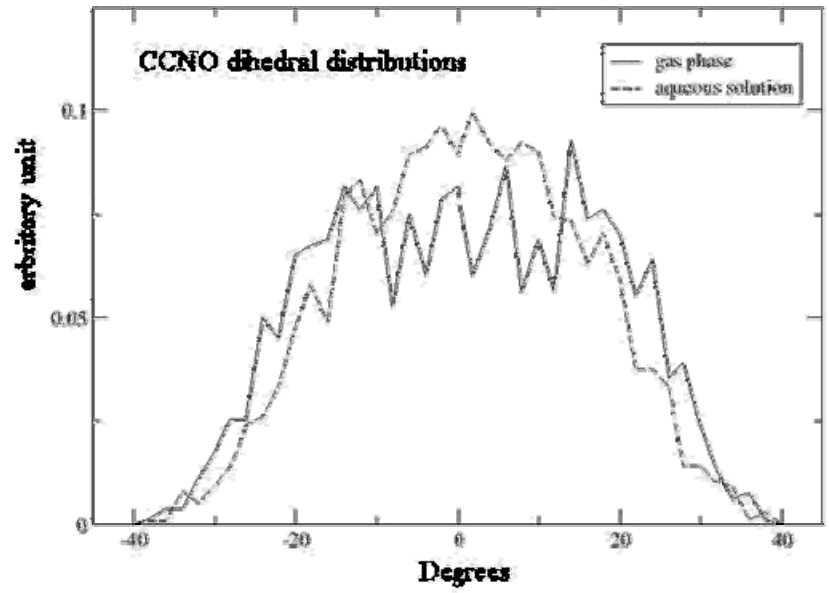

***Figure 5**. Distributions of NO bond length (a) and CNOC dihedral angle from CPMD (b).*

The structure of the solvation shell of the DTBN molecule in aqueous solution was analysed in terms of the aforementioned simple standard criteria for hydrogen bonds.

Table VII lists the results of this analysis. The average number of DTBN-water H-bonds is 1.2, and the average H-bonding structural parameters are in close agreement with the maximum peaks of the Radial Distribution Functions (RDF) shown in Figure 6.

Table VII. *Main characteristics of DTBN-H_2O hydrogen bonds from CPMD simulations: bond lengths in Å, angles in degrees, standard deviations in parenthesis.*

Average number of H-bonds	1.2 (0.5)
% 0 H-bond	7 %
% 1 H-bond	63 %
% 2 H-bond	30 %
O_{DTBN} … O_{water}	2.9 (0.2)
O_{DTBN} … H_{water}	1.9 (0.3)
O_{DTBN} … O_{water}—H_{water}	15 (7)

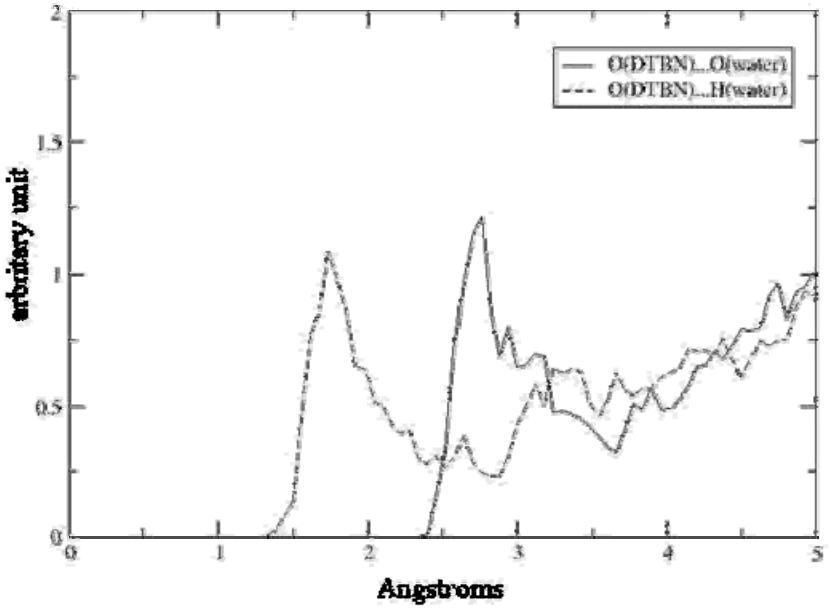

Figure 6*. Radial Distribution Functions O_{DTBN}—O_{water} (full line) O_{DTBN}—H_{water} (dashed line).*

The average number of H-bonds is significantly below the value of two suggested by experimental results for some spin probes and actually found in the simple DMNO

model. As a matter of fact, the presence of two bulky *tert*-butyl groups embedding the nitroxide moiety plays a key role in determining the space available to the solvent molecules for accessing the DTBN oxygen atom. This is well evidenced by the average CNC angle, which is around 115° in DMNO (as well as in the most widely used spin probes) and around 128° in DTBN: thus, in the latter case the methyl groups are pushed up crowding the space around the oxygen atom. Nevertheless, also in DTBN aqueous solution there is a significant number of structures (30%) characterized by two genuine solute-solvent hydrogen bonds, thus indicating that a proper dynamical average is needed to compute reliable spectroscopic parameters in solution.

Because of the lack of any experimental structure of the DTBN molecule, we must trust first-principle geometry optimizations. In this case we employed the PBE0 functional which provides very good geometrical results also for a wide range of organic free-radical species.[6] In order to minimize the differences between plane waves and Gaussian Type Orbital (GTO) approaches, we tested a number of basis sets with respect to the most important geometrical parameters of the DTBN radical. Table VIII lists the results obtained with different and very large basis sets, and shows that the 6-311++G(3df,2pd) basis set represents a very good compromise between reliability and computational burden.

As a consequence, all the geometry optimizations have been carried out with this basis set. In order to quantify the effect of the exchange contribution on the geometry we carried out a geometry optimization of the DTBN isolated molecule at the PBE and PBE0 levels of theory, obtaining the results listed in Table IX. As a matter of fact, the conventional GGA functional (PBE) overestimates the NO bond length: this behaviour is quite general for GGA models and can be partially corrected by the inclusion of an amount of non local Hartree-Fock (HF) exchange.[13]

Table VIII. *Test of basis set convergence, for geometry optimization, at the PBE0 level of theory: bond lengths in Å, valence and dihedral angles in degrees (°).*

Basis functions		**DTBN geometrical parameters**		
		N–O	**C–N–C**	**C–N–O…C**
6-31G(d)	186	1.276	127.6	160.9
6-31+G(d,p)	280	1.277	127.5	161.4
6-311G(d)	234	1.270	127.3	161.0
6-311+G(d,p)	328	1.272	127.3	161.6
6-311++G(2d,2p)	450	1.271	127.3	161.7
6-311++G(3df,2pd)	660	1.268	127.3	161.8
cc-pVDZ	230	1.271	127.5	161.0
cc-pVTZ	552	1.270	127.4	162.0
aug-cc-pVTZ	874	1.269	127.3	162.1
cc-pVQZ	1090	1.268	127.3	162.0

Table IX. *Geometric (bond lengths in Å and angles in degrees) and magnetic (a_N in gauss and Δg_{iso} in ppm) properties of DTBN computed at the PBE and PBE0 levels.*

	PBE	**PBE0**
Geometry [a]		
N–O	1.284	1.268
C–N–C	127.0	127.3
C–N–O…C	160.8	161.8
a_N [b]	13.04	12.28
Δg_{iso} [b]	3823	3736

(a) 6-311++G(3df,2pd) basis set; (b) single point PBE0/EPR-II property evaluation

The CNC valence angle and the out of plane distortion of the NO moiety are much less sensitive to the form of the density functional. Dynamical effects on the geometry of DTBN are evidenced by comparison between the average structure along the gas-phase CPMD trajectory and the PBE energy minimum. Since the employed GTO basis set is

at convergence with respect to the geometrical parameters, we think it is reasonable to compare these two data sets. As a matter of fact, the minimum and the average dynamical structures are in pretty good agreement, and the very small differences (within the standard deviations) are in the range of reasonable vibrational contributions.

Furthermore, we performed a calculation of the geometrical structure of the DTBN–$(H_2O)_n$ (n=0,1,2) with and without the PCM for modelling the solvent bulk. Table X lists the results on structural and magnetic properties. Interestingly, there is a very small shift of geometrical parameters going from gas-phase to solution minima: the trend of the NO bond displacements going from DTBN to DTBN–(H_2O) and to DTBN–$(H_2O)_2$ is the same in the gas-phase and in PCM embedded structures. Eventually, in order to have a flavour of the energies involved in nitroxide-water interaction we carried out single point calculations on the structures optimized in the gas phase for the above mentioned adducts and for the water dimer again at the PBE0/6-311+G(3df,2pd) level (see Table XI).

In the gas phase both the first and second nitroxide-water H-bonds provide an energetic balance (-5.7 and -6.6 kcal/mol, respectively) more favourable than that of solvent-solvent interaction (-4.5 kcal/mol for the H_2O dimer). The situation changes taking the solvent bulk into account, since now the energy corresponding to the water dimer, -2.1 kcal/mol, is larger than those of both DTBN-water clusters, -1.4 and -0.5 kcal/mol, respectively. Furthermore, the contribution of the second H-bond is now energetically unfavourable (0.9 kcal/mol), and the whole trend is also confirmed taking into account the solvent in the geometry optimisations. Remarkably, all these results are consistent with the H-bonding analysis of the aqueous solution trajectories where for the most part of the time there is just one DTBN-water H-bond.

Table X. *Structural and magnetic parameters computed for DTBN and its water adducts in vacuum and with a PCM representation of solvent bulk: bond lengths in Å, valence and dihedral angles in degrees, energies in kcal/mol, a_N in Gauss and Δg_{iso} in ppm.*

	in vacuum geometry optimisation.			**geometry optimisation with PCM**		
	DTBN	**DTBN(H_2O)**	**DTBN(H_2O)$_2$**	**DTBN**	**DTBN(H_2O)**	**DTBN(H_2O)$_2$**
Geometry [a]						
N–O	1.268	1.269	1.271	1.270	1.271	1.273
C–N–C	127.3	127.4	127.8	127.1	127.3	128.0
C–N–O…C	161.8	163.1	164.5	163.3	163.6	165.2
O…O_{water}	-	2.821	2.889	-	2.806	2.867
O…H_{water}	-	1.856	1.947	-	1.835	1.922
O…O-H_{water}	-	7.9	10.5	-	0.5	10.4
a_N [b]						
No PCM	12.28	12.74	13.51	-	-	-
PCM	13.06	13.31	14.06	12.77	13.22	13.91
Δg_{iso} [b]						
No PCM	3736	3502	3304	-	-	-
PCM	3591	3397	3222	3574	3396	3211

(a) PBE0/6-311++G(3df,2pd) level of theory; (b) PBE0/EPR-II level of theory, PCM radii=UAHF

Table XI. *Relative interaction energies (kcal/mol) of DTBN-H_2O, DTBN-$(H_2O)_2$ and H_2O-H_2O; single points at the PBE0/6-311++G(3df,2pd) level of theory on optimised geometries.*

Structure / Single Point	**Gas phase / Gas phase**	**Gas phase / PCM**	**PCM / PCM**
H_2O-H_2O	- 4.5	- 2.1	- 2.5
DTBN-H_2O	- 5.7	- 1.4	- 1.2
DTBN-$(H_2O)_2$ [a]	- 12.3 (- 6.6)	- 0.5 (0.9)	- 0.9 (0.3)

(a) the energetic contribution of the second DTBN-H_2O H-bond is given in parenthesis.

In order to achieve a consistent level of theory for the prediction of hyperfine coupling constants we performed a series of calculations with several basis sets: Table XII lists the computed a_N on a single DTBN structure extracted from the gas-phase CPMD simulation.

Table XII. *Test of basis set convergence, for hyperfine coupling constant calculations, at the PBE0 level of theory. A_N values in Gauss. Values computed on a DTBN geometry randomly extracted from the gas-phase Car-Parrinello dynamics.*

Basis functions		a_N
6-31G(d)	186	15.73
6-31+G(d,p)	280	15.57
6-311G(d)	234	12.55
6-311+G(d,p)	328	12.68
EPR-II	296	14.32
EPR-III	598	14.33
cc-pVDZ	230	16.73
cc-pVTZ	552	11.31
aug-cc-pVTZ	874	11.02

As is well known, none of the density functionals proposed till now allows a quantitative evaluation of a_N's. Thus, we followed the aforementioned QCISD-DFT approach (sketched in Figure 7) that has already been tested and validated for a large series of nitroxide radicals.[6]

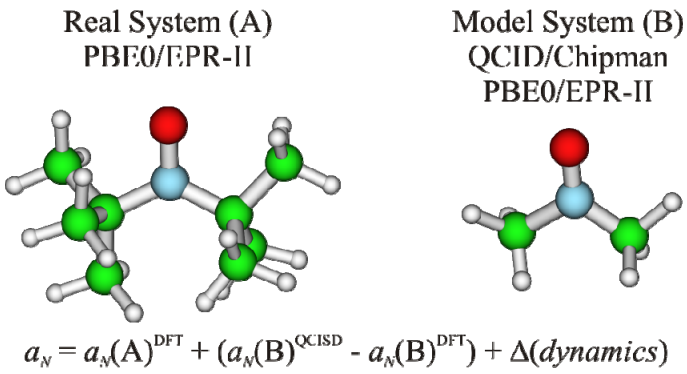

Figure 7*. Use of the combined QCISD-DFT approach for the calculation of a_N*

In particular, the PBE0 hybrid functional and the EPR-II basis set were used for most of the calculations and the QCISD correction was only computed for the DTBN gas-phase equilibrium value. In other words, in the present work the dynamical effect on the a_N was computed at the PBE0 level of theory by averaging the values obtained along the CPMD trajectories. To this end we extracted equally-time-spaced structures of DTBN (for the gas-phase) and DTBN–$(H_2O)_2$ (for the aqueous solution) along the CPMD trajectories and we repeated on each of these frames a calculation of the EPR spectral observables. Since the number of water-nitroxide hydrogen bonds in individual CPMD frames ranges from zero to two, we extracted from the aqueous solution trajectory clusters containing the solute plus the two water molecules closest to the nitroxide oxygen, the rest of the solvent being well described by the PCM. This should be considered a general procedure derived from the H-bond analysis that has been also proven effective in previous studies about other molecules involving oxygen atoms.[13] Figure 8 shows the a_N values in gas-phase (a) and in aqueous solution (b) as well as the Δg_{iso} values (c,d) computed along the trajectories together with the average value: it is quite apparent that two hundreds frames are largely sufficient to obtain well converged average results. Table XIII lists the data obtained from the Car-Parrinello dynamics. Structural modifications induced by the solvent (collectively referred to as indirect solvent effect) do not affect very much the a_N and g-tensor values, the spectral parameters computed on the isolated solute as extracted from the aqueous solution dynamics differing by 0.5 Gauss and 33 ppm from the average values obtained from the gas phase.

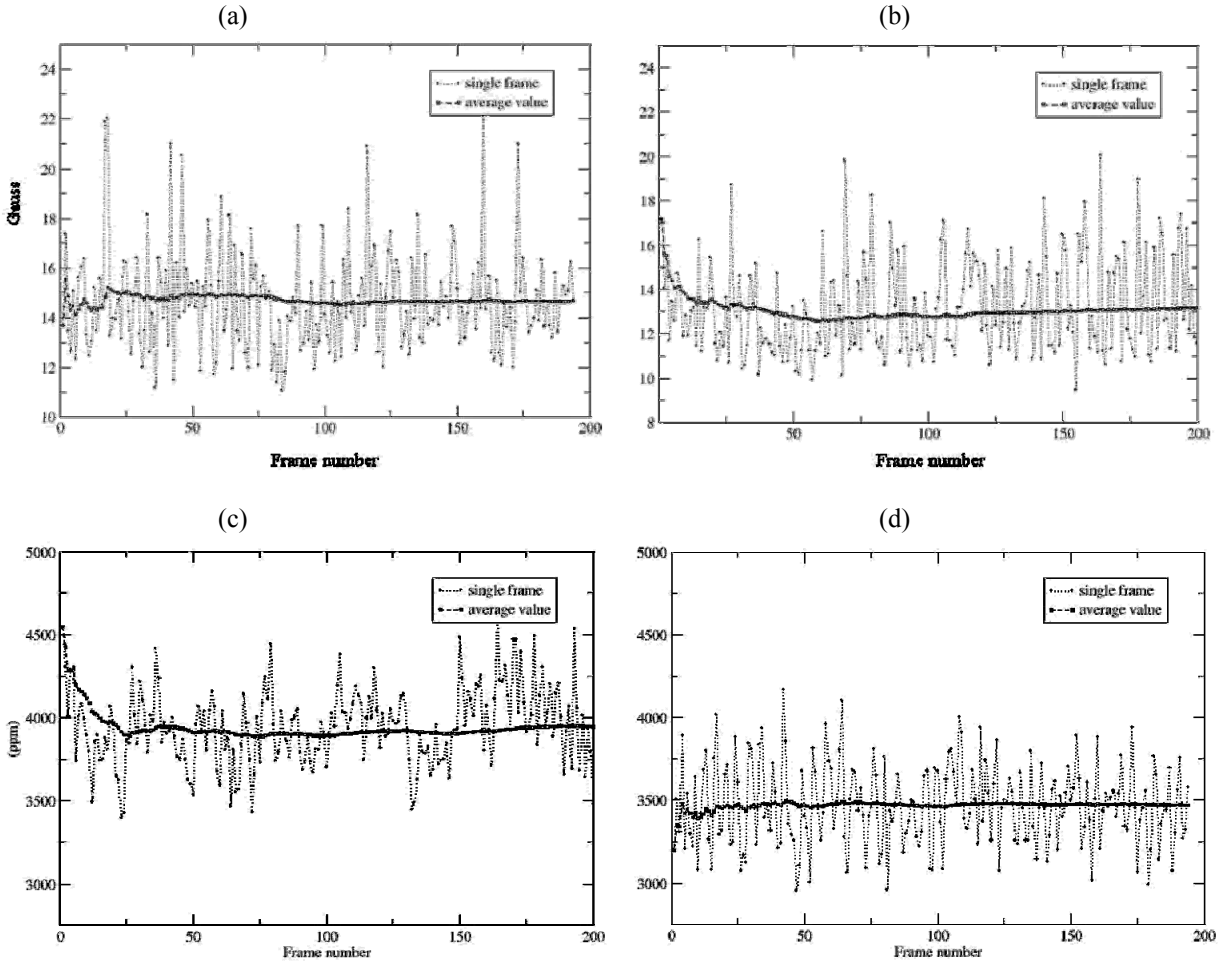

***Figure 8**: Convergence of a_N (in Gauss) and Δg_{iso} (in ppm) computed along the CPMD trajectories: (a) a_N in gas phase; (b) a_N in aqueous solution; (c) Δg_{iso} in gas phase; (d) Δg_{iso} in aqueous solution.*

On the other hand, direct solvent shifts (related to solute polarization at constant geometry) are significant: interestingly, the water environment enforces the hyperfine splitting in an opposite direction than the structural effect, whereas it decreases the value of the *g*-tensor shift following the same trend of the indirect solvent effect. To the best of our knowledge there is no value for the ***g***-tensor of DTBN in gas-phase, whereas estimates of a_N *in vacuum* have been obtained by extrapolation from experimental data in different solvents.[86] The CPMD average results are pretty far from reproducing absolute experimental data, but the a_N solvent shift is in very good agreement with its experimental counterpart. This failure in the reproduction of absolute data from CPMD simulation is related to the level of theory employed for the molecular dynamic simulations: as a matter of fact, the use of plane-wave basis sets for the CPMD simulation prevents the calculation of non local HF exchange with an affordable

computational cost. Conventional GGA functionals, employed in CPMD, provide equilibrium structures that are less accurate than those obtained from hybrid HF/KS models and this limitation affects also the MD trajectories and consequently the MD averaged spectroscopic values.[27] The effect of the exchange functional on the accuracy of the computed spectroscopic data can be highlighted by looking at the differences between PBE and its hybrid counterpart, PBE0, in calculating the structural and magnetic properties of the isolated DTBN molecule; the results are listed in Table IX. As a matter of fact, compared to the more reliable PBE0, the PBE structure provides a difference of 0.76 Gauss and 87 ppm in the case of a_N and Δg_{iso} values, respectively.

Table XIII. *Average values of a_N (in Gauss) and Δg_{iso} (in ppm) computed at the PBE0/EPR-II level of theory using structures issuing from CPMD simulations; standard deviations are given in parenthesis.*

	A_N	Δg_{iso}
Gas phase		
DTBN	13.1 (0.2)	3946 (17)
Exp [a, b]	15.5	
Aqueous solution		
DTBN	12.6 (0.2)	3913 (27)
DTBN-$(H_2O)_2$	14.7 (0.2)	3471 (18)
Exp [a, d]	17.17	3241
Solvent shifts		
CPMD	1.6	- 475
Exp [a]	1.7	-

(a) Ref. [86]; (b) Derived by a linear un-weighted least square fitting of the DTBN a_N in 31 different solvents related to the solvent dielectric constants; (c) DTBN-$(H_2O)_2$ clusters extracted from the MD plus the PCM for solvent bulk; (d) ref. [116]

A further analysis can be carried out from the computed EPR values on equilibrium DTBN and DTBN-water cluster geometries, as listed in Table X. The alternative inclusion of the PCM for the solution bulk and of just two explicit water molecules give us the chance to decouple the effects of the solvent dielectric properties to those arising

from the solute-solvent hydrogen bonding. Concerning a_N, specific interactions (e.g. H-bond) shift the computed value by 0.56 Gauss for the first H-bond and by 1.23 for the second one, whereas the effect of the dielectric contribution goes from 0.78 Gauss when one does not consider any explicit solvent molecule to a value of roughly 0.55 for both the single and double H-bond adducts. Interestingly, considering also the relaxation of the cluster induced by the solvent, the a_N shift from gas-phase to aqueous solution (in particular the DTBN$(H_2O)_2$/PCM value) of 1.63 Gauss is close to that obtained from the CPMD average values (1.6 Gauss). There should certainly be an error compensation that leads to results comparable to those obtained by considering the finite-temperature internal and solvent motions. As a matter of fact, the Δg_{iso} values computed on cluster structures optimized in gas-phase and in solution lead to a solvent shift quite different from that issuing from CPMD trajectories (-525 and -475 ppm, respectively). On the other hand, the dielectric (PCM) effect on both a_N and g-tensor decreases when explicit solvent molecules are included, thus showing the need of taking both short- and long-range solvent effects into the proper account. Thus, we tried to rationalise the computed spectroscopic observables by decoupling the different effects that tune the DTBN molecular properties. As the reference structure of DTBN in gas-phase, we took the PBE0/6-311++G(3df,2pd) energy minimum: using this geometry we extracted the model where the QCISD/Chipman calculation was carried out, i.e., di-methyl-nitroxide kept frozen at the geometry of DTBN. The intra-molecular dynamics of DTBN has certainly a non negligible effect on the computed spectroscopic value, which is quantified by the difference between the spectral parameters of the PBE gas-phase minimum and those averaged over the PBE CPMD gas-phase trajectory. The solvent effect was eventually taken into account by comparing the results obtained from the gas-phase and the aqueous solution dynamics. With this straightforward combination of the computed data, we obtained Nitrogen hyperfine coupling constant and g-tensor in quantitative agreement with their experimental counterparts. As summarized by Table XIV, the computed a_N of 17.2 Gauss is directly comparable to the experimental value of 17.17 Gauss; and the computed g-tensor shift (3384 ppm) is in close agreement with the experimental one (3241 ppm) with a relative error lower than 5%, which is well within the expected error bar of the DFT-GIAO approach.[117]

Table XIV. *EPR parameters of DTBN in aqueous solution.*

	QCISD/DFT + ***Δ(dynamics)*** + ***Δ(solvent)***			**TOTAL**	**EXP.** [b, c]
a_N (Gauss)	15.5	0.1	1.6	17.2	17.17
	GIAO-DFT + ***Δ(dynamics)*** + ***Δ(solvent)***			**TOTAL**	
Δg_{iso} (ppm)	3736	123	-475	3348	3241

(a) Solvent Shifts, see Table V; (b) ref. [86]; (c) ref. [116]

III. *2,2,5,5-tetramethyl-1-pyrrolidinyloxy (PROXYL)*

Structure, labelling and orientation of the proxyl molecule are depicted in Figure 1c. Geometrical parameters of the nitroxide moiety averaged over the Car-Parrinello simulation are listed in Table XV: a slight lengthening of the NO bond occurs when going from gas phase to solution, while angle and dihedral values are marginally affected. A first rough indication of the average number of hydrogen bonds between proxyl oxygen and solvent molecules is obtained by integrating the first peaks of the radial distribution functions (RDFs), depicted by Figure 9. The average number of solvent molecules coordinating the nitroxyl moiety is around two for the aqueous solution, but is close to one in the case of methanol. In order to avoid artefacts due to the limited statistics of CPMD, we generated a second trajectory starting from a configuration with two methanol-nitroxide H-bonds; however, after few picoseconds one of the solvent molecules leaves the first coordination shell of the nitroxide oxygen. Further insight was sought by adopting the usual set of purely structural criteria to compute the number of H-bonds and to measure their average geometries (see Table XV). Comparison between methanol and aqueous solution shows that the structural features of the hydrogen bonds are quite similar, as is the position of the first peak of the RDFs: the average number of proxyl-solvent H-bonds computed by the geometrical criteria is consistent with that obtained by integration of the RDFs. The higher standard deviation of the parameters associated to water-nitroxide H-bonds could be diagnostic of higher solvent mobility.

Table XV: *Geometrical parameters of the proxyl molecule, number and geometrical features of the solute-solvent hydrogen bonds, and magnetic parameters, averaged over the CPMD simulations. Distances in Angstroms, angles and dihedrals in degrees; a_N and $T_{N,zz}$ in Gauss, Δg in ppm. Standard deviations are reported in parenthesis.*

	Gas phase	**Aqueous solution**	**Methanol solution**
N-O	1.29 (0.03)	1.30 (0.02)	1.30 (0.02)
C-N-C	114 (3)	115 (2)	114 (2)
Abs(C-N-O-C)	165 (10)	167 (9)	166 (9)
r.m.s.(C-N-O-C - 180°)	18	16	17
No. of H-bonds [a]	-	1.9 (0.7)	1.0 (0.2)
(N)O…H(O) $_{solvent}$	-	2.0 (0.2)	1.9 (0.2)
(N)O…O $_{solvent}$	-	2.9 (0.2)	2.8 (0.2)
(N)O…H-O $_{solvent}$	-	15 (7)	12 (6)
a_N	11.8 (0.2) [b]	14.1 (0.2) [c] 14.2 (0.2) [d]	13.4 (0.2) [e]
$T_{N,zz}$	17.6 (0.6)	20.1 (0.9) [c] 20.1 (1.0) [d]	19.9 (1.0) [e]
Δg_{iso}	3741 (26) [b]	3333 (21) [c] 3313 (24) [d]	3414 (25) [e]
Δg_{xx}	7416 (63) [b]	6366(53) [c] 6311 (55) [d]	6605 (54) [e]
Δg_{yy}	4042 (18) [b]	3856 (19) [c] 3851 (19) [d]	3858 (29) [e]
Δg_{zz}	-234 (2) [b]	-226 (2) [c] -223 (2) [d]	-221 (2) [e]

(a) Identified based on the aforementioned structural criteria

(b) Computed at the PBE0/EPR-II level

(c) Computed at the PBE0/EPR-II/PCM (water) level on proxyl-$(H_2O)_2$ clusters

(d) Computed at the PBE0/EPR-II/PCM (water) level on proxyl-$(H_2O)_3$ clusters

(e) Computed at the PBE0/EPR-II/PCM (methanol) level on proxyl-CH_3OH clusters

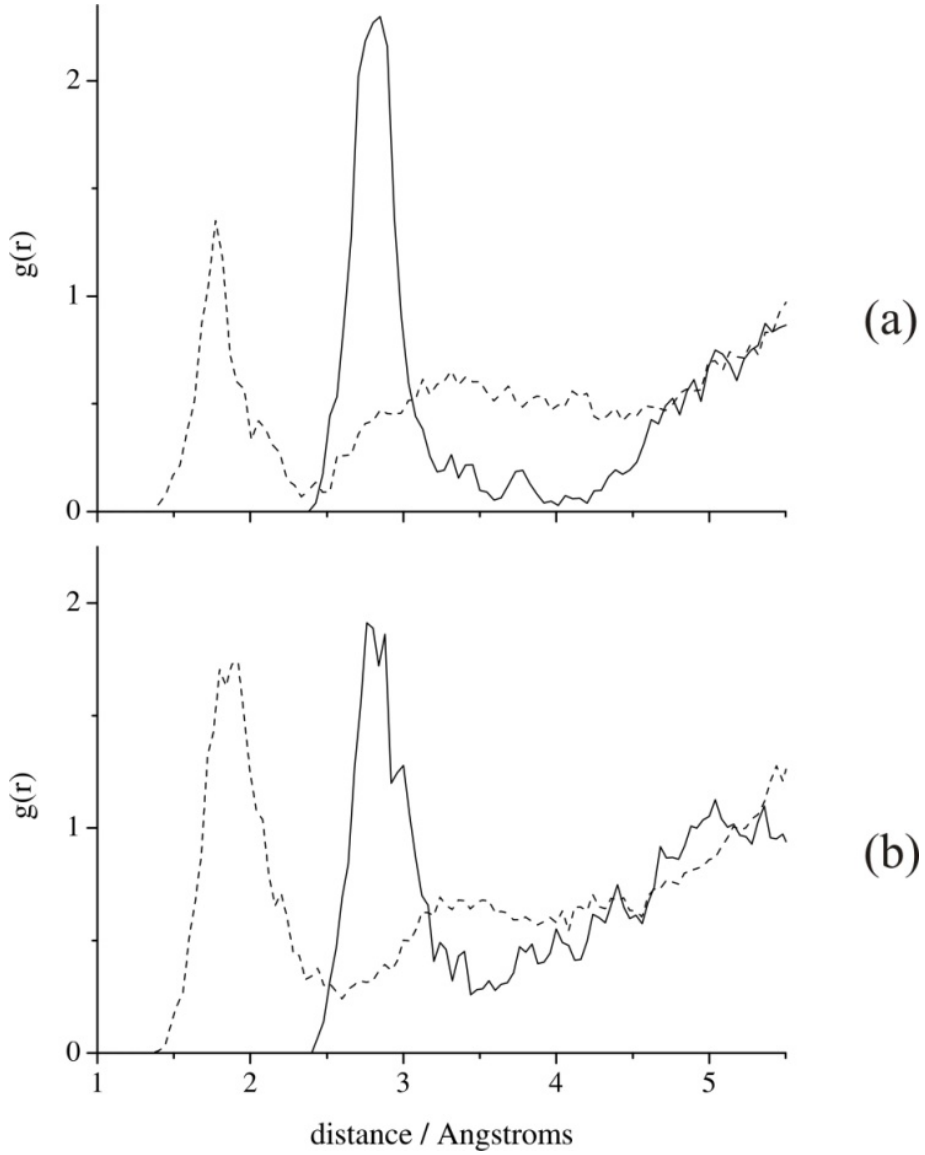

Figure 9. *Radial distribution functions computed on the Car-Parrinello trajectories in methanol (a) and aqueous solution (b); full lines correspond to (N)O…O $_{solvent}$ distances, dashed lines to (N)O…H(O) $_{solvent}$*

From another perspective, one can quantify the percentage of configurations sampled along the CPMD trajectories that display a definite number of H-bonds: in the methanol simulation, essentially all the frames (97 %) feature a single H-bond, and the remaining 3 % display no H-bond at all. In aqueous solution, more than half of the frames (52 %) present two genuine H-bonds; configurations with only one (25 %) and with three (20%) proxyl-water H-bonds are also populated, while the percentage of frames without H-bonds is small (3%). As it appears from visual inspection of the trajectory, configurations with only one and with three H-bonds are transient, and tend to evolve

towards the favoured state with two H-bonds: thus, they may be interpreted as instances of different mechanisms (dissociative and associative, respectively) by which an H-bonded water molecule can be exchanged with another one coming from the bulk. However, a more quantitative analysis of the exchange dynamics is prevented by the rather sporadic occurrence of the exchange events on the timescale sampled by the CPMD simulation. Overall, the geometrical analysis confirms the change in average number of solvent molecules coordinating the NO moiety, from two in aqueous solution to one in methanol. It is interesting to remark that the experimental information available, albeit indirect, seems to support the formation of a rather stable 1:1 "complex" between cyclic nitroxides and methanol.[118]

As an aid to the interpretation of the results issuing from CP dynamics, we carried out a quantum-chemical analysis of the interaction energies within nitroxide-solvent clusters. These calculations were performed with the same PBE functional employed for CPMD, and with the large 6-311++G(3df,2pd) basis set. However, we did make sure that the overall picture is not altered if the more reliable, hybrid functional known as PBE0 is used instead. Structural minima of the proxyl - *n* (solvent) (*n* = 1, 2) clusters, as well as of isolated proxyl and solvent molecules, have been computed both in the gas phase and in solution; in the latter case, the PCM was employed to take into proper account bulk solvent effects. In the gas phase, both water and methanol adducts feature a first H-bond with a stabilizing energy of ~ 7 kcal mol^{-1}; formation of an additional H-bond with a second solvent molecule results in a slightly lower energy gain (~ 6 kcal mol^{-1}), for a total interaction energy of ~ 13 kcal mol^{-1} with respect to isolated proxyl and solvent molecules. These conclusions are apparently uncorrelated with the results from CPMD. However, a satisfactory description of solvent effects should account not only for short-range interaction (H-bonding), but also for long-range contributions from the bulk solvent: this can be achieved by a cluster-PCM approach. In water, H-bonding with both the first and the second solvent molecule is favourable, with energy gains of 1.7 and 0.6 kcal mol^{-1}, respectively. On the other hand, in methanol solution, formation of the first solute-solvent H-bond remains favourable (by 0.5 kcal mol^{-1}), whereas coordination of a second methanol molecule is disfavoured by 0.8 kcal mol^{-1}. Thus, this more accurate description level predicts two genuine H-bonds in the case of water and just one in the case of methanol, a picture which fits nicely with the results from CPMD simulations. It

would be tempting to invoke steric effects to explain the shift from a preferred proxyl - 1 (solvent) cluster in methanol to a proxyl - 2 (solvent) cluster in water: as a matter of fact, the four α-methyl groups surrounding the proxyl oxygen define an accessible region where two H-bonded waters can fit easily, but two methanol molecules are more tightly accommodated. However, since the purely energetic description which emerges from the in vacuum interaction energies does not discriminate between formation of the proxyl - 2 (water) and proxyl - 2 (methanol) clusters, this effect can at most play an entropic role, in the sense that the tight fit of two methanol molecules around the proxyl group must involve a larger loss of entropy with respect to the corresponding binding of water molecules. This effect is clearly not accounted for in the static cluster calculations, but presumably it contributes to define the picture issuing from CMPD. From another viewpoint, one can compare the solvation free energies, as computed by the PCM, for proxyl, proxyl - 1 (solvent) and proxyl -2 (solvent) clusters (Table XVI).

Table XVI. *Computed [PBE/6-311++G(3df,2pd)/PCM // PBE/6-311++G(3df,2pd)/PCM] solvation free energies (kcal mol^{-1}) of proxyl, proxyl - solvent clusters, and solvent molecules. The separate electrostatic and non-electrostatic contributions are also listed.*

	ΔG_{solv}	ΔG_{elec}	$\Delta G_{non\text{-}elec}$
Aqueous solution			
H_2O / PCM	-6.0	-6.7	0.7
Proxyl / PCM	-3.0	-5.6	-2.6
Proxyl-H_2O / PCM	-4.5	-9.4	4.8
Proxyl-$(H_2O)_2$ / PCM	-4.0	-11.6	7.6
Methanol solution			
CH_3OH / PCM	-5.9	-5.4	-0.5
Proxyl / PCM	-6.2	-5.4	-0.9
Proxyl-CH_3OH / PCM	-6.3	-7.0	0.7
Proxyl-$(CH_3OH)_2$ / PCM	-4.3	-7.4	3.1

In aqueous solution, the solvation free energies of the individual proxyl - *n* (solvent) clusters are more or less constant, whereas in methanol solvation of the proxyl-CH_3OH cluster is appreciably more favourable (by 2 kcal mol^{-1}) with respect to proxyl-$(CH_3OH)_2$. Since, in agreement with experiment, the computed solvation free energy of a solvent molecule is almost exactly the same for water and methanol,[10] these opposite

trends are the crucial factors that determine the change in preferred cluster sizes in methanol and water. To push further the analysis, one can decompose the PCM solvation free energies into an electrostatic term, which accounts for solute polarization and interaction with the solvent reaction field, and a non-electrostatic contribution, which describes dispersion-repulsion and cavitation effects.[39] When the free energy trends along the proxyl - *n* (solvent) clusters are analyzed in this perspective, it transpires that in aqueous solution an increasingly positive non-electrostatic contribution is balanced by the large, negative electrostatic term; in methanol changes are smaller, but the electrostatic term is unable to overcome the larger and larger dispersion-repulsion and cavitation energies.

Regarding magnetic properties, we must first consider that the 'magnetic orbitals' (see below for a more detailed definition) of non conjugated nitroxides are strongly localized on the NO moiety (see Figure 10), so that the principal axes of both $\boldsymbol{T}_N$ and $\boldsymbol{g}$ tensors are practically aligned with the NO bond (by convention *x* axis) and with the average direction of π-orbitals (*z* axis). Since this conventional reference frame (see Figure 1) nearly coincides with the principal inertia frame, off-diagonal tensor elements can be safely neglected in the interpretation of EPR and ENDOR spectra. Furthermore, $T_{N,xx} \approx T_{N,yy}$ and, since $\boldsymbol{T}_N$ is a traceless tensor (i.e. $-T_{N,zz} = T_{N,xx} + T_{N,yy}$), we will discuss in the following only the largest component $T_{N,zz}$, which conveys the whole information about dipolar interactions. Since both direct and spin-polarization contributions to a_N are roughly proportional to the spin population in the π* SOMO (see Figure 10),[6] a_N and $T_{N,zz}$ show closely parallel trends. As a consequence, we report in the tables all the hyperfine parameters, but the discussion will be concentrated on a_N (which shows stronger solvent shifts and more direct connection with experimental results). In the same vein, the behaviour of the $\boldsymbol{g}$-tensor is dominated by its largest component g_{xx} (vide infra), so that Δg_{iso} and g_{xx} show parallel trends.

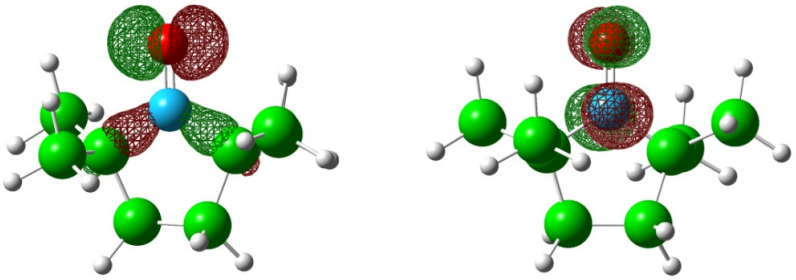

***Figure 10**. Selected molecular orbitals of PROXYL.*

Gas-phase minimum energy structures and their corresponding magnetic parameters are listed in Table XVII together with a comparison between the PBE functional and its HF-DFT hybrid counterpart, known as PBE0. The only significant difference between PBE and PBE0 structures concerns the NO bond length, the conventional GGA functional predicting a larger value, possibly because of the larger self-interaction error. Interestingly, a relative difference of 1 % in NO bond length translates into 5 % and 2 % relative errors on the nitrogen hyperfine coupling constant and the isotropic *g* shift, respectively. Moreover, the choice of the functional has a larger impact on computed magnetic parameters than on structural parameters: this points out the importance of selecting improved theory levels for the computation of spectroscopic properties, no matter which technique has been used for structural sampling.

Table XVII. Optimized structures [a] and magnetic parameters [b] of proxyl in the gas phase. Distances in Angstroms, angles and dihedrals in degrees, a_N and $T_{N,zz}$ in Gauss, and Δg in ppm.

Optimization	**PBE**				**PBE0**		
N-O	1.274				1.257		
C-N-C	114.8				115.1		
Abs(C-N-O-C)	180.0				180.0		
Magnetic parameters	**PBE**	**PBE0**	**PBE0/PCM (water)**	**PBE0/PCM (methanol)**	**PBE0**	**PBE0/PCM (water)**	**PBE0/PCM (methanol)**
a_N	6.45	9.76	10.83	10.78	9.32	10.30	10.27
$T_{N,zz}$	17.42	17.95	19.29	19.21	17.92	19.18	19.14
Δg_{iso}	3300	3596	3405	3417	3528	3352	3358
Δg_{xx}	6519	7084	6615	6643	6954	6526	6539
Δg_{yy}	3581	3932	3828	3833	3852	3751	3754
Δg_{zz}	-201	-228	-226	-226	-222	-220	-220

(a) Basis set: 6-311++G(3df,2pd)

(b) Basis set: EPR-II

Nevertheless, there is close correspondence between structural fluctuations measured along the CPMD trajectory and the computed observables (Figure 11): the nitrogen hyperfine coupling constant is mainly dependent on the out-of-plane motion of the nitroxide group, but is apparently uncorrelated to the NO bond length. Conversely, the isotropic *g* shift is mainly affected by changes in nitroxide bond length, but is quite insensitive to the C-N-O-C improper dihedral (hereafter θ). These correlations can be used to characterize the level of accuracy required during the structural sampling phase: the method chosen should provide a reliable description of those geometrical features of the molecule that mostly affect the spectroscopic observables of interest.

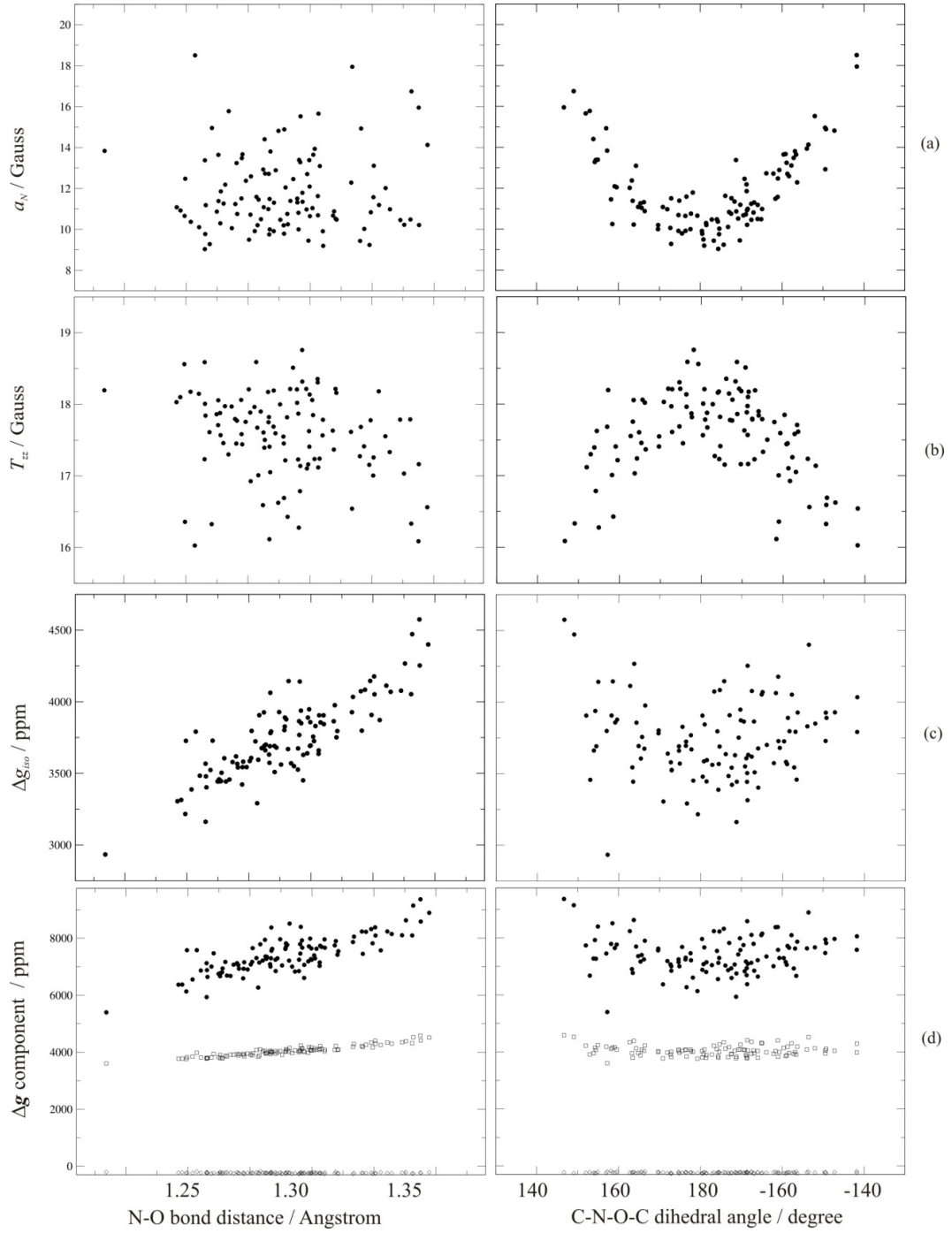

Figure 11. *Structure - property correlations computed along the gas phase CPMD trajectory: a_N (a), $T_{N,zz}$ (b), Δg_{iso} (c), and the principal components of the* ***g*** *tensor shift (d) are plotted against the NO bond length and the C-N-O-C out-of-plane dihedral. In panel (d), filled circles correspond to Δg_{xx}, empty squares to Δg_{yy}, and empty diamonds to Δg_{zz}.*

Table XVIII. *Optimized structures [a] and magnetic parameters [b] of proxyl-solvent adducts. Distances in Angstroms, angles and dihedrals in degrees, a_N and $T_{N,zz}$ in Gauss, and* ***Δg*** *in ppm.*

	Proxyl-H_2O				Proxyl-$(H_2O)_2$				Proxyl-CH_3OH				Proxyl-$(CH_3OH)_2$			
Optimization	PBE	PBE/ PCM	PBE0	PBE0/ PCM	PBE	PBE/ PCM	PBE0	PBE0/ PCM	PBE	PBE/ PCM	PBE0	PBE0/ PCM	PBE	PBE/ PCM	PBE0	PBE0/ PCM
N-O	1.278	1.282	1.260	1.263	1.280	1.285	1.263	1.266	1.278	1.283	1.260	1.263	1.282	1.285	1.263	1.266
C-N-C	115.1	115.0	115.3	115.3	115.3	115.2	115.4	115.3	115.1	115.1	115.3	115.2	115.2	115.1	115.4	115.2
abs(C-N-O-C)	176.9	177.3	177.7	178.0	179.9	180.0	179.8	179.7	177.5	177.0	178.2	178.5	179.0	179.7	179.8	180.0
(N)O…H(O) $_{solvent}$	1.83	1.82	1.85	1.84	1.88	1.86	1.87	1.87	1.83	1.80	1.84	1.81	1.86	1.86	1.87	1.87
(N)O…O $_{solvent}$	2.82	2.81	2.81	2.81	2.85	2.84	2.84	2.85	2.81	2.79	2.81	2.78	2.84	2.85	2.84	2.84
(N)O…H-O $_{solvent}$	4.7	2.0	4.8	0.1	4.4	0.8	4.5	0.0	3.7	3.2	4.0	4.5	3.5	1.0	3.7	1.3
Magnetic parameters	PBE0	PBE0/ PCM	PBE0	PBE0/ PCM	PBE0	PBE0/ PCM	PBE0	PBE0/ PCM	PBE0	PBE0/ PCM	PBE0	PBE0/ PCM	PBE0	PBE0/ PCM	PBE0	PBE0/ PCM
a_N	10.85	11.66	10.33	11.08	11.68	12.26	11.20	11.67	10.84	11.64	10.33	11.09	11.76	12.29	11.21	11.69
$T_{N,zz}$	19.20	20.16	19.13	20.04	20.25	20.90	20.19	20.74	19.21	20.11	19.14	20.05	20.30	20.92	20.20	20.77
Δg_{iso}	3341	3230	3278	3175	3135	3066	3074	3017	3343	3238	3278	3177	3131	3051	3068	3002
Δg_{xx}	6418	6148	6314	6073	5900	5726	5798	5664	6419	6158	6310	6061	5876	5676	5776	5613
Δg_{yy}	3826	3764	3737	3666	3722	3685	3636	3597	3829	3777	3739	3680	3733	3696	3640	3603
Δg_{zz}	-222	-222	-215	-215	-216	-213	-210	-210	-221	-222	-215	-210	-217	-217	-212	-210

(a) Basis set: 6-311++G(3df,2pd)

(b) Basis set: EPR-II

Conversely, it is clear that a MD trajectory generated at a given theory level may be a perfectly appropriate starting point for the computation of one kind of spectroscopic parameter, while being quite unsuitable for a different property. This is one of the reasons why in the present study, in which we wish to discuss all the principal magnetic parameters (a_N, $\boldsymbol{T}_N$, and $\boldsymbol{\Delta g}$) the accuracy of the CPMD has been cross-checked by comparison with minimum-energy structures obtained with the PBE and PBE0 functionals and large Gaussian basis sets.

Structural minima and magnetic parameters of nitroxide-solvent adducts are listed in Table XVIII. From both structural and spectroscopic viewpoints there is strict similarity between the proxyl-water and proxyl-methanol hydrogen bonding: moreover, in both cases, the solute-solvent distances computed at the PBE/PCM level reflect the position of the first peaks in the RDF, and the separate effects of the first and second H-bond on magnetic parameters are similar. As discussed above, when bulk solvent effects are taken into account by means of the PCM, the second H-bond is energetically unfavourable in methanol; nevertheless, the magnetic features of corresponding proxyl-water and proxyl-methanol clusters remain strikingly similar.

Thus, it appears that the differences in magnetic parameters measured in aqueous and in methanol solution should be essentially ascribed to an altered balance of the populations of proxyl- *n* (solvent) clusters, each type of cluster sharing quite similar magnetic properties in both solvents. Again, geometry optimizations at the PBE0 level predict shorter NO distances (by about 0.02 Å) with respect to the corresponding PBE minima, with little change in other geometric parameters. This translates into significantly different values of both a_N and the isotropic *g* shift; however, most of the difference disappears when changes from gas to solution phases are considered. Overall, it appears that in the present case "second order" effects related to the theory level adopted for cluster geometry optimizations have a marginal impact, as far as solvent shifts of magnetic parameters are concerned. This conclusion allows for a particularly simple interpretation of the results from the CPMD dynamics (based, as already remarked, on the PBE functional): in particular, the solvent shifts issuing from solution *versus* gas phase CPMD runs can be compared directly to those computed for specific, optimized solute-solvent clusters. Moreover, once the presence of clusters of different size has

been accounted for, the remaining discrepancies should provide some indication of dynamical effects, e.g. distortions from optimal (cluster) geometries.

It is interesting to note that, while both a_N and Δg_{iso} values are markedly sensitive to solvent effects, the relative influence of first shell solvent molecules and of the bulk are rather different for the two parameters. In aqueous solution, even when the two hydrogen bonded solvent molecules are described explicitly, i.e. in the proxyl-$(H_2O)_2$ cluster, the computed a_N value changes significantly in the presence of the PCM (23% of the total solvent shift, about one fifth of which is due to geometry relaxation with respect to the cluster structure optimized in vacuum); however, Δg_{iso} is less affected (13% of the total solvent shift). The trend is similar in methanol: in the most representative solute-solvent cluster, which is now proxyl-CH_3OH, the bulk accounts for 43 % of the total solvent shift for a_N, and 29 % for Δg_{iso}. As a matter of fact, the behavior of the $\boldsymbol{g}$ tensor in this respect becomes more complex if analyzed at the level of its principal components: while Δg_{zz} is too small to contribute in an appreciable way, the "residual" sensitivity to the PCM is relatively high for Δg_{yy}, but this is compensated by the reduced response of Δg_{xx}, which is by far the largest component of the tensor and therefore dominates the isotropic value.

Convergence of the computed magnetic parameters with respect to the number of solvent molecules which are included explicitly in a cluster-PCM calculation is an issue that in principle should be verified on a case by case basis: as a matter of fact, specific spectroscopic properties can display markedly different solvent sensitivities, as well as an altered balance of specific versus bulk effects. However, in the present instance the unambiguous indication that emerges from structural analysis of the dynamics, coupled with the experience accumulated on previously studied nitroxyl compounds, concur to define the most suitable choice, i.e., to describe at the QM level a constant number of solvent molecules, corresponding to the maximum number of hydrogen bonds that are formed with appreciable probability. Therefore, in aqueous solution the cluster-PCM computations of magnetic parameters refer to a proxyl molecule with the three water molecules closest to the oxygen atom, while in methanol solution only one solvent molecule is kept explicit. As a matter of fact, the aqueous solution is described rather well even if only two explicit water molecules are included: Δa_N is basically unchanged,

and $\Delta\Delta g_{iso}$ rises by 20 ppm, a 5 % change with respect to the computations with three water molecules at the QM level. One reason for this behavior is the fact that configurations with three water molecules H-bonded to proxyl are relatively little represented in the dynamics; moreover, these cases do not reflect a distinct minimum-energy cluster structure (or at most a very shallow one), since at least one of the water molecules needs to be displaced from the preferred H-bonding site: in this situation, the PCM is expected to correctly account for most of the influence of the third, furthest water molecule. However, apart from this special case, it is crucial that the explicit solvent molecules are described at a suitable QM level (in this study, for the sake of simplicity we adopted the same level as for the solute). Needless to say, the PCM alone (i.e. with no explicit solvent molecules) does not provide satisfactory results (compare the magnetic parameters listed in Tables XVII and XVIII); however, even a description of the hydrogen-bonded solvent molecules in terms of point charges does not perform well. Taking as example the optimized (PBE0/PCM) proxyl-$(H_2O)_2$ cluster, if one adopts the TIP3P charges[112] for water the computed a_N is 10.88 G and the isotropic *g*-shift 3196 ppm; with SPC charges[119], the corresponding results are 10.86 G and 3202 ppm. From one side, the closeness of the results obtained by different choices of the charges is reassuring; however, on the other side, the agreement with the values computed at the QM level (11.20 G and 3074 ppm, respectively; see Table XVIII) is quite poor. Analysis of the electron and spin density distributions in the QM clusters does not reveal any major transfer from the nitroxyl group to the solvent molecules: therefore, the inability of purely electrostatic models to fully account for the influence of solvent on magnetic parameters should be traced back to other quantum chemical effects, most likely Pauli repulsion. It is probable that a similar explanation also underlies the necessity to include explicit solvent molecules in order to correctly predict spectroscopic parameters of different kinds, e.g., NMR chemical shifts and low-lying electronic transitions.[13, 120]

Table XV also lists the magnetic parameters computed along the CPMD trajectories: convergence with respect to the sampling set was achieved by including ~ 100 configurations (Figure 12).

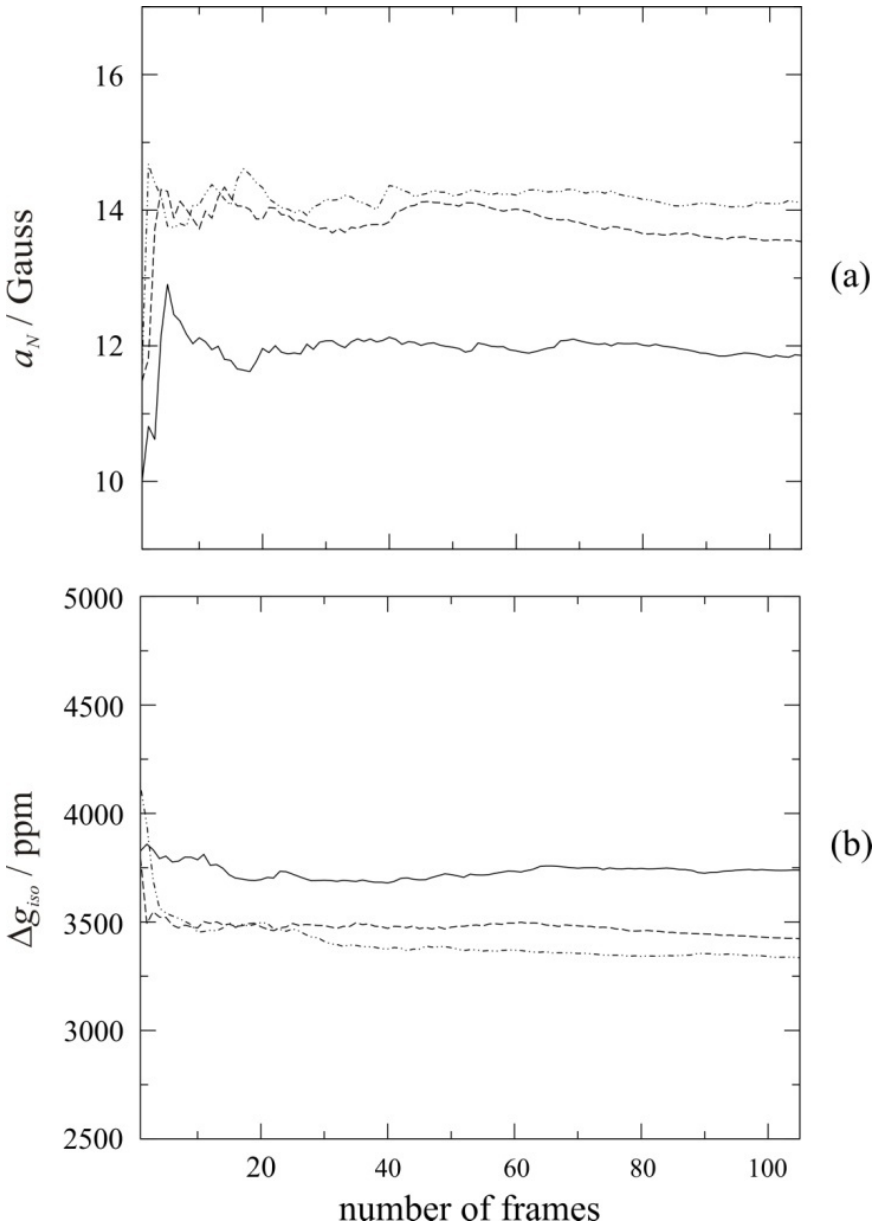

***Figure 12**. Average values of magnetic parameters obtained for different samplings along the CPMD trajectories: (a), hyperfine coupling constant; (b), isotropic g-shift. Full line corresponds to the gas phase, dotted-dashed line to the aqueous solution, and dashed line to the methanol solution.*

By referencing to the corresponding gas-phase values, a comparison of "static" and "dynamic" solvent shifts of a_N and $\boldsymbol{g}$ tensor values can be obtained: this is presented in Table XIX.

***Table XIX**. Solvent shifts of isotropic magnetic parameters computed on proxyl and proxyl-solvent cluster minima (from Tables XVII and XVIII), and corresponding values averaged over the CPMD trajectories (from Table 1). Δa_N in Gauss, $\Delta\Delta g_{iso}$ in ppm.*

	Δa_N	$\Delta\Delta g_{iso}$
Aqueous solution		
Proxyl / PCM	1.13	-159
Proxyl-H_2O / PCM	1.90	-366
Proxyl-$(H_2O)_2$ / PCM	2.50	-530
< CPMD >	2.4	-428
Methanol solution		
Proxyl / PCM	1.09	-155
Proxyl-CH_3OH / PCM	1.88	-358
Proxyl-$(CH_3OH)_2$ / PCM	2.53	-545
< CPMD >	1.7	-327

As far as a_N values are concerned, solvent shifts obtained from the CPMD are in nice agreement with those computed on the optimized cluster which corresponds to the prevailing solvation, i.e. proxyl-$(H_2O)_2$ in water, proxyl-CH_3OH in methanol. This explains why solvent shifts of hyperfine couplings have been reproduced with good accuracy by static continuum (for non protic solvents) or discrete/continuum (for protic solvents) models.[6] In the latter cases agreement with experiment was obtained including one explicit solvent molecules for chloroform and alcohols and two molecules for aqueous solutions.[88]

As expected, the ***g*** tensor is more sensitive to the details of the solute-solvent interaction, and the CPMD solvation shifts do not coincide with those computed on minimum energy structures: these latter overestimate solvent effects. The observed differences will in part reflect dynamical features of the hydrogen-bond geometries within the cluster. Thus, for example, relaxed geometry scans of the proxyl-$(H_2O)_2$ cluster in the presence of PCM show that distortions of the two water molecules away from the plane of the nitroxyl group significantly affect the magnetic parameters: for large distortions a_N increases by up to 0.35 G, and Δg_{iso} by about 100 ppm. The corresponding figures for the proxyl-CH_3OH cluster are about 0.25 G and 70 ppm. The energy changes involved are quite small [~ 0.8 and 0.4 kcal mol^{-1}, respectively for proxyl-$(H_2O)_2$ and proxyl-CH_3OH]: this is due in part to the bulky α-substitution, since

solute-solvent steric interactions are more unfavorable when the solvent molecules are close to the proxyl molecular plane, and are relieved when they move away from it (this effect can be highlighted by a comparison with DMNO). Moreover, because of the presence of the unpaired electron in a π^* orbital, the hydrogen bonding of nitroxyls is intrinsically less directional than for typical sp^2 oxygens, e.g., in ketones, as will be discussed in the next chapter. At this level of analysis, the presence of solute-solvent clusters of different composition should also be taken into account, since in the case of aqueous solution its impact on the computed values becomes of comparable importance. The fractional populations of different clusters during the CPMD have been quantified before, and could be employed directly to compute a weighted average of magnetic parameters for the corresponding optimized clusters. In this connection, it seems reasonable to co-add the occurrences of proxyl-$(H_2O)_3$ clusters and proxyl-$(H_2O)_2$ clusters, since the explicit presence of a third water molecule has a minor impact on the magnetic parameters computed along the CPMD, its effect being well accounted for by the PCM. Averaging of the magnetic parameters computed for proxyl (with a statistical weight of 3 %), proxyl-H_2O (25 %) and proxyl-$(H_2O)_2$ clusters (72 %), each at their minimum-energy PBE/PCM geometries, leads to estimated values of -478 ppm for $\Delta\,\Delta g_{iso}$ and 2.31 G for $\Delta\, a_N$. When the geometrical distortions of the proxyl-$(H_2O)_2$ cluster are introduced into the picture by straightforward Boltzmann averaging, the values change to -460 ppm and 2.35 G, respectively, which represents an even better agreement with the data issuing from CPMD (see Table XIX). While the present comparison is clearly lacking quantitative rigor, inter alia because of the limited exploration of the potential energy surface of proxyl-solvent clusters, it highlights in a qualitative way the delicate interplay of cluster size distribution and exact cluster geometries, which is sampled by the CPMD, and also allows to gauge to some extent the influence that such factors exert on magnetic parameters.

The solvent shifts of magnetic parameters computed from the CPMD trajectories compare well with their experimental counterparts: thus, for proxyl the measured change in a_N between water and dodecane solutions is 2.35G,[100] consistent with the computed difference of 2.4 G between aqueous solution and gas phase. For a related five-membered ring nitroxide derivative[116] the experimental a_N shift between water and methanol is ~ 1.0 G, in fair agreement with the computed value of 0.7 G. For the same

molecule, the experimental $\Delta\,\Delta g_{iso}$ between toluene and water (-430 ppm) is reproduced quite well by our value of -428 ppm (gas phase to aqueous solution). However, the agreement is just reasonable in the case of methanol (computed -327 ppm, measured -200 ppm).

Absolute values of $\boldsymbol{T}_N$ and $\boldsymbol{g}$ tensor elements are in good agreement with experiment, since they are dominated by the shape and energies of *n* and π* orbitals, which are well reproduced by current DFT methods and are only marginally affected by vibrational averaging effects.[121, 122] However, a quantitative computation of the nitrogen hyperfine coupling constant is more involved, due to its strong sensitivity to the large amplitude out of plane motion of the NO moiety and to the limitations of current density functionals in describing the NO spin polarization. As a matter of fact, the intra-molecular dynamics of proxyl is very close in vacuum and in solution, so that vibrational averaging effects effectively cancel out when computing solvent shifts: this explains the remarkable agreement between the shifts obtained by geometry optimizations and by CPMD. On the other hand, the significant difference between the equilibrium value of a_N in the gas-phase and the average along the CPMD trajectory shows that detailed comparison between computed and experimental spectroscopic parameters requires proper account of nuclear motions, which must be performed, in principle, by a QM approach. For semi-rigid molecules low-order perturbative methods are particularly effective and have been applied with remarkable success also to quite large systems.[123] Unfortunately, the perturbative approach is ill adapted to treat large amplitude vibrations, because of their strong curvilinear character and of the poor convergence of the Taylor expansion of the potential. When a single large amplitude motion can be singled out (here NO inversion) it becomes possible to build an effective one-dimensional Hamiltonian, whose eigenvalues and eigenvectors can be found by standard numerical procedures. A number of studies have shown that this approach provides accurate vibrationally averaged values for π-radicals.[124] In the particular case of proxyl, the correction issuing from this treatment (1.8 G) is very close to that provided by the CPMD classical simulation (2.0), possibly due to the large masses of the moving atoms. However, we have still to deal with the underestimation of spin polarization by current DFT models. In order to obtain accurate estimates, more demanding theory levels are required, e.g., QCISD[125] with purposely tailored basis

sets,[110] possibly integrated into the aforementioned mixed QCISD-DFT approach.[6] In order to apply this procedure, we fitted the difference between QCISD and PBE0 hyperfine coupling constants of DMNO as a function of θ, available from Improta *et al.*,[6] and then corrected the computed values for the different frames of proxyl and its adducts by the difference corresponding to the specific θ value. It is noteworthy that a very good fitting (see Figure 13) is obtained using 0.86 + 1.99 cos(2θ), which is exactly the trend expected for spin polarization. Furthermore, the a_N obtained in this way for the gas-phase (13.91 G) compares nicely with the experimental vales in dodecane (14.02 G).[100] Thus, our general procedure provides accurate results both for absolute values and solvent shifts for all the magnetic parameters of nitroxides.

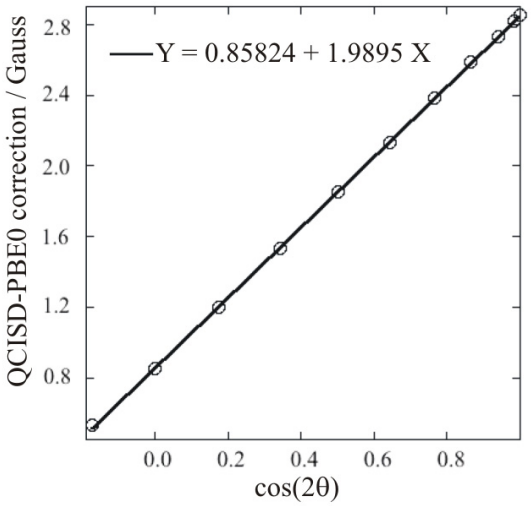

Figure 13. *Difference between QCISD and PBE0 hyperfine coupling constants of dimethylnitroxide as a function of the improper dihedral θ (see text for details).*

To conclude, it may be worthwhile to put into a more general perspective some trends of the magnetic parameters which have emerged in the above discussion. The characteristic dependence of a_N and $T_{N,zz}$ on the out-of-plane dihedral at the nitroxide group can be rationalized based on simple physical considerations. In the planar conformation (which does not necessarily correspond to a minimum on the potential energy surface) the only contribution to a_N is provided by spin polarization; however, pyramidalization at the nitrogen center allows for the direct involvement of the nitrogen *s* orbital in the SOMO, and this results into a large contribution to the Fermi contact

term, which overcomes the spin polarization contribution and determines the observed increase in a_N. $T_{N,zz}$ reports on the sole π spin density, and as a consequence decreases with increasing nitrogen pyramidalization. Concerning solvent effects, both the polarity of the environment and formation of specific hydrogen bonds to the nitroxide oxygen contribute to the selective stabilization of the charge-separated resonance form of the NO functional group (see Scheme 1) which entails a larger spin density on nitrogen with the consequent increase of a_N and $T_{N,zz}$.

A qualitative explanation of the ***g*** tensor in organic free radicals is provided by the Stone theory.[126, 127]. In these systems, the significant amount of spin density localized on heteroatoms such as nitrogen or oxygen leads to distinct ***g*** tensor anisotropy. This is related on one hand to the relatively large spin-orbit coupling constants of heteroatoms, which results into significant spin-orbit mixing, and, on the other hand, to the presence of nonbonding orbitals that are energetically close to the SOMO. In the specific case of nitroxide radicals, three *g*-shifts of significantly different magnitude are expected, with $\Delta g_{xx} > \Delta g_{yy} > \Delta g_{zz}$, the last value being always close to zero, i.e., $g_{zz} \approx g_e$.

The large Δg_{xx}, directed along the NO bond (see Figure 1), is particularly sensitive to the polarity of the surroundings. The most important contribution to this term comes from an electronic excitation from the SOMO-1 (an in-plane lone pair, hereafter referred to as *n*) to the SOMO (an out of plane π* orbital),[115, 128] both of which are sketched in Figure 10. Δg_{yy} is less sensitive to the surroundings, and Δg_{zz} is basically unaffected. The dependence of the ***g*** tensor on solvent polarity is related to the selective stabilization of lone pair orbitals by polar solvents: this increases the $n \rightarrow \pi^*$ gap, with the consequent reduction of ***g*** tensor shifts (especially Δg_{xx}). Together with this purely electrostatic interaction, formation of solute-solvent H-bonds also concurs to the stabilization of lone pair orbitals and, once again, to a decrease of the ***g*** tensor shifts. On the other hand, lengthening of the NO bond has a negligible effect on lone-pair orbitals, but stabilizes the π *-SOMO: this results into a smaller $n \rightarrow \pi^*$ gap, and therefore into larger ***g*** tensor values.

Conclusions

The present chapter deals with a thorough analysis of the structural and magnetic properties of widely used spin probes in the gas phase and in two different protic solvents, performed by means of an integrated computational tool including Car-Parrinello molecular dynamics and discrete/continuum solvent models. Analysis of the CPDM simulations reveals a marked, and to some extent unexpected change in the average number of solute-solvent hydrogen bonds, which drops from around two in aqueous solution to just one in methanol solution in the case of PROXYL, and goes to one in the case of DTBN aqueous solution too.

The static cluster energy calculations that were performed in order to rationalize this behavior pointed to a delicate balance of bulk solvent effects and explicit hydrogen bond interactions, and underline the necessity for a proper treatment of the bulk solvent (which in this study was provided by the PCM), along with the description of short-range, specific interactions. Such a cluster-PCM approach also allows for a further dissection of the factors which determine the preferred cluster size, in terms of electrostatic versus non-electrostatic contributions to the solvation free energy of specific solute-solvent clusters. Of course, the average solute-solvent cluster size plays a central role in defining the solute magnetic parameters. A specific information which is provided by the CPMD simulations is the impact of dynamic fluctuations (of both intra- and inter-molecular structural parameters) on magnetic properties; in the cases at hand, all the magnetic parameters (a_N, $\boldsymbol{T}_N$, $\boldsymbol{\Delta g}$) are affected by intramolecular dynamics, but their sensitivity to the geometrical features of the solute-solvent clusters differ.

Decoupling of structural, dielectric and hydrogen bonding contributions to the solvent shifts of magnetic parameters provides a framework for the conceptual rationalization and computational description of the physico-chemical behavior of a complex nitroxide-solvent system. From a different viewpoint, it is reassuring that the computed magnetic parameters are in fair agreement with the available experimental values: thus, the integrated computational protocol we presented is useful not only to analyze the different factors that tune the structural and magnetic properties of organic free radicals in different solvents, but also to provide reliable estimates of spectromagnetic data. This possibility can be of particular interest to setup detection protocols, based on specific

spectroscopic signatures, in unusual chemical situations. In more general terms, the coupling of effective dynamical treatments with the high-accuracy evaluation of spectroscopic properties for a statistically significant number of configurations opens exciting perspectives for a systematic study of free radicals of biological relevance in their natural environments.

Chapter 3

Spectroscopic properties of acetone in aqueous solution

Abstract: this chapter reports the theoretical investigation of the solvent effect on the n-π^* electronic transition energy and on the ^{13}C and ^{17}O nuclear magnetic shieldings of the carbonyl group of the acetone molecule in aqueous solution. A new classical force field has been developed in order to obtain MD trajectories on the time scale of nanoseconds. From these simulations, a statistically consistent set of acetone-water configurations have been extracted for computing spectroscopic parameters by using high level *ad initio* methods. Acetone was chosen as a suitable benchmark, given its relatively high polarity and the availability of suitable experimental data. Of course, the system, by itself, is a chemically interesting one; moreover, it can also be regarded as a simple model to probe the general features of the carbonyl-water interaction, which is an issue of still wide chemical and biochemical interest.

Introduction

In this chapter we consider the typical case of a solute/solvent system, where the solute molecule is the spectroscopically active moiety, which represents a large class of molecular systems in the condensed phase. The physical response of the solute to an applied electromagnetic field is generally quite a complex phenomenon, which is affected by both the interaction with the environment, for example the solvent, and the fluctuations of the solute geometry as well as the surrounding solvent molecules. As reported in the previous chapter, the problem of reproducing accurately spectroscopic parameters of molecules in solution can be decomposed into two parts: (a) sampling a representative region of the configurational space of the solute/solvent system, and (b) performing spectroscopic calculations, at a high level of theory, on the sampled molecular structures and then obtaining the physical observables from statistical averages. The latter point can be effectively pursued by recently developed QM methods based on post-HF or DFT calculations, especially when second-order properties are considered. In such methods, the environmental effects on the solute molecule are usually taken into account by including explicitly the solvent molecules in the QM treatment[129] or, more efficiently, by embedding the solute in a dielectric continuum that accounts for the solvent polarization.[37] [10] Also, mixed quantum/classical (QM/MM) methods are often used to treat explicitly extended molecular systems at low computational cost, by reducing the expensive ab initio calculations to the chemically important region of the system. [98, 130, 131] Less straightforward is the determination of an accurate and statistically significant sampling of the solute/solvent system, which is, in most cases, unavoidable due to the sensitivity of spectroscopic properties to the specific molecular configurations. First-Principle MD techniques represent the method of choice when high accuracy and reliability are required.[14] Unfortunately, *ab initio* MD simulations have some severe limitations due to the high computational cost: typically, system sizes are limited to few hundreds of atoms and simulation lengths are of the order of tens of picoseconds. Moreover, the usual QM models adopted in *ab initio* MD, for example, DFT with functionals based on the generalized gradient approximation (GGA), may not be accurate enough for reproducing geometrical and energetic features of molecular systems. On the other hand, classical MD methods are computationally very efficient but their reliability is

subject to the implicit approximations included in the empirically derived force fields. Nevertheless, classical MD is well-suited to computing statistical mechanical properties from extended simulations. As a part of the ongoing effort to develop and validate a general protocol for the QM computation of spectroscopic parameters for large molecules in solution, here we discuss an effective and flexible strategy based on both *ab initio* and classical methods. This computational strategy consists of a three-step procedure. (1) The parameterization of a reliable force field for the solute/solvent system to be used in long classical MD simulations. Parameters can be obtained from existing molecular force fields, such as OPLS[132] or AMBER,[133] and also derived, if necessary, from more sophisticated QM calculations and dynamics. In particular, intermolecular potentials can be conveniently adjusted to reproduce solute/solvent radial distribution functions as obtained from *ab initio* MD simulations of model system. (2) The extended sampling of the molecular system via classical MD simulations, whose force field has been previously obtained and tested, using the mean field (MF) method.[134] Briefly, the MF is a continuum model suited for simulation of solute/solvent systems: the solute molecule is placed at the center of a spherical cavity embedded in a dielectric continuum and solvated with a large number (hundreds or thousands) of explicit solvent molecules within the cavity. (3) QM computation of the spectroscopic parameters. Remarkably, for each sampled configuration, the whole molecular system is considered in such calculations, which also includes the dielectric continuum for consistency. As in the case of nitroxide radicals, only few solvent molecules along with the solute should be treated at the QM level, whereas the remaining molecules are included as point charges in what can be more properly named a QM/MM/MF calculation.

In a recent work,[44] it was shown that the MF model is very effective in reproducing the structural and thermodynamic properties of bulk water as well as aqueous solutions of simple solutes, as compared to conventional simulations using periodic boundary conditions (PBC). In this context, the use of the MF model is very well-suited because it elegantly allows retention of the same explicit molecular system, as obtained from the simulated trajectory (step 2) in the QM calculations (step 3). Moreover, the MF model can be conveniently used for QM or mixed QM/MM MD simulations of liquids and solutions [45, 46] by allowing the use of localized basis sets instead of plane waves.

Finally, within the procedure depicted above, a number of strictly system-dependent technical issues have to be addressed, such as the parameterization of a new force-field and the convergence of the spectroscopic properties with the number of configurations. In particular, special care is due to all those features of the molecular force field that highly affect the final results of the computed spectroscopic properties, and not just the geometrical parameters.

In particular, a theoretical investigation on the $n \rightarrow \pi^*$ electronic transition energies and on the ^{13}C and ^{17}O nuclear magnetic shielding constants of the carbonyl group of the acetone molecule in both gas-phase and aqueous solution is presented. Acetone was chosen as a suitable benchmark, given its relatively high polarity and the availability of suitable experimental data. Of course, the system, by itself, is a chemically interesting one; moreover, it can also be regarded as a simple model to probe the general features of the carbonyl-water interaction, which is an issue of still wide chemical and biochemical interest. First, a classical force field was derived for the intra- and intermolecular potentials of acetone from high-level QM calculations and Car-Parrinello MD.[13] Then, a large sampling of both the isolated molecule and the solute/solvent configurational spaces was obtained from MD simulations of about one nanosecond each. Therefore, on structures extracted from these trajectories the spectroscopic observables were computed with high accuracy, obtaining a quantitative agreement with available experimental data.

Methods and computational details

A. Force-field parameters

QM calculations were carried out on acetone and the acetone-$(H_2O)_2$ cluster at different levels of theory to obtain a reliable MM force field for the acetone intra- and inter-molecular interactions. In particular, the Perdew-Burke-Ernzerhov (PBE) functional[102] and its hybrid HF-DFT counterpart,[35] known as PBE0 were tested. As expected, the inclusion of some HF exchange into the functional formulation ensured a better agreement with experimental structural parameters. Also, the results of the latest room-temperature Car-Parrinello dynamics of acetone in aqueous solution[13] were used to adjust the acetone-water intermolecular parameters, as discussed below in the results. All QM results were obtained using the Gaussian03 package.[70]

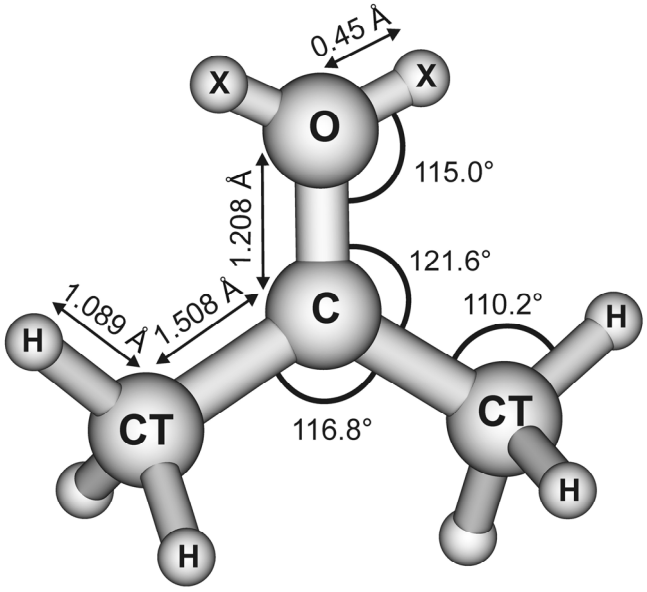

Figure 1. *Structure and atom type labelling of the acetone molecule.*

The final MM parameters are summarized in Table I and the minimum energy configuration, along with the atom-type labels, is depicted in Figure 1.

Table I. *Acetone and acetone/water force field parameters.*

Bonded interactions			Non-bonded interactions		
Parameter[a]	**Value**	**Unit**	**Parameter**	**Value**	**Unit**
D	810.82	kJ mol^{-1}	q_{O}	0.0	
B	2.2636	Å^{-1}	q_{X}	-0.302291	
$r_{CO,0}$	1.2080[b] (1.2170[c])	Å	q_{C}	0.582543	
$k_{b,CC}$	2652.66	kJ mol^{-1} Å^{-2}	q_{CT}	-0.320374	
$r_{CC,0}$	1.5088	Å	q_{H}	0.1104645	
$k_{b,CH}$	2845.12	kJ mol^{-1} Å^{-2}	$\varepsilon_{O,H}$	0.46965	kJ mol^{-1}
$r_{CH,0}$	1.0895	Å	$\sigma_{O,H}$	2.9500	Å
$k_{\theta,OCC}$	669.44	kJ mol^{-1} rad^{-2}	$\varepsilon_{CT,H}$	0.09310	kJ mol^{-1}
$\theta_{OCC,0}$	121.79	deg	$\sigma_{CT,H}$	3.0000	Å
$k_{\theta,CCC}$	527.18	kJ mol^{-1} rad^{-2}	$\varepsilon_{H,H}$	0.12552	kJ mol^{-1}
$\theta_{CCC,0}$	116.43	deg	$\sigma_{H,H}$	2.5000	Å
$k_{\theta,CCH}$	418.40	kJ mol^{-1} rad^{-2}	$\varepsilon_{Ow,O}$	0.76427	kJ mol^{-1}
$\theta_{CCH,0}$	110.26	deg	$\sigma_{Ow,O}$	3.2980	Å
$k_{\theta,HCH}$	292.88	kJ mol^{-1} rad^{-2}	$\varepsilon_{Ow,C}$	0.53438	kJ mol^{-1}
$\theta_{HCH,0}$	108.62	deg	$\sigma_{Ow,C}$	3.4580	Å
k_{ξ}	115.0	kJ mol^{-1} rad^{-2}	$\varepsilon_{Ow,CT}$	0.42367	kJ mol^{-1}
ξ_0	0.0	deg	$\sigma_{Ow,CT}$	3.3330	Å
k_{OCCH}	1.6736	kJ mol^{-1}	$\varepsilon_{Ow,H}$	0.28564	kJ mol^{-1}
n_{OCCH}	1		$\sigma_{Ow,H}$	2.5830	Å
$\phi_{OCCH,0}$	0.0	deg			
k_{OCCH}	0.16736	kJ mol^{-1}			
n_{OCCH}	3				
$\phi_{OCCH,0}$	180.0	deg			

(a) ξ is the OCCC improper dihedral angle; (b) gas-phase parameter; (c) condensed-phase parameter.

The important C=O bond stretching and out-of-plane modes of acetone were fitted on QM data with a Morse and harmonic potentials respectively, whereas all other force constants were taken from the OPLS-AA force field, and the equilibrium values were scaled to agree with QM-optimized structures. Note that two dummy atoms (atom label

X) representing the oxygen lone pairs, which are usually absent in standard force fields, were included to account for the hydrogen bond directionality. Partial charges of the acetone were computed by fitting an *ab initio*-derived electrostatic potential on a grid of points around the molecule, according to the RESP procedure.[135] The water model adopted for the MM calculations of the cluster and aqueous solution is the popular simple-point-charge (SPC) model.[119] A modified version of the GROMACS package was used for all the MM and MD calculations.

B. Classical molecular dynamics

Classical MD simulations of acetone in the gas-phase and in aqueous solution were performed in a canonical *ensemble* (NVT) at 300 K. In both cases, the overall simulation length was 1 ns, including an initial equilibration of 400 ps. The condensed-phase molecular dynamics has been carried out using the MF model with spherical boundary conditions.[134] It consists on simulating explicitly a molecular system, such as a liquid or a solution, inside a cavity of a continuum, which accounts for the long-range interactions with the environment, thus avoiding the use of periodic boundary conditions that, in principle, could introduce unwanted correlation effects. In particular, the MF model includes both an electrostatic reaction field and a dispersion-repulsion contribution. In this work, the acetone molecule, solvated with 1111 SPC water molecules ((N_{water} + 1) / V = 33.184 nm^{-3}), was placed at the center of a spherical cavity embedded in the continuum medium. The roto-traslation motions of the solute were removed during the dynamics. All simulations were performed in double precision with a modified version of the GROMACS simulation package, which includes the MF model and the Gaussian isokinetic thermostat.

C. Quantum-mechanical calculations of spectroscopic properties

All the spectroscopic properties were computed using the Gaussian03 package.[70] Excitation energies were computed within the Time-Dependent (TD)-DFT formalism [136] employing the PBE0 functional and a basis set that combines the 6-311++G(2d,2p) on the carbonyl atoms, namely C and O, and the 6-31+G(d,p) on the other acetone and water atoms (henceforth denoted as [6-311++G(2d,2p), 6-31+G(d,p)]). The consistency of this basis set has been already proven in other recent

work, in which it was successfully applied to the computation of UV parameters.[13] All the calculations of nuclear magnetic shielding tensors were carried out using the gauge-including atomic orbital (GIAO) formalism:[137]

$$\sigma_{ji} = \left[\frac{\partial^2 E}{\partial B_i \partial \mu_j} \right] = \sum_{\alpha,\beta} D_{\alpha\beta} \frac{\partial^2 h_{\alpha\beta}}{\partial B_i \partial \mu_j} + \sum_{\alpha,\beta} \frac{\partial D_{\alpha\beta} \partial h_{\alpha\beta}}{\partial B_i \partial \mu_j}$$

where σ_{ji} is the ji^{th} component of the shielding tensor, B_i is the i^{th} component of the external magnetic field and μ_j is the j^{th} component of the nuclear magnetic moment; $D_{\alpha\beta}$ and $h_{\alpha\beta}$ are generic elements of the one-electron density and Hamiltonian matrix, respectively in the GIAO basis. The isotropic shielding (σ_{iso}) is defined as one-third of the trace of the shielding tensor. The same [6-311++G(2d,2p), 6-31+G(d,p)] basis set was also employed for the NMR shielding tensor calculations at the PBE0 and at the Møller-Plesset second order perturbation theory (MP2)[138] levels of theory. The spectroscopic data were computed on different frames extracted from the gas phase and from the aqueous solution dynamics, after testing the sampling set in order to achieve a consistent number of snapshots and ensure converged average parameters. The solvent was taken into account within the MF approach in close agreement to the MD simulations. Water molecules embedded into the continuum sphere, modelling the polarizable medium, were treated as point charges and the closest water molecules to the carbonyl oxygen were included together to the acetone molecule into the QM layer. The charges on water atoms are those of the SPC model and both the sampling set and the number of water molecules to be included into the QM region were tested.

Results and Discussion

A. Force-field parameterization

The gas-phase structure of the acetone molecule is known experimentally from electron diffraction spectroscopy,[139] and was used as a reference to test the accuracy of the *ab initio* calculations as well as the molecular mechanics force field. First, we carried out QM calculations of acetone at different levels of theory to determine the optimal combination of *ab initio* methodology and basis set. To this end, both the PBE

functional and its hybrid HF-DFT counterpart, the PBE0, have been tested. The consistency of the structural parameters computed with the PBE0 functional was also checked with different basis sets, from double and triple ζ of Pople' series to the correlation consistent triple ζ of Dunning' series. Acetone structural parameters as obtained from experiments and computations are listed in Table II.

A significant difference in the computed values between PBE and PBE0 with the same 6-31+G(d,p) basis set is observed: the hybrid functional increases the accuracy of the bond distances, whereas the angle values are not affected. Among the basis sets considered with the PBE0 functional, the triple-ζ set of the Pople' series, with diffuse and d-polarization functions on carbon and oxygen and p-polarization functions on hydrogen atoms, provides geometrical parameters which are consistent with much larger basis sets, like cc-pVTZ and Aug-cc-pVTZ, and are in close agreement to experiments, with the exception of the C-H bond. Note that the experimental value of the latter is affected by a larger error and all computational results reported in this work are consistent.

Table II. *Geometrical parameters of acetone molecule. Bond distances are in Å, angles in degrees.*

	C = O	**C – C**	**C – H**	**C – C – C**	**C – C = O**
PBE 6-31+G(d,p)	1.229	1.520	1.102	116.6	121.7
PBE0 6-31+G(d,p)	1.214	1.510	1.094	116.6	121.7
PBE0 6-311+G(d,p)	1.208	1.509	1.090	116.4	121.8
PBE0 cc-pVTZ	1.206	1.507	1.091	116.4	121.8
PBE0 Aug-cc-pVTZ	1.207	1.506	1.091	116.4	121.8
MM	1.208	1.508	1.089	116.8	121.6
Exp.[a]	1.210(0.003)	1.507(0.002)	1.076(0.006)	116.7(0.3)	121.7[b]

(a) Ref. [139]; (b) assumed value

After all these tests we have found that PBE0/6-311+G(d,p) represents the best compromise between accuracy and efficiency, and all QM calculations used in the force field parameterization have been performed at this level of theory.

The acetone MM structure is also listed in Table II: a very good agreement with both high-level QM calculations and experimental data was obtained. PBE0/6-311+G(d,p) calculations were performed in order to fit a Morse potential for the C=O bond stretching (Eq. 1):

$$V_{bond}(r) = D\left[1 - \exp\left(-B\left(r_{CO} - r_{CO,0}\right)\right)\right]^2 \quad (1)$$

where D, B, and $r_{CO,0}$ are the usual Morse parameters. This functional form, rather than the usual harmonic potential, was chosen to account for the anharmonic character of the bond. Also, the harmonic dihedral parameters that correspond to the out-of-plane mode of the acetone were fitted at the same level of theory, thus ensuring a reliable force constant (Eq. 2):

$$V_{dihedral}(\xi) = k_{\xi}\left(\xi - \xi_0\right)^2 \quad (2)$$

where ξ is the dihedral angle and k_{ξ} the corresponding force constant (see Table I for parameter values). The correct sampling of these two modes during the dynamics was found to be crucial for an accurate calculation of the spectroscopic properties. Moreover, lone pairs have been added to the oxygen atom of the acetone molecule in order to reproduce the QM minimum energy structure of the acetone-$(H_2O)_2$ cluster: the correct hydrogen bond geometry, as shown in Table III, has been obtained with an O-X distance of 0.45 Å and a C=O-X angle of 115° (see Fig. 1).

Table III. *Geometric parameters of the Acetone–$(H_2O)_2$ cluster. QM corresponds to PBE0/6-311+G(d,p) calculations, MM corresponds to force field calculations, as given in Table I. Water atoms are indicated by the subscript W. Bond distances are in Å, angles in degrees.*

	MM	**QM**	**QM+PCM**
O … H_w	1.91	1.91	1.88
O … O_w	2.91	2.85	2.85
C = O … H_w	115.4	117.2	126.4
O … O_w – H_w	1.8	12.2	0.2
C=O	1.211[a] (1.220[b])	1.221	1.224

(a) value obtained with r_0 = 1.2080 Å; (b) value obtained with r_0 = 1.2170 Å.

Note that commonly used force fields, such as OPLS, CHARMM and AMBER, do not include lone pairs attached to the carbonyl oxygen and therefore are unable to provide some basic features of the hydrogen bond pattern. Also, it was necessary to impose a different equilibrium distance, r_0, for the C=O bond in the condensed phase simulation with respect to the gas phase ($r_{0,\text{gas-phase}}$ = 1.2080 Å; $r_{0,\text{cond.-phase}}$ = 1.2170 Å) to account for the elongation of the carbonyl, as observed in Table III. The C=O bond stretching is a result of the polarization effect of the solvent, which induces a change of the bond order from a purely double bond character to a mixed double/single bond. Such a structural modification ultimately depends on an electron-density rearrangement and cannot be trivially obtained with an effective force field. For such a reason, we decided to use two different parameters for the MM equilibrium distance of the carbonyl (see Table I), according to high-level *ab initio* molecular geometries.

***Table IV**. Average geometrical parameters of the acetone molecule from gas phase and aqueous solution dynamics Bond distances are in Å, angles in degrees, standard deviations inter parenthesis.*

	C = O	**C – C**	**C – H**	**C – C – C**	**C – C = O**
Gas-phase MM[a]	1.209 (0.002)	1.514 (0.003)	1.089 (0.002)	116.9 (1.1)	121.4 (0.6)
Gas-phase CPMD	1.23 (0.02)	1.52 (0.04)	1.11 (0.04)	116.9 (5.3)	121.4 (4.3)
Solution MM[b]	1.222 (0.002)	1.511 (0.002)	1.090 (0.001)	115.7 (0.6)	121.5 (0.5)
Solution CPMD	1.25 (0.01)	1.50 (0.03)	1.11 (0.02)	117.4 (3.1)	121.0 (3.4)

(a) value obtained with r_0 = 1.2080 Å; (b) value obtained with r_0 = 1.2170 Å.

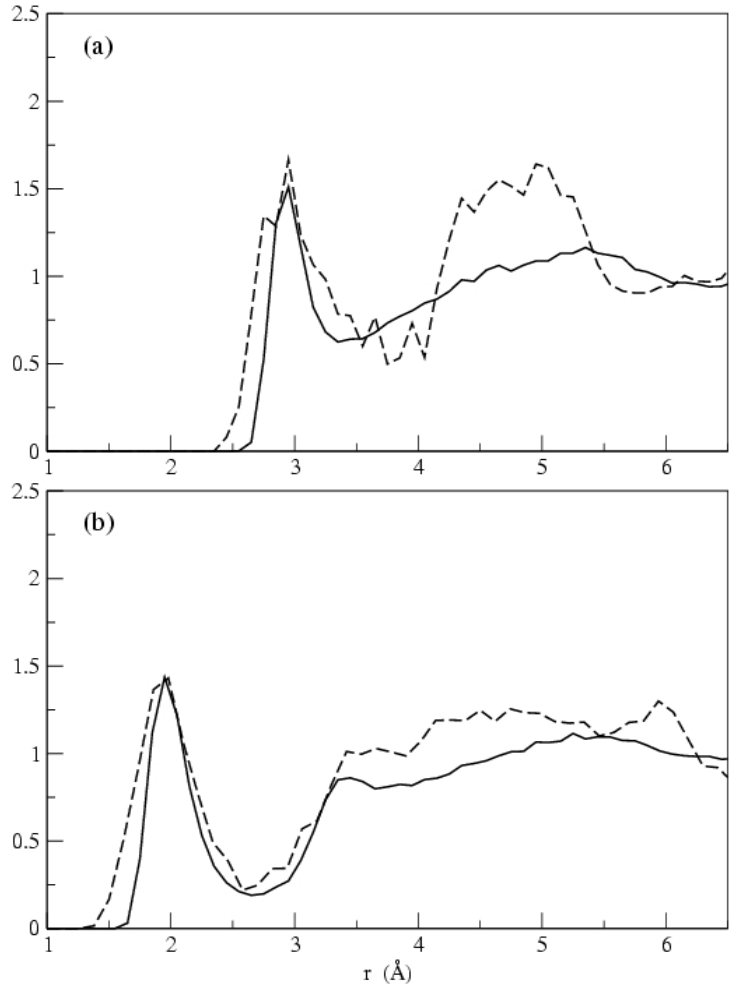

Figure 2. *(a) O(acetone)-O(water) and (b) O(acetone)-H(water) radial distribution functions. Solid line, MM molecular dynamics; dashed line, Car-Parrinello molecular dynamics.*

Furthermore, it is interesting to note that solvent has a negligible effect on the C=O bond distance beyond the two closest water molecules (~0.003 Å), as shown by the inclusion of solvent effect in the geometry optimization with the PCM model (see last column of Table III), which is also consistent with MM results (for acetone-$(H_2O)_2$ cluster: $r_{C=O}$ = 1.220 Å; for acetone in solution: $r_{C=O}$ = 1.222 Å, see Table IV).

Finally, the acetone/water intermolecular parameters, for example the Lennard-Jones interaction between the oxygen atoms, were adjusted to let structural properties to agree with our previous condensed-phase CPMD simulation[13] (see Figure 2).

B. Molecular dynamics simulations

Constant-temperature MD simulations of acetone at 300 K in both vacuum and aqueous solution were carried out to produce a large sampling of the configurational space. Here, we compare the results of the classical (MM) dynamics with the *ab initio* MD simulations, based on the Car-Parrinello scheme and the PBE density-finctional. Note that, as usual, CPMD simulations were quite short (about 5.5 ps), and, in some cases, only a qualitative comparison with MM results is possible.

In Table IV, some average geometrical parameters of acetone are reported. Overall the molecular structure has not changed significantly in going from gas-phase to liquid: only the C=O bond is slightly elongated, as a result of the interactions with the solvent. The main difference between CPMD and MM values consists of the C=O average distance. The MM carbonyl group was parameterized with an improved density-functional (PBE0) with respect to CPMD (PBE).

In condensed phase, the hydrogen bond arrangement is very similar in both *ab initio* and classical simulations, as shown by different structural analyses. The $O_{acetone}$-O_{water} and $O_{acetone}$-H_{water} radial distribution functions (RDFs) are comparable, as shown in Fig. 2: the first peaks show remarkably the same positions and heights, whereas a significant deviation is observed in the RDFs at larger distance. However, CPMD results are clearly too noisy due to the poor statistics and a detailed comparison seems meaningless. Somewhat more reliable are the results of the average number of hydrogen bonds formed by acetone and water, the corresponding distribution of one, two and three hydrogen bonds, and the average $O_{acetone}$-H_{water} distance: as reported in Table V,

Table V. *Acetone–water hydrogen bonds.*

	CPMD	**MM**
average number of hydrogen bonds[a]	2.1	2.0
% of 1 hydrogen bond	17	15
% of 2 hydrogen bonds	52	66
% of 3 hydrogen bonds	31	19
O … H_w	1.99 Å	2.06 Å

(a) H-bond criteria: (C)O…H(O)$_{water}$ ≤ 2.6 Å; (C)O…O $_{water}$ ≤ 3.5 Å; ∠ (C)O…H-O $_{water}$ ≤ 30°

MM and CPMD results agree nicely. Note that, in agreement with CPMD, a non negligible number of configurations in the MM simulation show one or three hydrogen bonds, with a slight preference for the latter. Further, we want to stress once more the importance of the inclusion of the lone pairs to the oxygen atom of the acetone molecule. In Figure 3, the structural effect of the lone pairs on the angular distribution of the hydrogen bonds is depicted. As expected, water molecules lie preferentially close to the acetone molecular plane (Fig. 3b), whereas the absence of lone pairs generates a spherically symmetric distribution around the carbonyl (Fig. 3a).

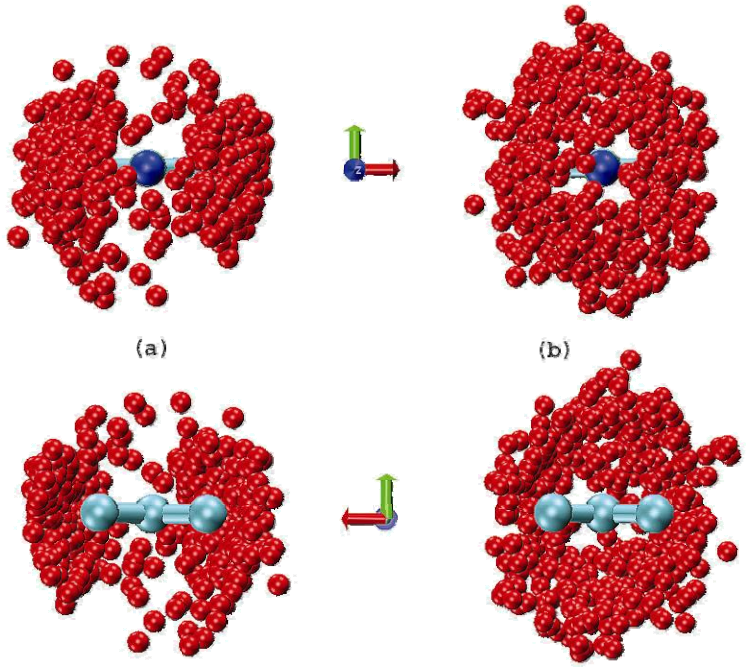

Figure 3. *Distribution of the water molecules that form hydrogen bonds with acetone: (a) acetone with lone pairs on the oxygen atom, (b) acetone without lone pairs on the oxygen atom; acetone oxygen is depicted in blue, carbon in light blue and water oxygens in red;. (hydrogen atoms are omitted for clarity).*

C. Spectroscopic parameters

In this section, we compare the solvent shifts of $n \rightarrow \pi^*$ electronic transition energy, ^{13}C and ^{17}O nuclear magnetic shieldings for the passage from gas-phase to aqueous solution obtained by high-level QM computations with their experimental counterparts.[43, 140, 141] According to the methodological approach proposed above, we extracted a large number of molecular configurations from the simulated trajectories

and we obtained the spectroscopic observables as averages of the corresponding computed parameters on each configuration. Depending on the molecular system considered and on the specific spectroscopic property, some technical issues should be addressed, such as the choice of the QM method, the size of the QM layer in the QM/MM calculations and the number of configurations required to reach a convergence of the computed spectroscopic values. UV transition energies were evaluated with the TD-DFT approach and NMR shieldings by GIAO-DFT calculations using in both cases the same level of thoey, PBE0 / [6-311++G(2d,2p), 6-31+G(d,p)]. NMR parameters were also computed at the MP2 level for comparison.

***Table VI**. Convergence of NMR parameters as a function of the number of explicit water molecules included in the QM layer.*

	σ_{iso} (ppm)[a]	σ_{iso} (ppm)[b]
0 QM + MM	- 258	- 249
2 QM + MM	- 253	- 243
3 QM + MM	- 253	- 244
5 QM + MM	- 252	- 241
0 QM + PCM	- 299	- 289
2 QM + PCM	- 261	- 243
3 QM + PCM	- 258	- 245
0 QM	-362	-349
2 QM	-	-283
3 QM	-	-280
5 QM	-	-260
35 QM	-	-235
55 QM	-	-239

(a) average values computed on 100 configurations; (b) values computed on one specific configuration

Some tests were carried out to check the convergence of spectroscopic parameters with the number of water molecules treated at the QM level along with the acetone, while the remaining solvent molecules are included in the Hamiltonian as point charges according to the SPC model (MM).

Table VII. *$n \rightarrow \pi^*$ excitation energies computed at the PBE0/6-311++G(2d,2p)/6-31+G(d,p) level as a function of the number of explicit water molecules included into the QM layer. MM waters are represented by SPC point charges and average values are computed over 100 configurations.*

	$\Delta E_{(n-\pi^*)}$ (eV)
0 QM + MM	4.56
2 QM + MM	4.57
3 QM + MM	4.57
5 QM + MM	4.57

In Table VI and Table VII, we report the results for the NMR ^{17}O shieldings and the $n \rightarrow \pi^*$ excitation energy, respectively, computed with 0, 2, 3 and 5 QM water molecules. In Table VI we also have included for comparison the results obtained by applying the PCM model directly on the QM region (*x*QM+PCM), that is, avoiding the inclusion of any point charges, and the values obtained for clusters of different size without the continuum (*x*QM). In particular, the slow convergence with cluster size of the computed NMR shieldings, as observed for one particular molecular configuration (see *x*QM results in last column of Table VI), clearly demonstrates the importance of the inclusion of long-range bulk solvent effects, either by continuum models (e.g. PCM) or by explicit point charges (MM). Moreover, the full QM result for the acetone-$(H_2O)_{55}$ cluster, σ_{iso}= -239 ppm, computed on a specific molecular configuration, is very close to the result obtained considering only 5 water molecules in the QM region, σ_{iso}= -244 ppm, for the same cluster (5 QM + 50 MM). Remarkably, the two approaches that include solvent effects (*x*QM+PCM and *x*QM+MM) do converge to values in close agreement to each other (a difference of about 5 ppm should be considered within the statistical error), and are both computationally very efficient for a given size of the QM region. It should be pointed out that, in general, a very limited number of water molecules, typically those which form hydrogen bonds with the carbonyl group, have to be included in the QM region in order to obtain an acceptable accuracy, as noted in our previous work. Here, we have found that UV energies are not very much affected by the number of QM water molecules, whereas NMR results are unchanged only with two or more QM molecules. In the latter case, the inclusion of quantum effects in the treatment of solute-solvent interactions is crucial, so that perturbative approaches, which account

only for the electrostatic contribution of the environment, are expected to be inadequate. In the following, according to the proposed methodology, we always performed spectroscopic calculations with the two closest water molecules to the carbonyl oxygen treated at QM level and the remaining water molecules treated as point charges plus a reaction field.

The accuracy of the spectroscopic observables was tested against the number of uncorrelated molecular configurations obtained from the MD simulations. As shown in Figure 4, few tens of configurations represent already a statistically significant data set for an accurate estimate of the spectroscopic parameters, both in gas-phase and in solution. Due to the low computational cost of such calculations, the results reported in the following are obtained from averages over 100 molecular configurations taken from the simulated trajectories at evenly spaced time intervals.

Table VIII. *Isotropic shielding constants (ppm) of acetone in the gas phase and in aqueous solution, PBE0 and MP2 calculation were carried out with the 6-311++G(2d,2p)/6-31+G(d,p) basis set. Aqueous solution data were computed including the two closest water molecules into the QM layer. Gas phase and aqueous solution results are averaged over 100 configurations.*

		PBE0	**MP2**	**Exp.**[a]
^{13}C	gas-phase	- 23	- 9	-
	solution	- 42	- 28	-
	$\Delta_{solvent}$	- 19	- 19	- 18.9
^{17}O	gas-phase	- 340	- 265	-
	solution	- 253	- 200	-
	$\Delta_{solvent}$	+ 87	+ 65	+ 75.5

(a) from ref.[141] *and* [43].

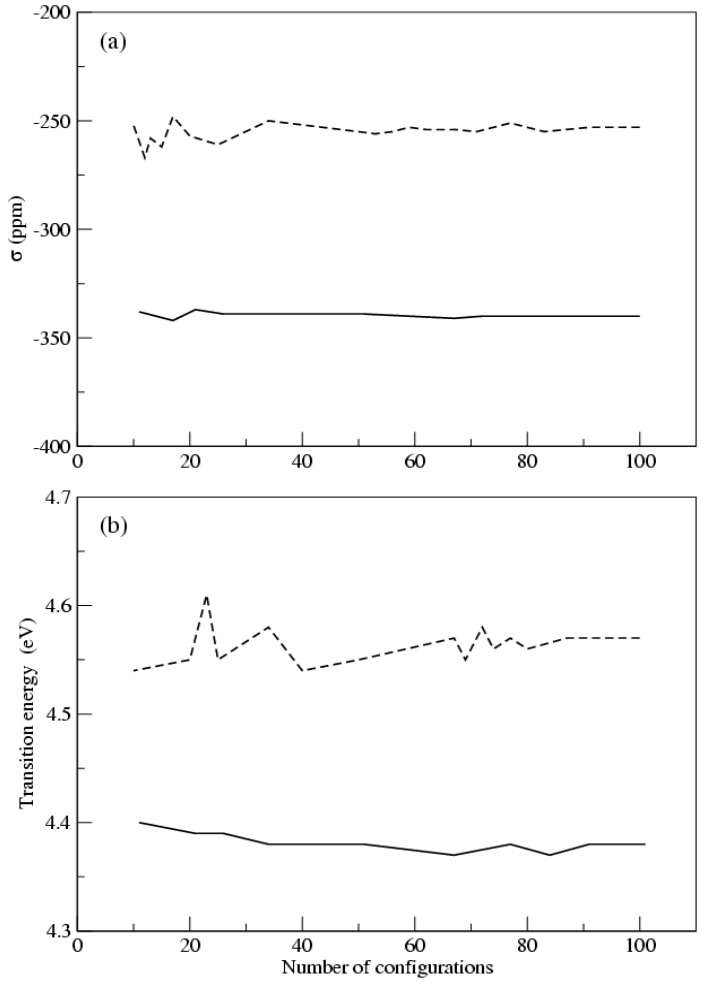

Figure 4. *(a) Average ^{17}O isotropic shielding constant of acetone as a function of the number of configurations. (b) Average $n \rightarrow \pi^*$ excitation energy as a function of the number of configurations. Solid line, gas phase; dashed line, aqueous solution. Aqueous solution data were computed including the two closest water molecules into the QM layer.*

In Table VIII, the ^{13}C and ^{17}O isotropic shielding constants relative to the corresponding carbonyl atoms of acetone are reported, as obtained from the acetone gas-phase and aqueous solution molecular dynamics and computed at both PBE0 and MP2 level of theory. The change on the ^{13}C NMR shieldings in going from gas-phase to liquid has shown no differences between PBE0 and MP2 results, and, notably, is in excellent agreement with experiment. On the other hand, the calculated ^{17}O shielding constants are somewhat less accurate: PBE0 overestimates the solvent effects on the NMR shieldings (σ_{iso} = 87 ppm) with respect to experiment (σ_{iso} = 75.5 ppm), whereas MP2 underestimates the same measure (σ_{iso} = 65 ppm). However, an error of about 10 ppm

should be considered acceptable and, besides, it should be noted that no scaling factors or other kind of corrections, based on empirical considerations, were applied to the reported results. Moreover, the solvent shifts of ^{13}C and ^{17}O shielding constants computed at the PBE0 level on the CPMD trajectories are respectively -23.1 and 105, which are significantly different from experiment due to the overestimated C=O bond length. Finally, the computed and experimental results for the $n \rightarrow \pi^*$ excitation energy are shown in Table IX: the agreement is apparent and, in particular, the solvent effect, as given by the blue shift in the energy band, is very well reproduced.

Table IX. *$n \rightarrow \pi^*$ excitation energy (eV). TD-DFT computations were performed by using the PBE0 functional and the 6-311++G(2d,2p)/6-31+G(d,p) basis set. Aqueous solution data were computed including the two closest water molecules into the QM layer. Gas phase and aqueous solution results are averaged over 100 configurations.*

	PBE0	**Exp[a]**
Gas-phase	4.38	~ 4.5
Solution	4.57	~ 4.7
$\Delta_{solvent}$	0.19	~ 0.2

(a) from ref. [140].

Conclusions

In the present chapter, a reliable and computationally efficient approach has been reported for the theoretical evaluation of spectroscopic observables of molecules in solution. Such challenging problem requires that solvent effects and thermal fluctuations of the molecular conformations should be properly taken into account. Our procedure has been schematically divided in three successive steps: (a) the parameterization of an effective classical force field for the solute intra-molecular and solute/solvent inter-molecular interactions, (b) the sampling of the configurational space of the system via molecular dynamics simulations using the MF model and (c) the QM computation of spectroscopic parameters on a representative set of molecular configurations. This computational approach has been illustrated considering as a first test case the acetone molecule in aqueous solution, which has extensively been studied both experimentally and, more recently, theoretically by different groups. First, we have shown that classical MD based on a reliable force field compares favourably with

CPMD simulations, as shown by acetone-water RDFs and hydrogen bond distributions, and can be used effectively to obtain extended sampling of the solute/solvent configurations. To remark once more the importance of point (a), it should be noted that it was necessary to modify standard OPLS-AA force field for acetone by including oxygen lone pairs and improve some geometrical features, such as the C=O stretching and out-of-plane mode, by an accurate re-parameterization. Indeed, force-field based MD could provide more reliable molecular geometries, and indirectly spectroscopic properties as seen for ^{13}C and ^{17}O shielding constants, with respect to standard Car-Parrinello MD, due to the well-known limitations of the DFT functionals used in the latter. Besides, the MF model has shown to be an effective methodology for simulating solute/solvent systems and particularly well-suited for post-*ab initio* calculations of spectroscopic parameters. Then, it has been shown how a mixed QM/MM approach can accurately reproduce experimental spectroscopic observables of acetone, such as NMR shielding constants and $n \rightarrow \pi^*$ excitation energy, once provided that an appropriate level of theory and a suitable number of solvent molecules are treated at QM level along with the solute. In particular, the present approach has the advantage of being highly flexible as far as it concerns the QM model used for the post-MD calculations, i.e., DFT or post-HF methods, and was found to be equivalent to more expensive full QM calculations as well as QM calculations using the PCM model, as shown for the case of acetone ^{17}O NMR chemical shifts. Moreover, it is worth noting that our procedure, due to a much longer simulation time scale, has provided results with a significant smaller statistical error for the computed UV transition energies than previous results based on full QM and QM/MM molecular dynamics simulations.

Conclusions and perspectives

The main topic of the work summarized in the thesis is the development and the successful application of an integrated computational approach to modelling complex physico-chemical processes from first principles. Such an approach consists of combining new developed density-functional models, *ab initio* and/or classical molecular dynamics, and discrete-continuum (QM/PCM) or hybrid approaches (QM/MM, QM/MM/MF) in order to predict accurate molecular parameters, to investigate thermal fluctuations, and to account for environmental effects. In particular, the spectroscopic properties of model systems with biological and technological relevance have been investigated: i.e., the EPR parameters of nitroxide spin probes in different protic solutions, the NMR and optical properties of the carbonyl group in the acetone-water system, and the aromatic π-π interaction in the prototypical case of the benzene dimer.

From the methodological point of view, three main achievements can be underlined: (1) the set up and validation of a scheme that combines molecular dynamics and *a posteriori* calculations of spectroscopic properties by means of high level *ab intio* methods; (2) the development of a protocol for the parameterization of classical force fields, based on first-principle molecular dynamics and DFT calculations; (3) the addition of a semi-empirical correction term to DFT for taking into account dispersion interactions.

Regarding the evaluation of spectroscopic properties of molecular systems in solution, Car-Parrinello molecular dynamics of nitroxide free radicals in aqueous and methanolic solutions were carried out: extraction of solute-solvent configurations from the trajectories and comparison with minimum-energy structures highlighted the delicate balance of bulk solvent effects and explicit hydrogen-bond interactions. Thus, a proper scheme to set discrete-continuum calculations (QM/PCM) of EPR parameters has been identified from the analysis of the hydrogen bonding networks. In the case of the acetone aqueous solution, a new classical force field was developed on the basis of Car-Parrinello simulations and high level *ab initio* calculations: the proposed MM potential was used to obtain trajectories on the time scale of nanoseconds within the framework

of a non-periodic mean-field approach for the simulation of molecular liquids. Then, similarly to the MD simulations, the hybrid QM/MM/MF scheme was exploited for computing the ^{13}C and ^{17}O magnetic shieldings and n-π^* electronic transition energy of the acetone molecule on a consistent set of structures extracted from the trajectories. The well-known failure of commonly used density functionals to describe van der Waals interactions has been also addressed. The addition of a semi-empirical term accounting for dispersion to hybrid density-functionals provided the best compromise between accuracy and computational feasibility. The implementation of this method for studying the benzene dimer provided results in quantitative agreement with expensive post-Hartree-Fock methods in a fraction of computer time. Furthermore, beyond the description of stationary points along the potential energy surface, it allowed to compute vibrational frequencies and to perform *ab initio* molecular dynamics. According to the simple concept that weak forces correspond to large amplitude motions, our results highlighted the importance of zero-point vibrational energies and thermal fluctuations for a consistent comparison between computed data and experimental observations.

In conclusion, the proposed computational approach ensured an excellent agreement between predicted spectroscopic parameters and experimental data. Eventually, the study of semi-empirically corrected density functionals could be further developed by the formulation of a brand-new functional, which integrates the proposed dispersion correction with a kinetic-energy dependent exchange-correlation functional (meta-GGA) and with the long-range corrected (LC) inclusion of HF exchange, since they amend the self-interaction error and the incorrect asymptotic behaviour of hybrid HF-DFT exchange, respectively. On these grounds, *ad hoc* force-fields for classical molecular dynamics will be parameterized, which will allow simulations long enough to compute spectroscopic properties for complex systems, e.g., for supporting the interpretation of EPR experiments carried out for spin probes embedded in biological macromolecules. Within this context, it is worth noting that the proposed approach for the *ab initio* evaluation of magnetic tensors is currently being and will be further integrated with methods based on the stochastic Liouville equation (SLE), which allow to predict EPR spectral shapes. This further step paves the route toward quantitative evaluations of EPR spectra in different phases and large temperature intervals starting from the chemical formula of the radical and the physical parameters of the solvent.

Appendix A

Electron Paramagnetic Resonance parameters of organic free radicals

The direct characterization of organic free radicals, generally short-lived species, is quite difficult: electron paramagnetic resonance (EPR) spectroscopy emerged as the most effective technique to detect and characterize them in different conditions and environments.[142, 143] Up to the last years EPR has been essentially a continuous wave (cw) method, i.e. the samples sitting in a static magnetic field were irradiated by a continuous microwave (mw) electromagnetic field to drive electron spin transitions. Despite the breakthroughs in nm and sub-nm microwave technologies in the last decade, a peaceful coexistence between cw and pulse EPR will continue to persist and will be determined entirely by the sample properties and relaxation times. The difference of EPR with respect to nuclear magnetic resonance (NMR) spectroscopy, where pulse techniques have completely replaced cw ones, is related to the shorter relaxation times (μs in place of ms), which imply severe technical problems connected to the generation of pulses and the handling of transient signals in the ns time scale. At the same time, for low-symmetry species, particularly in frozen solution samples, standard EPR suffers from low spectral resolution due to strong inhomogeneous broadening. Such problems arise, for instance, because several radical species or different magnetic sites of rather similar characteristics are present, or quite small anisotropies of the magnetic tensors do not allow observation of canonical orientations in the powder EPR spectrum. Some of these situations can effectively be dealt with by electron-nuclear-double (ENDOR) or even triple (TRIPLE) resonance techniques, which can be seen as variants of NMR on paramagnetic systems, the unpaired electron serving as highly sensitive detector for the NMR transitions. In other circumstances high-field EPR can be of help since unresolved

hyperfine interactions do not depend on the magnetic field, whereas the Zeeman interactions are field dependent. Thus, measurements at various field/frequency settings allow to separating different interactions in complex biological systems. The above experimental developments represent powerful tools for the exploration of molecular structure and dynamics, complementary to other techniques. However, as is often the case for spectroscopic techniques, only interaction with effective and reliable computational models allows interpretation in structural and dynamical terms. The tools needed by EPR spectroscopists are from the world of quantum mechanics (QM), as far as the parameters of the spin Hamiltonian are concerned, and from the world of molecular dynamics (MD) and statistical thermodynamics for the simulation of spectral line-shapes. The introduction of methods rooted into the Density Functional Theory (DFT) represents a turning point for the calculations of spin-dependent properties.[6, 144, 145] Before DFT, QM calculations of magnetic tensors were either prohibitively expensive already for medium size radicals[146, 147] or not sufficiently reliable for predictive and interpretative purposes. Today, last generation density-functionals and purposely tailored basis sets allow to computing magnetic tensors in remarkable agreement with their experimental counterparts:[6, 41, 117, 144, 145] computed data can take into the proper account both average environmental effects and short-time dynamical contributions like, e.g., vibrational averaging from intramolecular vibrations and/or solvent librations ,[123, 148-150] therefore providing a set of tailored parameters that can be confidently used for further calculations. The other challenging experimental-theoretical match, EPR spectral shape versus probe dynamics, has a long history too. The two limits of essentially fixed molecular orientation as in a crystal, and of rapidly rotating probes in solutions of low viscosity (Redfield limit),[151] have been overcome by methods based on the stochastic Liouville equation (SLE), allowing the simulation of spectra in any régime of motion and in any type of orienting potential.[91-93] The ongoing integration of the above two aspects, namely improved QM methods for the calculation of magnetic tensors, and effective implementations of SLE approaches for increasing numbers of degrees of freedom, paves the route toward quantitative evaluations of EPR spectra in different phases and large temperature intervals starting from the chemical formula of the radical and the physical parameters of the solvent.[90] Here, the main framework of a recently proposed general model is sketched, paying the most attention

to the ab initio computation of magnetic parameters, whereas the problem of spectral line-shapes will be only briefly illustrated.

The general model

The calculation of ESR observables can be in principle based on a 'complete' Hamiltonian $\hat{H}\left(\{\mathbf{r}_i\},\{\mathbf{R}_k\},\{\mathbf{q}_\alpha\}\right)$, including electronic $\{\mathbf{r}_i\}$ and nuclear $\{\mathbf{R}_k\}$ coordinates of the paramagnetic probe together with solvent coordinates $\{\mathbf{q}_\alpha\}$:

$$\hat{H}\left(\{\mathbf{r}_i\},\{\mathbf{R}_k\},\{\mathbf{q}_\alpha\}\right)=\hat{H}_{\text{probe}}\left(\{\mathbf{r}_i\},\{\mathbf{R}_k\}\right)+\hat{H}_{\text{probe-solvent}}\left(\{\mathbf{r}_i\},\{\mathbf{R}_k\},\{\mathbf{q}_\alpha\}\right)+\hat{H}_{\text{solvent}}\left(\{\mathbf{q}_\alpha\}\right) \quad (1)$$

Any spectroscopic observable can then be linked to the density matrix $\hat{\rho}\left(\{\mathbf{r}_i\},\{\mathbf{R}_k\},\{\mathbf{q}_\alpha\},t\right)$ governed by the Liouville equation

$$\begin{aligned}\frac{\partial}{\partial t}\hat{\rho}\left(\{\mathbf{r}_i\},\{\mathbf{R}_k\},\{\mathbf{q}_\alpha\},t\right)&=-i\left[\hat{H}\left(\{\mathbf{r}_i\},\{\mathbf{R}_k\},\{\mathbf{q}_\alpha\}\right),\hat{\rho}\left(\{\mathbf{r}_i\},\{\mathbf{R}_k\},\{\mathbf{q}_\alpha\},t\right)\right]\\&=-\hat{\mathcal{L}}\left(\{\mathbf{r}_i\},\{\mathbf{R}_k\},\{\mathbf{q}_\alpha\}\right)\hat{\rho}\left(\{\mathbf{r}_i\},\{\mathbf{R}_k\},\{\mathbf{q}_\alpha\},t\right)\end{aligned} \quad (2)$$

Solving Eq. (2) as a function of time would allow, in principle, a direct evaluation of $\hat{\rho}\left(\{\mathbf{r}_i\},\{\mathbf{R}_k\},\{\mathbf{q}_\alpha\},t\right)$ and hence calculation of any molecular property. However, the diverse time scales characterizing different sets of coordinates allow to introduce a number of generalized adiabatic approximations. In particular, the nuclear coordinates $\mathbf{R}\equiv\{\mathbf{R}_k\}$ can be separated into fast vibrational coordinates $\mathbf{R}_{\text{fast}}$ and slow probe coordinates (e.g., overall probe rotations and, if required, large amplitude intra-molecular degrees of freedom) $\mathbf{R}_{\text{slow}}$, relaxing at least in a picoseconds time scale. Then, the probe Hamiltonian is averaged on *i)* femtoseconds and sub-picoseconds dynamics, pertaining to probe electronic coordinates and *ii)* picoseconds dynamics, pertaining to fast intra-probe degrees of freedom. The averaging on the electron coordinates is the usual implicit procedure for obtaining a spin Hamiltonian from the complete electronic Hamiltonian of the probe. In the frame of Born-Oppenheimer approximation, the averaging on the picosecond dynamics of nuclear coordinates allows to introduce in the calculation of magnetic parameters the effect of the vibrational motions, which can be

very relevant in some cases.[123] The effective probe Hamiltonian obtained in this way is characterized by magnetic tensors. By taking into account only the electron Zeeman and hyperfine interactions, for a probe with a single unpaired electron and *N* nuclei we can define an averaged magnetic Hamiltonian $\hat{H}\left(\mathbf{R}_{\text{slow}},\{\mathbf{q}_\alpha\}\right)$:

$$\begin{aligned}\hat{H}\left(\mathbf{R}_{\text{slow}},\{\mathbf{q}_\alpha\}\right) = \frac{\beta_e}{\hbar}\mathbf{B}_0\cdot\mathbf{g}\left(\mathbf{R}_{\text{slow}},\{\mathbf{q}_\alpha\}\right)\cdot\hat{\mathbf{S}} + \gamma_e\sum_n \hat{\mathbf{I}}_n\cdot\mathbf{A}_n\left(\mathbf{R}_{\text{slow}},\{\mathbf{q}_\alpha\}\right)\cdot\hat{\mathbf{S}} \\ + \hat{H}_{\text{probe-solvent}}\left(\mathbf{R}_{\text{slow}},\{\mathbf{q}_\alpha\}\right) + \hat{H}_{\text{solvent}}\left(\{\mathbf{q}_\alpha\}\right)\end{aligned} \tag{3}$$

The first term is the Zeeman interaction depending upon the $\mathbf{g}\left(\mathbf{R}_{\text{slow}},\{\mathbf{q}_\alpha\}\right)$ tensor, external magnetic field $\mathbf{B}_0$ and electron spin momentum operator $\hat{\mathbf{S}}$; the second term is the hyperfine interaction of the *n*-th nucleus and the unpaired electron, defined in terms hyperfine tensor $\mathbf{A}_n\left(\mathbf{R}_{\text{slow}},\{\mathbf{q}_\alpha\}\right)$ and nuclear spin momentum operator $\hat{\mathbf{I}}_n$. The following terms do not affect directly the magnetic properties and account for probe-solvent [$\hat{H}_{\text{probe-solvent}}\left(\mathbf{R}_{\text{slow}},\{\mathbf{q}_\alpha\}\right)$] and solvent-solvent [$\hat{H}_{\text{solvent}}\left(\{\mathbf{q}_\alpha\}\right)$] interactions. An explicit dependence is left in the magnetic tensor definition from slow probe coordinates (e.g. geometrical dependence upon rotation), and solvent coordinates. The averaged density matrix becomes $\hat{\rho}\left(\mathbf{R}_{\text{slow}},\{\mathbf{q}_\alpha\},t\right) = \left\langle\hat{\rho}\left(\{\mathbf{r}_i\},\{\mathbf{R}_k\},\{\mathbf{q}_\alpha\},t\right)\right\rangle_{\{\mathbf{r}_i\},\mathbf{R}_{\text{fast}}}$ and the corresponding Liouville equation, in the hypothesis of no residual dynamic effect of averaging with respect to sub-picoseconds processes, can be simply written as in Eq. (2) with $\hat{H}\left(\mathbf{R}_{\text{slow}},\{\mathbf{q}_\alpha\}\right)$ instead of $\hat{H}\left(\{\mathbf{r}_i\},\{\mathbf{R}_k\},\{\mathbf{q}_\alpha\}\right)$.

Finally, the dependence upon solvent or bath coordinates can be treated at a classical mechanical level, either by solving explicitly the Newtonian dynamics of the explicit set $\{\mathbf{q}_\alpha\}$ or by adopting standard statistical thermodynamics arguments leading to an effective averaging of the density matrix with respect to solvent variables $\hat{\rho}\left(\mathbf{R}_{\text{slow}},t\right) = \left\langle\hat{\rho}\left(\mathbf{R}_{\text{slow}},\{\mathbf{q}_\alpha\},t\right)\right\rangle_{\{\mathbf{q}_\alpha\}}$. One of the most effective way of dealing with the modified time evolution equation for $\hat{\rho}\left(\mathbf{R}_{\text{slow}},t\right)$ is represented by the SLE, i.e. by the direct inclusion of motional dynamics in the form of stochastic (Fokker-Planck / diffusive) operators in the Liouvillean governing the time evolution of the system [91-93]

$$\frac{\partial}{\partial t}\hat{\rho}(\mathbf{R}_{\text{slow}},t)=-i\left[\hat{H}(\mathbf{R}_{\text{slow}}),\hat{\rho}(\mathbf{R}_{\text{slow}},t)\right]-\hat{\Gamma}\hat{\rho}(\mathbf{R}_{\text{slow}},t)=-\hat{\mathcal{L}}(\mathbf{R}_{\text{slow}})\hat{\rho}(\mathbf{R}_{\text{slow}},t) \tag{4}$$

The effective Hamiltonian, averaged with respect to the solvent coordinates, is

$$\hat{H}(\mathbf{R}_{\text{slow}})=\frac{\beta_e}{\hbar}\mathbf{B}_0\cdot\mathbf{g}(\mathbf{R}_{\text{slow}})\cdot\hat{\mathbf{S}}+\gamma_e\sum_n\hat{\mathbf{I}}_n\cdot\mathbf{A}_n(\mathbf{R}_{\text{slow}})\cdot\hat{\mathbf{S}} \tag{5}$$

and $\mathbf{g}(\mathbf{R}_{\text{slow}})$, $\mathbf{A}_n(\mathbf{R}_{\text{slow}})$ are now averaged tensors with respect to solvent coordinates, while $\hat{\Gamma}$ is the stochastic operator modelling the dependence of the reduced density matrix on relaxation processes described by stochastic coordinates $\mathbf{R}_{\text{slow}}$.

This is a general scheme, which can allow for additional considerations and further approximations. First, the average with respect to picoseconds dynamic processes is carried on, in practice, together with the average with respect to solvent coordinates to allow the QM evaluation of magnetic tensors corrected for solvent effects and for fast vibrational and solvent librational motions. The effective treatment of these aspects represents the heart of second chapter.

Dynamics on longer time scales determines spectral line-shapes and requires more 'coarse-grained' models rooted into a stochastic approach. For semirigid systems the relevant set of stochastic coordinates can be restricted to the set of orientational coordinates $\mathbf{R}_{\text{slow}}\equiv\Omega$, which can be described, in turn, in terms of a simple formulation for a diffusive rotator, characterized by a diffusion tensor $\mathbf{D}$,[90] i.e.

$$\hat{\Gamma}=\hat{\mathbf{J}}(\Omega)\cdot\mathbf{D}\cdot\hat{\mathbf{J}}(\Omega) \tag{6}$$

where $\hat{\mathbf{J}}(\Omega)$ is the angular momentum operator for body rotation.

Once the effective Liouvillean is defined, the direct calculation of the cw-ESR signal is possible without resorting to a complete solution of the SLE by evaluating the spectral density from the expression.[90-93]

$$I(\omega-\omega_0)=\frac{1}{\pi}\text{Re}\left\langle v\,|\,[i(\omega-\omega_0)+i\hat{\mathcal{L}}]^{-1}\,|\,vP_{eq}\right\rangle \tag{7}$$

where the Liouvillean $\hat{\mathcal{L}}$ acts on a starting vector which is defined as proportional to the *x* component of the electron spin operator $\hat{S}_x$.

Magnetic tensors

First considering the electron-field interactions ruled by the so-called ***g***-tensor, the shift with respect to the free-electron value (g_e=2.002319) is $\Delta\mathbf{g} = \mathbf{g} - g_e\mathbf{1}_3$ where $\mathbf{1}_3$ is the 3x3 unit matrix. Upon complete averaging by rotational motions, only the isotropic part of the ***g*** tensor survives, which is given by g_{iso} = 1/3Tr(***g***). The corresponding shift from the free electron value is $\Delta g_{iso} = g_{iso} - g_e$.

$\Delta\boldsymbol{g}$ includes three main contributions [2, 152]

$$\Delta\mathbf{g} = \Delta\mathbf{g}^{RMC} + \Delta\mathbf{g}^{GC} + \Delta\mathbf{g}^{OZ/SOC} \tag{8}$$

$\Delta\boldsymbol{g}^{RMC}$ and $\Delta\boldsymbol{g}^{GC}$ are first order contributions, which take into account relativistic mass (RMC) and gauge (GC) corrections, respectively. The first term can be expressed as:

$$\Delta\mathbf{g}^{RMC} = -\frac{\alpha^2}{S}\sum_{\mu\nu} P_{\mu\nu}^{\alpha-\beta}\left\langle\varphi_\mu\left|\hat{T}\right|\varphi_\mu\right\rangle \tag{9}$$

where α is the fine structure constant, *S* the total spin of the ground state, $\mathbf{P}_{\mu\nu}^{\alpha-\beta}$, is the spin density matrix, φ the basis set and $\hat{T}$ is the kinetic energy operator.

The second term is given by:

$$\Delta\mathbf{g}^{GC} = \frac{1}{2S}\sum_{\mu\nu} P_{\mu\nu}^{\alpha-\beta}\left\langle\varphi_\mu\left|\sum_n \xi(\mathbf{r}_n)\left(\mathbf{r}_n\mathbf{r}_0 - \mathbf{r}_{n,\mathbf{r}}\mathbf{r}_{0,\mathbf{s}}\right)\hat{T}\right|\varphi_\nu\right\rangle \tag{10}$$

where r_n is the position vector of the electron relative to the nucleus n, r_0 the position vector relative to the gauge origin and $\xi(r_n)$ depends on the effective charge of the nuclei, as defined below. These two terms are usually small and have opposite signs so that their contributions tend to cancel out.

The last term in equation (8), $\Delta \boldsymbol{g}^{OZ/SOC}$, is a second-order contribution arising from the coupling of the Orbital Zeeman (OZ) and the Spin-Orbit Coupling (SOC) operators. The OZ contribution in the system Hamiltonian is:

$$\hat{H}_{OZ} = \beta \sum_i \mathbf{B} \cdot \hat{\mathbf{l}}(i) \tag{11}$$

The gauge origin dependence of this term, arising from the angular momentum $\hat{\mathbf{l}}(i)$ of the i^{th} electron, can be effectively treated by the so-called Gauge Including Atomic Orbital (GIAO) approach.[117, 137]

Eventually, the SOC term is a true two-electron operator, which can be, however, approximated by a one-electron operator involving adjusted effective nuclear charges. Several studies have shown that this model operator works fairly well in the case of light atoms, providing results close to those obtained using more refined expressions for the SOC operator.[153] The one-electron approximate SOC operator reads:

$$\hat{H}_{SOC} = \sum_{n,i} \xi\left(\mathbf{r}_{i,n}\right) \hat{\mathbf{l}}_n(i) \cdot \hat{\mathbf{s}}(i) \tag{12}$$

where $\hat{\mathbf{l}}_n(i)$ is the angular momentum operator of the i^{th} electron relative to the nucleus n and $\hat{\mathbf{s}}(i)$ its spin-operator. The function $\xi\left(\mathbf{r}_{i,n}\right)$ is defined as:[154]

$$\xi\left(\mathbf{r}_{i,n}\right) = \frac{\alpha^2}{2} \frac{Z_{eff}^n}{\left|\mathbf{r}_i - \mathbf{R}_n\right|^3} \tag{13}$$

where Z_{eff}^n is the effective nuclear charge of atom n at position R_n. Starting from zero-order Kohn-Sham (KS) spin-orbitals, the OZ/SOC contribution is evaluated by the GIAO extension of the coupled perturbed formalism.[117, 137]

The hyperfine coupling tensor ($\boldsymbol{A}_X$), which describes the interaction between the electronic spin density and the nuclear magnetic momentum of nucleus X, can be broken into three terms:[155]

$$\boldsymbol{A}_X = a_X \boldsymbol{I}_3 + \boldsymbol{T}_X + \boldsymbol{\Lambda}_X \tag{14}$$

where $\mathbf{1}_3$ is the 3x3 unit matrix.

The first term (a_X), usually referred to as Fermi-contact interaction, is an isotropic contribution also known as hyperfine coupling constant (hcc), and is related to the spin density at the corresponding nucleus X by

$$a_X = \frac{8\pi}{3}\frac{g_e}{g_0} g_X \beta_X \sum_{\mu,\nu} P^{\alpha-\beta}_{\mu,\nu} \left\langle \varphi_\mu \left| \delta(r_X) \right| \varphi_\nu \right\rangle \tag{15}$$

The second contribution ($\mathbf{T}_X$) is anisotropic and can be derived from the classical expression of interacting dipoles,

$$T_{X,ij} = \frac{g_e}{g_0} g_X \beta_X \sum_{\mu,\nu} P^{\alpha-\beta}_{\mu,\nu} \left\langle \varphi_\mu \left| r_X^{-5} \left(r_{Xi}^2 \delta_{ij} - 3 r_{Xi} r_{Xj} \right) \right| \varphi_\nu \right\rangle \tag{16}$$

The last term, $\mathbf{\Lambda}_X$, is due to second-order spin-orbit coupling and can be determined by methods similar to those described in the following for the gyromagnetic tensor. Due to the small spin-orbit coupling constants of second-row atoms its contribution can be safely neglected and will not be discussed in the following.

In the above equations the vector $\mathbf{r}_X$ points from nucleus X to the electron. Of course, upon complete averaging by rotational motions, only the isotropic part survives. Since both a_X and $\mathbf{T}_X$ are ruled by one-electron operators, their evaluation is, in principle, quite straightforward. However, hyperfine coupling constants have been among the most challenging quantities for conventional QM approaches for two main reasons. From one hand, conventional Gaussian basis sets are ill adapted to describe nuclear cusps and, on the other hand, the overall result derives from the difference between large quantities of opposite sign. However, the last few years have shown that coupling of some hybrid functionals (e.g., PBE0[35]) to purposely tailored basis sets performs a remarkable job both for isotropic and dipolar terms.[41]

Bibliography

[1] E. A. Carter, P. J. Rossky, *Accounts Of Chemical Research* **2006**, *39*, 505.

[2] R. McWeeny, *Methods of Molecular Quantum Mechanics*, Academic Press, London, **1992**.

[3] V. Barone, P. Cimino, O. Crescenzi, M. Pavone, *Journal Of Molecular Structure-Theochem* **2007**, *811*, 323.

[4] R. G. Parr, W. Yang, *Density-Functional Theory of Atoms and Molecules*, Oxford University Press, New York, **1989**.

[5] W. Koch, M. C. Holthausen, *A Chemist's Guide to Density Functional Theory*, Wiley-VCH, Weinheim, **2002**.

[6] R. Improta, V. Barone, *Chemical Reviews* **2004**, *104*, 1231.

[7] A. R. Leach, *Molecular Modelling: Principles and Applications, 2nd ed.*, Prentice Hall, London, **2001**.

[8] J. Tomasi, M. Persico, *Chemical Reviews* **1994**, *94*, 2027.

[9] J. Tomasi, B. Mennucci, R. Cammi, **2005**, *105*, 2999.

[10] V. Barone, M. Cossi, J. Tomasi, *Journal Of Chemical Physics* **1997**, *107*, 3210.

[11] C. Benzi, O. Crescenzi, M. Pavone, V. Barone, *Magnetic Resonance In Chemistry* **2004**, *42*, S57.

[12] R. Improta, V. Barone, *Journal Of The American Chemical Society* **2004**, *126*, 14320.

[13] O. Crescenzi, M. Pavone, F. De Angelis, V. Barone, *Journal Of Physical Chemistry B* **2005**, *109*, 445.

[14] R. Car, M. Parrinello, *Physical Review Letters* **1985**, *55*, 2471.

[15] S. Kristyán, P. Pulay, *Chemical Physics Letters* **1994**, *229*, 175.

[16] W. Kohn, Y. Meir, D. E. Makarov, *Physical Review Letters* **1998**, *80*, 4153.

[17] T. Helgaker, P. Jørgensen, J. Olsen, *Molecular Electronic-structure Theory*, J. Wiley, New York, **2000**.

[18] S. Grimme, *Journal Of Computational Chemistry* **2006**, *27*, 1787.

[19] E. B. Wilson, J. C. Decius, P. C. Cross, *Molecular Vibrations: The Theory of Infrared and Raman Vibrational Spectra*, Dover, New York, **1980**.

[20] J. Franck, *Transactions of the Faraday Society* **1926**, *21*, 536.

[21] E. Condon, *Physical Review* **1928**, *32*, 858.

[22] F. Santoro, R. Improta, A. Lami, J. Bloino, V. Barone, *Journal of Chemical Physics* **2007**, *126*, 084509.

[23] M. Born, R. Oppenheimer, *Annalen der Physik* **1927**, *20*, 457.

[24] A. Szabo, N. S. Ostlund, *Modern Quantum Chemistry*, McGraw-Hill, New York, **1989**.

[25] V. Barone, *Journal Of Chemical Physics* **2005**, *122*, 14108.

[26] V. Barone, *Journal Of Chemical Physics* **2004**, *120*, 3059.

[27] M. Pavone, V. Barone, I. Ciofini, C. Adamo, *Journal Of Chemical Physics* **2004**, *120*, 9167.

[28] D. C. Rapaport, *The Art of Molecular Dynamics Simulations*, University Press, Cambridge, UK, **1997**.

[29] N. Rega, *Theoretical Chemical Accounts* **2006**, *116*, 347.

[30] M. Buhl, *Journal Of Physical Chemistry A* **2002**, *106*, 10505.

[31] G. Pastore, E. Smargiassi, F. Buda, *Physical Review A* **1991**, *44*, 6334.

[32] W. Andreoni, A. Curioni, *Parallel Computing* **2000**, *26*, 819.

[33] D. A. Gibson, I. V. Ionova, E. A. Carter, *Chemical Physics Letters* **1995**, *240*, 261.

[34] H. B. Schlegel, S. S. Iyengar, X. Li, J. M. Millam, G. A. Voth, G. E. Scuseria, M. J. Frisch, *Journal Of Chemical Physics* **2002**, *117*, 8694.

[35] C. Adamo, V. Barone, *Journal Of Chemical Physics* **1999**, *110*, 6158.

[36] C. J. Cramer, D. G. Truhlar, *Chemical Reviews* **1999**, *99*, 2161.

[37] M. Cossi, G. Scalmani, N. Rega, V. Barone, *Journal Of Chemical Physics* **2002**, *117*, 43.

[38] G. Scalmani, V. Barone, K. N. Kudin, C. S. Pomelli, G. E. Scuseria, M. J. Frisch, *Theoretical Chemistry Accounts* **2004**, *111*, 90.

[39] M. Cossi, V. Barone, *Journal Of Chemical Physics* **1998**, *109*, 6246.

[40] M. Cossi, V. Barone, *Journal Of Chemical Physics* **2001**, *115*, 4708.

[41] I. Ciofini, C. Adamo, V. Barone, *Journal Of Chemical Physics* **2004**, *121*, 6710.

[42] M. Pavone, A. Sillanpaa, P. Cimino, O. Crescenzi, V. Barone, *Journal Of Physical Chemistry B* **2006**, *110*, 16189.

[43] M. Cossi, O. Crescenzi, *Journal Of Chemical Physics* **2003**, *118*, 8863.

[44] G. Brancato, N. Rega, V. Barone, *Journal Of Chemical Physics* **2006**, *124*.

[45] N. Rega, G. Brancato, V. Barone, *Chemical Physics Letters* **2006**, *422*, 367.

[46] G. Brancato, N. Rega, V. Barone, *Journal Of Chemical Physics* **2006**, *125*.

[47] S. K. Burley, G. A. Petsko, *Science* **1985**, *229*, 22.

[48] J.-Y. Ortholand, A. M. Z. Slawin, N. Spencer, J. F. Stoddart, D. J. Williams, *Angewandte Chemie-International Edition* **1989**, *28*, 1394.

[49] E. A. Meyer, R. K. Castellano, F. Diederich, *Angewandte Chemie-International Edition* **2003**, *42*, 1210.

[50] T. Janowski, P. Pulay, *Chemical Physics Letters* **2007**, *447*, 27.

[51] M. Dion, H. Rydberg, E. Schrëder, D. C. Langreth, B. I. Lundqvist, *Physical Review Letters* **2004**, *92*, 246401.

[52] A. D. Becke, E. R. Johnson, *Journal Of Chemical Physics* **2007**, *127*, 124108.

[53] R. Podeszwa, R. Bukowski, K. Szalewicz, *Journal of Physical Chemistry A* **2006**, *110*, 10345.

[54] O. Anatole-von-Lilienfeld, I. Tavernelli, U. Rothlisberger, D. Sebastiani, *Physical Review Letters* **2004**, *93*, 153004.

[55] Y. Zaho, D. G. Truhlar, *Journal of Chemical Theory and Computation* **2007**, *3*, 289.

[56] M. Elstner, P. Hobza, T. Frauenheim, S. Suhai, E. Karixas, *Journal Of Chemical Physics* **2001**, *114*, 5149.

[57] X. Wu, M. C. Vargas, S. Nayak, V. Lotrich, G. Scoles, *Journal Of Chemical Physics* **2001**, *115*, 8748.

[58] E. J. Meijer, M. Sprik, *Journal Of Chemical Physics* **1996**, *105*, 8684.

[59] Q. Wu, W. Yang, *Journal Of Chemical Physics* **2002**, *116*, 515.

[60] E. C. Lee, D. Kim, P. Jurečka, P. Tarakeshwar, P. Hobza, K. S. Kim, *Journal of Physical Chemistry A* **2007**, *111*, 3446.

[61] P. M. Felker, P. M. Maxton, M. W. Schaeffer, *Chemical Reviews* **1994**, *84*, 1787.

[62] P. Hobza, H. L. Selzle, E. W. Schlag, *Chemical Reviews* **1994**, *94*, 1767.

[63] J. GrantHill, J. A. Platts, H.-J. Werner, *Physical Chemistry Chemical Physics* **2006**, *8*, 4072.

[64] M. O. Sinnokrot, C. D. Sherrill, *Journal of Physical Chemistry A* **2006**, *110*, 10656.

[65] R. A. J. DiStasio, G. von-Helden, R. P. Steele, M. Head-Gordon, *Chemical Physics Letters* **2007**, *437*, 277.

[66] A. Puzder, M. Dion, D. C. Langreth, *Journal of Chemical Physics* **2006**, *124*, 164105.

[67] T. Sato, T. Tsuneda, K. Hirao, *Journal of Chemical Physics* **2007**, *126*, 234114.

[68] J.-M. Ducéré, L. Cavallo, *Journal of physical Chemistry B* **2007**, *111*, 13124.

[69] S. F. Boys, F. Bernardi, *Molecular Physics* **1970**, *19*, 553.

[70] M. J. Frish, G. W. Trucks, H. B. Schlegel, G. E. Scuseria, M. A. Robb, J. R. Cheeseman, J. A. Montgomery, T. Vreven, K. N. Kudin, J. C. Burant, J. M. Millam, S. S. Iyengar, J. Tomasi, V. Barone, B. Mennucci, M. Cossi, G. Scalmani, N. Rega, G. A. Petersson, H. Nakatsuji, M. Hada, M. Ehara, K. Toyota, R. Fukuda, J. Hasegawa, M. Ishida, T. Nakajima, Y. Honda, O. Kitao, H. Nakai, M. Klene, X. Li, J. E. Knox, H. P. Hratchian, J. B. Cross, V. Bakken, C. Adamo, J. Jaramillo, R. Gomperts, R. E. Stratmann, O. Yazyev, A. J. Austin, R. Cammi, C. Pomelli, J. W. Ochterski, P. Y. Ayala, K. Morokuma, G. A. Voth, P. Salvador, J. J. Dannenberg, V. G. Zakrzewski, S. Dapprich, A. D. Daniels, M. C. Strain, O. Farkas, D. K. Malick, A. D. Rabuck, K. Raghavachari, J. B. Foresman, J. V. Ortiz, Q. Cui, A. G. Baboul, S. Clifford, J. Cioslowski, B. B. Stefanov, G. Liu, A. Liashenko, P. Piskorz, I. Komaromi, R. L. Martin, D. J. Fox, T. Keith, M. A. Al-Laham, C. Y. Peng, A. Nanayakkara, M. Challacombe, P. M. W. Gill, B. Johnson, W. Chen, M. W. Wong, C. Gonzalez, J. A. Pople, Gaussian, Inc., Wallingford CT, **2004**.

[71] A. D. Becke, *Journal Of Chemical Physics* **1993**, *98*, 5648.

[72] R. A. Kendall, T. H. J. Dunning, R. J. Harrison, *Journal Of Chemical Physics* **1992**, *96*, 6796.

[73] V. Barone, unpublished.

[74] W. C. Swope, H. C. Andersen, P. H. Berens, K. R. Wilson, *Journal Of Chemical Physics* **1982**, *76*, 637.

[75] G. R. Dennis, G. L. Ritchie, *Journal Of Physical Chemistry* **1993**, *97*, 8403.

[76] M. Okruss, R. Müller, A. Hese, *Journal Of Chemical Physics* **1999**, *110*, 10393.

[77] U. Erlekam, M. Frankowski, G. Meijer, G. v. Helden, *Journal Of Chemical Physics* **2006**, *124*, 171101.

[78] E. Arunan, H. S. Gutowsky, *Journal Of Chemical Physics* **1993**, *98*, 4294.

[79] J. F. W. Keana, *Chemical Reviews* **1978**, *78*, 37.

[80] L. J. Berliner, *Spin Labelling: Theory and Applications*, Academic Press, New York, **1976**.

[81] A. H. Buchaklian, C. S. Klug, *Biochemistry* **2005**, *44*, 5503.

[82] C. Adamo, A. di Matteo, P. Rey, V. Barone, *Journal Of Physical Chemistry A* **1999**, *103*, 3481.

[83] J. E. Baur, S. Wang, M. C. Brandt, *Analytical Chemistry* **1996**, *68*, 3815.

[84] A. M. Tedeschi, G. D'Errico, E. Busi, R. Basosi, V. Barone, *Physical Chemistry Chemical Physics* **2002**, *4*, 2180.

[85] K. Mobius, A. Savitsky, A. Schnegg, M. Plato, M. Fuchs, *Physical Chemistry Chemical Physics* **2005**, *7*, 19.

[86] B. R. Knauer, J. J. Napier, *Journal of the American Chemical Society* **1976**, *98*, 4395.

[87] V. I. Krinichnyi, Y. Grinberg, V. R. Bogatyrenko, G. I. Likhtenshtein, Y. S. Lebedev, *Biophysics* **1985**, *30*, 233.

[88] V. Barone, A. Bencini, M. Cossi, A. Di Matteo, M. Mattesini, F. Totti, *Journal Of The American Chemical Society* **1998**, *120*, 7069.

[89] D. G. Wu, A. D. Malec, M. Head-Gordon, M. Majda, *Journal Of The American Chemical Society* **2005**, *127*, 4490.

[90] V. Barone, A. Polimeno, *Physical Chemistry Chemical Physics* **2006**, *8*, 4609.

[91] A. Polimeno, J. H. Freed, *Adv. Chem. Phys.* **1992**, *83*, 89.

[92] D. J. Schneider, J. H. Freed, *Adv. Chem. Phys.* **1989**, *73*, 387.

[93] G. Moro, J. H. Freed, *Journal of Chemical Physics* **1981**, *74*, 3757.

[94] H. J. Steinhoff, M. Muller, C. Beier, M. Pfeiffer, *Journal Of Molecular Liquids* **2000**, *84*, 17.

[95] T. Yagi, O. Kikuchi, *Journal Of Physical Chemistry A* **1999**, *103*, 9132.

[96] D. Sebastiani, M. Parrinello, *Journal Of Physical Chemistry A* **2001**, *105*, 1951.

[97] O. V. Yazyev, I. Tavernelli, L. Helm, U. Rothlisberger, *Physical Review B* **2005**, *71*.

[98] S. Canuto, K. Coutinho, M. C. Zerner, *Journal Of Chemical Physics* **2000**, *112*, 7293.

[99] M. Buhl, M. Parrinello, *Chemistry-A European Journal* **2001**, *7*, 4487.

[100] J. F. Keana, T. D. Lee, E. M. Bernard, *Journal Of The American Chemical Society* **1976**, *98*, 3052.

[101] A. Pasquarello, K. Laasonen, R. Car, C. Y. Lee, D. Vanderbilt, *Physical Review Letters* **1992**, *69*, 1982.

[102] J. P. Perdew, K. Burke, M. Ernzerhof, *Physical Review Letters* **1996**, *77*, 3865.

[103] D. Vanderbilt, *Physical Review B* **1990**, *41*, 7892.

[104] J. C. Grossman, E. Schwegler, E. W. Draeger, F. Gygi, G. Galli, *Journal Of Chemical Physics* **2004**, *120*, 300.

[105] B. Hetenyi, F. De Angelis, P. Giannozzi, R. Car, *Journal Of Chemical Physics* **2004**, *120*, 8632.

[106] S. Nosé, *Journal Of Chemical Physics* **1984**, *81*, 511.

[107] M. M. Francl, W. J. Pietro, W. J. Hehre, J. S. Binkley, M. S. Gordon, D. J. DeFrees, J. A. Pople, *Journal Of Chemical Physics* **1982**, *77*, 3654.

[108] T. H. J. Dunning, *Journal Of Chemical Physics* **1989**, *90*, 1007.

[109] V. Barone, *Theoretica Chimica Acta* **1995**, *91*, 113.

[110] D. M. Chipman, *Theoretica Chimica Acta* **1992**, *82*, 93.

[111] F. Neese, *Journal Of Chemical Physics* **2005**, *122*.

[112] W. L. Jorgensen, J. Chandrasekhar, J. D. Madura, R. W. Impey, M. L. Klein, *Journal Of Chemical Physics* **1983**, *79*, 926.

[113] M. Ferrario, M. Haughney, I. R. McDonald, M. L. Klein, *Journal Of Chemical Physics* **1990**, *93*, 5156.

[114] S. M. Mattar, A. D. Stephens, *Chemical Physics Letters* **2001**, *347*, 189.

[115] Z. Rinkevicius, L. Telyatnyk, O. Vahtras, K. Ruud, *Journal Of Chemical Physics* **2004**, *121*, 5051.

[116] R. Owenius, M. Engstrom, M. Lindgren, M. Huber, *Journal Of Physical Chemistry A* **2001**, *105*, 10967.

[117] F. Neese, *Journal Of Chemical Physics* **2001**, *115*, 11080.

[118] M. Romanelli, M. F. Ottaviani, G. Martini, L. Kevan, *Journal Of Physical Chemistry* **1989**, *93*, 317.

[119] H. J. C. Berendsen, J. R. Grigera, T. P. Straatsma, *Journal Of Physical Chemistry* **1987**, *91*, 6269.

[120] M. Pavone, G. Brancato, G. Morelli, V. Barone, *Chemphyschem* **2006**, *7*, 148.

[121] A. V. Arbuznikov, M. Kaupp, V. G. Malkin, R. Reviakine, O. L. Malkina, *Physical Chemistry Chemical Physics* **2002**, *4*, 5467.

[122] S. M. Mattar, A. D. Stephens, *Chemical Physics Letters* **2000**, *319*, 601.

[123] V. Barone, P. Carbonniere, C. Pouchan, *Journal Of Chemical Physics* **2005**, *122*.

[124] V. Barone, C. Adamo, Y. Brunel, R. Subra, *Journal Of Chemical Physics* **1996**, *105*, 3168.

[125] I. Carmichael, *Journal Of Physical Chemistry A* **1997**, *101*, 4633.

[126] A. J. Stone, *Molecular Physics* **1963**, *6*, 509.

[127] A. J. Stone, *Molecular Physics* **1964**, *7*, 311.

[128] S. Sinnecker, A. Rajendran, A. Klamt, M. Diedenhofen, F. Neese, *Journal Of Physical Chemistry A* **2006**, *110*, 2235.

[129] M. Krauss, S. P. Webb, *Journal Of Chemical Physics* **1997**, *107*, 5771.

[130] K. Coutinho, S. Canuto, *Journal Of Chemical Physics* **2000**, *113*, 9132.

[131] U. F. Rohrig, I. Frank, J. Hutter, A. Laio, J. VandeVondele, U. Rothlisberger, *Chemphyschem* **2003**, *4*, 1177.

[132] D. Kony, W. Damm, S. Stoll, W. F. van Gunsteren, *Journal Of Computational Chemistry* **2002**, *23*, 1416.

[133] W. D. Cornell, P. Cieplak, C. I. Bayly, I. R. Gould, K. M. Merz, D. M. Ferguson, D. C. Spellmeyer, T. Fox, J. W. Caldwell, P. A. Kollman, *Journal Of The American Chemical Society* **1995**, *117*, 5179.

[134] G. Brancato, A. DiNola, V. Barone, A. Amadei, *Journal Of Chemical Physics* **2005**, *122*, 154109.

[135] P. Cieplak, W. D. Cornell, C. Bayly, P. A. Kollman, *Journal Of Computational Chemistry* **1995**, *16*, 1357.

[136] E. K. U. Gross, W. Kohn, *Physical Review Letters* **1985**, *55*, 2850.

[137] J. R. Cheeseman, G. W. Trucks, T. A. Keith, M. J. Frisch, *Journal Of Chemical Physics* **1996**, *104*, 5497.

[138] C. Møller, M. S. Plesset, *Physical Review* **1934**, *46*, 618.

[139] R. L. Hilderbrandt, A. L. Andreassen, S. H. Bauer, *Journal Of Physical Chemistry* **1970**, *74*, 1586.

[140] N. S. Bayliss, E. G. McRae, *Journal Of Physical Chemistry* **1954**, *58*, 1006.

[141] B. Tiffon, J.-E. Dubois, *Organic Magnetic Resonance* **1978**, *11*, 295.

[142] B. C. Gilbert, M. J. Davies, D. M. Murphy, *Electron Paramagnetic Resonance, Vol. 18*, Royal Society of Chemistry, Cambridge, UK, **2002**.

[143] N. J. Turro, M. H. Kleinman, E. Karatekin, *Angewandte Chemie-International Edition* **2000**, *39*, 4437.

[144] V. Barone, *Journal Of Chemical Physics* **1994**, *101*, 6834.

[145] V. Barone, *Journal Of Chemical Physics* **1994**, *101*, 10666.

[146] D. Feller, E. R. Davidson, *Journal Of Chemical Physics* **1988**, *88*, 5770.

[147] S. A. Perera, L. M. Salemi, R. J. Bartlett, *Journal Of Chemical Physics* **1997**, *106*, 4061.

[148] F. Jolibois, J. Cadet, A. Grand, R. Subra, V. Barone, N. Rega, *Journal Of The American Chemical Society* **1998**, *120*, 1864.

[149] J. A. Nillson, L. A. Eriksson, A. Laaksonen, *Molecular Physics* **2001**, *99*.

[150] M. Pavone, P. Cimino, F. De Angelis, V. Barone, *Journal Of The American Chemical Society* **2006**, *128*, 4338.

[151] C. P. Slichter, *Principles of Magnetic Resonance*, Harper & Row, New York, **1963**.

[152] A. J. Stone, *Proc. R. Soc. London, Ser. A* **1963**, *271*, 424.

[153] O. L. Malkina, J. Vaara, B. Schimmelpfennig, M. Munzarova, V. G. Malkin, M. Kaupp, *Journal Of The American Chemical Society* **2000**, *122*, 9206.

[154] S. Koseki, M. W. Schmidt, M. S. Gordon, *Journal Of Physical Chemistry* **1992**, *96*, 10768.

[155] R. A. Frosch, H. M. Foley, *Physical Review* **1952**, *88*, 1337.

List of acronyms and abbreviations

ADMP	Atom-centred Density Matrix Propagation
AMBER	Assisted Model Building with Energy Refinement
B3LYP	Becke 3-parameter Lee-Yang-Parr
B3LYP-D	B3LYP plus Dispersion correction
BO	Born-Oppenheimer approximation
BOMD	BO Molecular Dynamics
BSSE	Basis-Set Superposition Error
CC	Coupled Clusters
CCSD(T)	CC with Singles and Doubles, plus perturbative treatment of Triples
CHARMM	Chemistry at HARvard Molecular Mechanics
CP	Car-Parrinello
CPMD	Car-Parrinello Molecular Dynamics
cw	continuous wave
DFT	Density Functional Theory
DFT-D	Density Functional Theory plus Dispersion
ENDOR	Electron-Nuclear DOuble-Resonance
EPR	Electron Paramagnetic Resonance
GGA	Generalized Gradient Approximation
GIAO	Gauge-Including Atomic Orbital
GROMACS	GROningen MAchine for Chemical Simulations
GTO	Gaussian Type Orbital
hcc	hyperfine coupling constant
HF	Hartree-Fock
KS	Kohn-Sham

LC	Long-range Corrected
LDA	Local Density Approximation
MD	Molecular Dynamics
MF	Mean Field
MM	Molecular Mechanics
MP2	Møller-Plesset second order perturbation theory
mw	microwave
N07T	Napoli 2007 Triple-ζ basis set
NMR	Nuclear Magnetic Resonance
NVE	Number of particles, Volume, and Energy (micro-canonical ensemble)
NVT	Number of particles, Volume, and Temperature (canonical ensemble)
OPLS	Optimized Potential for Liquid Simulations
OPLS-AA	Optimized Potential for Liquid Simulations – All Atoms
OZ	Orbital-Zeeman
PBC	Periodic Boundary Conditions
PBE	Perdew-Burke-Ernzerhov
PBE0	Perdew-Burke-Ernzerhov with no empirical parameters (Zero)
PCM	Polarizable Continuum Model
PES	Potential Energy Surface
PW	Plane Waves
QCISD	Quadratic Configuration Interaction with Single and Double excitations
QM	Quantum Mechanics
RDF	Radial Distribution Functions
SLE	Stochastic Liouville Equation
SOC	Spin-Orbit Coupling
SOMO	Singly Occupied Molecular Orbital
SPC	Simple Point-Charge
TD	Time-Dependent

TIP3P	Transferable Intermolecular Potential-function 3 Point-charges
TRIPLE	electron-nuclear-triple resonance
UAHF	United Atom Hartree-Fock
UV	UltraViolet
xc	exchange-correlation
ZPE	Zero-Point vibrational Energy

List of publications

Michele Pavone,Vincenzo Barone, Ilaria Ciofini, Carlo Adamo

Journal of Chemical Physics 120, 9167 (2004)

Title. First-principle molecular dynamics of the Berry pseudorotation: insights on ^{19}F NMR in SF_4

Abstract. First-principles [density-functional theory (DFT)] molecular-dynamic simulations of the Berry pseudorotation mechanism in SF_4 were performed using the atom-centered density-matrix propagation method. The reaction was monitored by following the chemical shieldings of the fluorine atoms, computed on snapshots along the trajectories. In particular we compared the results obtained using a standard functional based on the generalized gradient approximation with those issuing from its hybrid Hartree–Fock–DFT counterpart using a number of basis sets. Our results show that both the basis set and the functional choice rule the quality of the molecular properties monitored as well as the trajectory over the potential-energy surface.

Michele Pavone, Caterina Benzi, Filippo De Angelis, Vincenzo Barone

Chemical Physics Letters 395, 120–126 (2004)

Title. Hyperfine coupling constants of dimethyl nitroxide in aqueous solution: Car–Parrinello molecular dynamics and discrete-continuum approaches

Abstract. Vibrational averaging and solvent effects on the isotropic hyperfine coupling constants of dimethyl nitroxide have been investigated by an integrated computational tool including Car–Parrinello molecular dynamics and discrete-continuum solvent models. The results allow an unbiased judgement of the role of different effects in determining the observed EPR parameters.

Caterina Benzi, Orlando Crescenzi, **Michele Pavone**, Vincenzo Barone∗

Magnetic Resonance in Chemstry 42, S57–S67 (2004)

Title. Reliable NMR chemical shifts for molecules in solution by methods rooted in density functional theory

Abstract. The conceptual and numerical problems involved in the computation of reliable NMR chemical shifts for molecules in condensed phases are analyzed with reference to a number of case studies ranging from aromatic compounds in low-polarity solvents to carbonyl and amidic models in aqueous solution and to large polypeptides. The results show that an integrated tool including the most recent density functionals, mixed discrete-continuum solvent models, hybrid QM/MM approaches and, when needed, averaging from molecular dynamics simulations are becoming an invaluable complement to experimental results.

Anna Lisa Piccinelli, Osmany Cuesta-Rubio, Mariano Barrios Chica, Naheed Mahmood, Bruno Pagano, **Michele Pavone**, Vincenzo Barone, Luca Rastrelli

Tetrahedron 61, 8206–8211 (2005)

Title. Structural revision of clusianone and 7-epi-clusianone and anti-HIV activity of polyisoprenylated benzophenones

Abstract. For the first time, the tautomeric pairs of clusianone and 7-epi-clusianone were isolated from the same source, Clusia torresii fruits. An extensive NMR spectroscopic study is described to establish 1H and 13C chemical shift assignments and the C-7 relative configuration of these epimers and to clarify contradictory NMR spectroscopic data previously reported. Quantum mechanical computations than pointed out the relationship between indirect coupling constants and the equilibrium between the B-ring chair and twist-boat forms of the bicyclo-[3.3.1.]-nonane system. Clusianone, 7-epi-clusianone and polyisoprenylated benzophenones 18,19-dihydroxyclusianone, propolone A and nemorosone were screened for their activity against HIV infection in C8166 cells. All compounds inhibited infection with selectivity index values ranging from 2.25 to 15.6. Only clusianone derivatives inhibited infection by binding to viral protein gp120 and prevented its interaction with cellular receptor CD4 as detected by ELISA using recombinant proteins.

Orlando Crescenzi, **Michele Pavone**, Filippo De Angelis, Vincenzo Barone

Journal of Physical Chemistry B 109, 445-453 (2005)

Title. Solvent Effects on the UV ($n \rightarrow \pi^*$) and NMR (^{13}C and ^{17}O) Spectra of Acetone in Aqueous Solution. An Integrated Car-Parrinello and DFT/PCM Approach

Abstract. The accurate reproduction of ultraviolet and nuclear magnetic resonance spectra of acetone in aqueous solution is used as a test of an integrated computational tool rooted in the density functional theory, the polarizable continuum model, and the Car-Parrinello dynamics. The analysis and solution of several conceptual and practical

issues results in a robust and effective approach, which also can be used by nonspecialists and provides a general and powerful complement to experimental techniques.

Paola Cimino, **Michele Pavone**, Vincenzo Barone

Chemical Physics Letters 419, 106–110 (2006)

Title. Structural, thermodynamic, and magnetic properties of adducts between TEMPO radical and alcohols in solution: New insights from DFT and discrete–continuum solvent models

Abstract. Structural, thermodynamic, and magnetic properties of adducts between the TEMPO radical and representative hydrogen bond donors in solution have been investigated by an integrated computational tool including hybrid density functionals and discrete–continuum solvent models. The results allow an unbiased judgement of the role of different effects in determining the observed thermodynamic and spectroscopic parameters.

Laurent Joubert, **Michele Pavone**, Vincenzo Barone, Carlo Adamo

Journal of Chemical Theory and Computation 2, 1220-1227 (2006)

Title. Comparative Static and Dynamic Study of a Prototype S_N2 Reaction

Abstract. Ab initio molecular-dynamic simulations, using density functional theory (DFT) and the recent atom-centered density-matrix propagation method (ADMP), were used to study the bond formation process in a prototypical S_N2 reaction, namely the Walden inversion. Using the real space partition schemes of both electronic density and electron localization function gradient fields, we analyzed different quantum chemical topology (QCT) properties along the ADMP trajectory. In particular, atomic charges derived from the Bader's atoms-in-molecules (AIM) theory were used to analyze intra- and intermolecular charge transfers between atoms, while the electronic population of the forming bonding basin obtained from the electron localization function (ELF) gradient field was employed to describe the bond formation process. These results were compared to the corresponding QCT properties issuing from a static approach based on the intrinsic reaction path (IRP). Although similar features are found for both static and dynamic approaches, the dynamic QCT analysis provides some explanation of the differences observed during the formation of the ion-molecule complex. In particular, it suggests a stronger electron exchange leading to an effective maximization of both covalent and noncovalent interactions.

Michele Pavone, Orlando Crescenzi, Giovanni Morelli, Nadia Rega, Vincenzo Barone

Theoretical Chemistry Accounts 116, 456–461 (2006)

Title. Solvent effects on the UV (n→ π*) and NMR (^{17}O) spectra of acetone in aqueous solution: development and validation of a modified Amber force field for an integrated MD/DFT/PCM approach

Abstract. A modified Amber force field has been developed and used to compute UV and NMR spectra of acetone in aqueous solution by an integrated computational tool rooted in the density functional theory, the polarizable continuum model, and classical molecular dynamics. The results show that, provided that classical force fields are carefully reparameterized and validated, they can be part of a robust and effective approach, which can be used also by non-specialists and provides a general and powerful complement to experimental techniques.

Michele Pavone, Giuseppe Brancato, Giovanni Morelli, and Vincenzo Barone

ChemPhysChem 7, 148 – 156, (2006)

Title. Spectroscopic Properties in the Liquid Phase: Combining High-Level *ab initio* Calculations and Classical Molecular Dynamics

Abstract. We present an integrated computational tool, rooted in density functional theory, the polarizable continuum model, and classical molecular dynamics employing spherical boundary conditions, to study the spectroscopic observables of molecules in solution. As a test case, a modified OPLS-AA force field has been developed and used to compute the UV and NMR spectra of acetone in aqueous solution. The results show that provided the classical force fields are carefully reparameterized and validated, the proposed approach is robust and effective, and can also be used by non-specialists to provide a general and powerful complement to experimental techniques.

Michele Pavone, Paola Cimino, Filippo De Angelis, Vincenzo Barone

Journal of the American Chemical Society 128, 4338-4347, (2006)

Title. Interplay of Stereoelectronic and Enviromental Effects in Tuning the Structural and Magnetic Properties of a Prototypical Spin Probe: Further Insights from a First Principle Dynamical Approach

Abstract. The nitrogen isotropic hyperfine coupling constant (hcc) and the g tensor of a prototypical spin probe (di-tert-butyl nitroxide, DTBN) in aqueous solution have been investigated by means of an integrated computational approach including Car-Parrinello molecular dynamics and quantum mechanical calculations involving a discrete-continuum embedding. The quantitative agreement between computed and experimental parameters fully validates our integrated approach. Decoupling of the structural, dynamical, and environmental contributions acting onto the spectral observables allows an unbiased judgment of the role played by different effects in determining the overall experimental observables and highlights the importance of finite-temperature vibrational averaging. Together with their intrinsic interest, our results pave the route toward more reliable interpretations of EPR parameters of complex systems of biological and technological relevance.

Michele Pavone, Atte Sillanpää, Paola Cimino, Orlando Crescenzi, Vincenzo Barone

Journal of Physical Chemistry B 110, 16189-16192 (2006)

Title. Evidence of Variable H-Bond Network for Nitroxide Radicals in Protic Solvents

Abstract. This letter presents the results of a thorough computational investigation of two prototypical nitroxide spin probes in two different protic solvents, namely water and methanol, based on the combined use of Car-Parrinello molecular dynamic simulations and static cluster/continuum quantum chemical computations. Remarkable changes in solvation networks were found on going from aqueous to methanolic solutions. Moreover, despite their structural similarity, the two nitroxide probes display quite different behaviors in water. This provides a rationalization of indirect experimentally available indications. Eventually, the combination of static and dynamical ab initio methods exploited in the present study allows to dissect many subtle features of the nitroxide-solvent interaction, and also allows for an analysis of solvent effects on magnetic parameters (hyperfine coupling constants and g-tensor shift).

Paola Cimino, **Michele Pavone**, Vincenzo Barone

Journal of Physical Chemistry A 111, 8482-8490 (2007)

Title. Halogen Bonds between 2,2,6,6-Tetramethylpiperidine-N-oxyl Radical and $C_xH_yF_zI$ Species: DFT Calculations of Physicochemical Properties and Comparison with Hydrogen Bonded Adducts

Abstract. Structural, thermodynamic, and magnetic properties of adducts between the 2,2,6,6-tetramethylpiperidine-N-oxyl radical and representative hydrogen and halogen bond donors in solution have been investigated by an integrated computational tool

including hybrid density functionals and discrete-continuum solvent models. From a quantitative point of view, the computed values show a fair agreement with experiment when environmental effects are taken into the proper account. From a more general point of view, our analysis points out a number of analogies, but also some difference, between hydrogen and halogen bond, which have been interpreted in terms of the various effects tuning thermodynamic and spectroscopic parameters.

Vincenzo Barone, Paola Cimino, Orlando Crescenzi, **Michele Pavone**

Journal of Molecular Structure: THEOCHEM 811, 323–335 (2007)

Title. Ab initio computation of spectroscopic parameters as a tool for the structural elucidation of organic systems

Abstract. Computation of spectroscopic parameters is rapidly evolving from a highly specialized research field into a versatile tool, capable of providing a crucial aid for the interpretation of experimental information. The present paper focuses on the application of computed spectroscopic parameters in organic chemistry, both in terms of assignment of observed transitions, and also in the more demanding task of discrimination among alternative structural hypotheses. The impact of dynamical and environmental effects, and some computational approaches that allow to properly take into account their influence on specific spectroscopic parameters, are also discussed based on some recent examples from the authors' experience.

Michele Pavone, Paola Cimino, Orlando Crescenzi, Atte Sillanpää, Vincenzo Barone

Journal of Physical Chemistry B 111, 8928-8939 (2007)

Title. Interplay of Intrinsic, Environmental, and Dynamic Effects in Tuning the EPR Parameters of Nitroxides: Further Insights from an Integrated Computational Approach

Abstract. The role of stereoelectronic, environmental, and short-time dynamic effects in tuning the hyperfine and gyromagnetic tensors of a prototypical nitroxide spin probe has been investigated by an integrated computational approach based on extended Lagrangian molecular dynamics and discrete-continuum solvent models. Trajectories were generated in two protic solvents as well as in the gas phase for reference; structural analysis of the dynamics, and comparison with optimized solute-solvent clusters, allowed for the identification of the prevailing solute-solvent hydrogen-bonding patterns and helped to define the strategy for the computation of magnetic parameters. This was performed in a separate step, on a large number of frames, by a high-level DFT approach coupling the PBE0 hybrid functional with a tailored basis set and with proper account of specific and bulk solvent effects. Remarkable changes in solvation networks

are found on going from aqueous to methanol solution, thus providing a rationalization of indirect experimentally available evidence. The computed magnetic parameters are in satisfactory agreement with the available measured values and allow for an unbiased evaluation of the role of different effects in tuning the overall EPR observables. Apart from their intrinsic interest, our results pave the route toward the development of tunable detection protocols based on specific spectroscopic signatures.

Malgorzata Biczysko, Giovanni Piani, Massimiliano Pasquini, Nicola Schiccheri, Giangaetano Pietraperzia, Maurizio Becucci, **Michele Pavone**, Vincenzo Barone

Journal of Chemical Physics 127, 144303 (2007)

Title. On the properties of microsolvated molecules in the ground (S_0) and excited (S_1) states: The anisole-ammonia 1:1 complex

Abstract. State-of-the-art spectroscopic and theoretical methods have been exploited in a joint effort to elucidate the subtle features of the structure and the energetics of the anisole-ammonia 1:1 complex, a prototype of microsolvation processes. Resonance enhanced multiphoton ionization and laser-induced fluorescence spectra are discussed and compared to high-level first-principles theoretical models, based on density functional, many body second order perturbation, and coupled cluster theories. In the most stable non-planar structure of the complex, the ammonia interacts with the delocalized π electron density of the anisole ring: hydrogen bonding and dispersive forces provide a comparable stabilization energy in the ground state, whereas in the excited state the dispersion term is negligible because of electron density transfer from the oxygen to the aromatic ring. Ground and excited state geometrical parameters deduced from experimental data and computed by quantum mechanical methods are in very good agreement and allow us to unambiguously determine the molecular structure of the anisole-ammonia complex.

Massimiliano Pasquini, Nicola Schiccheri, Giovanni Piani, Giangaetano Pietraperzia, Maurizio Becucci, Malgorzata Biczysko, **Michele Pavone**, Vincenzo Barone

Journal of Physical Chemistry A 111, 12363-12371 (2007)

Title. Isotopomeric Conformational Changes in the Anisole-Water Complex: New Insights from HR-UV Spectroscopy and Theoretical Studies

Abstract. Resonance enhanced multiphoton ionization and rotationally resolved $S_1 \leftarrow S_0$ electronic spectra of the anisole-^2H_2O complex have been obtained. The experimental results are compared with high level quantum mechanical calculations and with data already available in the literature. Quite surprisingly, the equilibrium structure of the

anisole-$^{2}H_2O$ complex in the S_0 state shows some non-negligible differences from that of the isotopomer anisole-$^{1}H_2O$ complex. Actually, the structure of the deuterated complex is more similar to the corresponding structure of the anisole-$^{1}H_2O$ complex in the S_1 state. In anisole-water, two equivalent H(D) atoms exist as revealed by line splitting in the rotationally resolved spectra. It is possible to suggest a mechanism for the proton/deuteron exchange ruled by a bifurcated transition state for the exchange reaction, with both water hydrogen atoms interacting with the anisole oxygen atom. From the analysis of all of the available experimental data and of computational results, we can demonstrate that in the S_1 excited state the hydrogen bond in which the water molecule acts as an acid is weaker than in the electronic ground state but is still the principal interaction between water and the anisole molecules.

Michele Pavone, Nadia Rega, Vincenzo Barone

Submitted to *Chemical Physics Letters*

Title. Implementation and validation of DFT-D for molecular vibrations and dynamics: the benzene dimer as a case study

Abstract. Semi-empirical correction to density-functional theory for dispersion (DFT-D) has been implemented for energies, analytical gradients, and Hessians in order to explore potential energy surfaces by means of a complete set of first-principle methods. The impact of non-bonding interactions on structures, binding energies and zero-point energy contributions as well as on ab-initio molecular dynamics trajectories have been investigated for the well known case of benzene dimer. While the static results are in remarkable agreement with the most sophisticated post-Hartree-Fock approaches, the low cost of DFT-D allows to unravel dynamical aspects too, which are mandatory for situations ruled by weak interactions

Vincenzo Barone, Malgorzata Biczysko, **Michele Pavone**

Submitted to *Chemical Physics*

Title. The role of dispersion correction to DFT for modelling weakly bound molecular complexes in the ground and excited electronic states

Abstract. Several computational methodologies rooted into Density Functional Theory (DFT) or Møller-Plesset second order perturbation theory (MP2) have been applied to study the anisole-ammonia and anisole-water 1:1 molecular complexes in the ground and first excited electronic states, with a special reference to the role of dispersion interactions. Semi-empirical correction to account for dispersion (DFT-D), a recently parameterized semi-local density-functional (M05-2X), and longrange correction

scheme (LC-ωPBE and LC-PBETPSS) have been tested. All the results are compared with Coupled-Cluster calculations and with state-of-the-art experimental spectroscopic data. Regarding the ground electronic state, the best description of structures and energies has been achieved by MP2 computations by including a counterpoise correction for the basis-set superposition error. Besides, the tested density functionals corrected for dispersion have provided qualitative and in some cases also quantitative agreement with the experimental and reference data at a much lower computational cost.

Malgorzata Biczysko, **Michele Pavone**,Vincenzo Barone

Submitted to *Physical Chemistry Chemical Physics*

Title. Modified DFT-D scheme for stacking/dispersion and hydrogen bonding interactions

Abstract. Starting from the DFT-D approach (S. Grimme, J. Comput.Chem. 2006, 27, 1787), we propose a modified dispersion scheme based on a chemical context of atoms in molecular systems (DM): it neglects all the dispersion contributions for hydrogen atoms bonded to electronegative atoms like, e.g., N and O. The B3LYP, B3LYP-D, B3LYP-DM, and M052X functionals have been tested on a small set of prototypical systems: namely, the water, benzene, and phenol dimers and two molecular adducts, i.e., anisole-ammonia and anisole-water 1:1 complexes. Our results show that the DM scheme represents a viable route toward improving the DFT-D approach for those systems ruled by a delicate balance between stacking/dispersion and hydrogen bonding forces.